FULL FREQUENCY-DEPENDENT PHASE-DOMAIN MODELLING OF TRANSMISSION LINES AND CORONA PHENOMENA

by

Fernando Castellanos

Electrical Engineer, Universidad de Los Andes, 1983
M.A.Sc, Elec. Engr., Universidad de Los Andes, 1986

A THESIS SUBMITTED IN PARTIAL FULFILLMENT OF
THE REQUIREMENTS FOR THE DEGREE OF
DOCTOR OF PHILOSOPHY
in
THE FACULTY OF GRADUATE STUDIES
DEPARTMENT OF ELECTRICAL ENGINEERING

We accept this thesis as conforming
to the required standard

THE UNIVERSITY OF BRITISH COLUMBIA
February 1997
© Fernando Castellanos,1997

In presenting this thesis in partial fulfilment of the requirements for an advanced degree at the University of British Columbia, I agree that the Library shall make it freely available for reference and study. I further agree that permission for extensive copying of this thesis for scholarly purposes may be granted by the head of my department or by his or her representatives. It is understood that copying or publication of this thesis for financial gain shall not be allowed without my written permission.

Department of Electrical Engineering

The University of British Columbia
Vancouver, Canada

Date April 29th 1997

DE-6 (2/88)

ABSTRACT

This thesis presents two main developments in the modelling of power transmission lines for the simulation of electric networks. The first one is a wide bandwidth circuit corona model and the second a phase-domain multiphase full frequency-dependent line model. The latter can be easily used in connection with the former. Both models have been developed for implementation in time domain simulation computer programs, such as the ElectroMagnetic Transients Program (EMTP).

Corona in overhead transmission lines is a highly nonlinear and non-deterministic phenomenon. Circuit models have been developed in the past to represent its behaviour, but the response of these models is usually limited to a narrow band of frequencies. The corona model presented in this thesis overcomes this problem by: 1) matching closely the topology of the circuit to the topology of the physical system, and 2) duplicating the high-order dynamic response of the phenomenon with a high-order transient circuit response. The resulting model is valid for a wide range of frequencies and is able to represent waveshapes from switching to lightning surges.

A unique set of model parameters can be obtained directly from test-cage measurements, and the same set can be used directly for an arbitrary overhead line configuration. The model uses only standard EMTP circuit elements and requires no iterations. Simulations of corona charge-voltage (q-v) curves and of travelling surges were performed and compared to existing field test measurements.

The proposed new transmission line model (z-line) can be used for the representation of multicircuit transmission lines in time-domain transient solutions. The model includes a full representation of the frequency-dependent line parameters and is formulated directly in phase coordinates. The solution in phase coordinates, as opposed to modal coordinates, avoids the problems associated with the representation of the frequency-dependent transformation matrices that relate the two domains. The main obstacle in phase-domain modelling, which is the mixing or superposition of propagation modes with different travelling times in the elements of the phase-domain propagation matrix $[\mathbf{e}^{-\gamma(\omega)x}]$ is effectively circumvented by discretizing in space rather than in time. In simple terms, instead of synthesizing the elements of $[\mathbf{e}^{-\gamma(\omega)x}]$ by rational functions as in the traditional approach ("time discretization"), propagation on a discrete-length segment of line can be represented as propagation on a discretized segment of ideal line (which has an exact solution) plus wave shaping by the line losses. The losses are represented by a frequency-dependent impedance matrix $[\mathbf{Z}^{loss}(\omega)]$ which is synthesized directly in the phase-domain by rational function approximations. A new coordinated-fitting procedure is introduced to ensure numerically stable fitting functions. An additional advantage of space discretization is that it allows the interface of transversal line phenomena between sections (such as corona models, tower models, grounding connections, etc.).

The z-line model is accurate, efficient, and numerically stable, and is specially suited for strongly asymmetrical line configurations where conventional models can give inaccurate results. A number of simulations were performed for highly asymmetrical line configurations and system conditions and the results compared against other time domain

and frequency-domain models. The new z-line model was combined with the proposed corona circuit model in the simulation of a field test measurement of travelling-wave propagation under corona conditions.

TABLE OF CONTENTS

LIST OF TABLES

Number *Page*

LIST OF FIGURES

Number *Page*

ACKNOWLEDGMENTS

The completion of this work represents another valuable accomplishment in my professional life. As any other person I have reached this stage of my existence only through the love, encouragement, support, work and dedication of many people over the span of my entire life. I would like to thank and remember all those that have crossed my path and helped me in any way on this continuous and fantastic experience called life. Particularly, I have to thank those whom are closer to my heart and have taught and guided me through the arduous development of this thesis.

To the memory of my grandmother Susana who taught me the love for mathematics and gave me my first arithmetic lessons. My deepest love and gratitude to my dear parents Pepe and Menelly for the infinite love, support and encouragement through all my dreams, adventures and life; I only wish I can be such a good parent one day. To my fabulous sister Pilar, her husband Fernando and my new-born nephew Camilo for their constant readiness to help and unconditional love; their faith in our families have made us reach new dimensions. To my mother in-law Seedai who has welcomed me as one of her sons and provides me with so much love, understanding and patience. To my extraordinary, beautiful and magnificent wife Cintra, for being my companion, the rock to hold on to during my weak moments and the calypso to dance to during my happy times; thanks for your endless love, patience, support and incentive.

A very special thank you to my professor Alberto Gutierrez who introduced me several years ago to the EMTP and opened for me the door to this area of knowledge and research. My deepest gratitude to my supervisor Dr. J. R. Martí for his sapient, broad and original technical guidance, his personal time, advice and his invaluable friendship; thanks for helping me stretch my intellectual horizons. I want to thank Dr. H. Dommel, whom I respect and admire tremendously, for his keen suggestions, support and time; his pioneering and unique research work was the reason I came to UBC. To Dr. M. L. Wedepohl for his insights in modal domain, idempotents and allowing me to use his FDTP program as a reference for some of the results in this work.

A warm and special thanks to all my friends and colleagues in the Power Group; their friendship through the past years have been a constant source of knowledge, enjoyment and energy. Thank you and the best luck on your research. Thanks to all the Professors and staff in the Department of Electrical Engineering who taught, guided and helped me constantly. I will like to thank UBC, Dr. Martí, Dr. Dommel, the Natural Sciences and Engineering Research Council of Canada (NSERC), BC-Hydro and my wife for providing the funds for my graduate study.

Finally, I would like to thank my beloved and beautiful country Colombia and it's people for giving me the basis to build what I have achieved; I believe in you. Last, but not least, I want to thank the mountains for their strength and beauty, for their silent and unconditional companionship, for taking me so deep inside myself; thanks and I will be seeing you soon.

"... A heavy gypsy with an untamed beard and sparrow hands, who introduced himself as Melquíades, put on a bold public demonstration of what he himself called the eight wonder of the learned alchemists of Macedonia. He went from house to house dragging two metal ingots and everybody was amazed to see pots, pans, tongs, and braziers tumble down from their places and beams creak from the desperation of nails and screws trying to emerge, an even objects than have been lost for a long time appeared from where they had been searched for most and went dragging along in turbulent confusion behind Melquíades' magical irons. "Things have a life of their own," the gypsy proclaimed with a harsh accent. "It's simply a matter of waking up their souls."..."

Gabriel García Márquez (1928-), Colombian author. *One Hundred Years of Solitude.*

"I seem to have been only like a boy playing on the seashore, and diverting myself in now and then finding a smoother pebble or a prettier shell than ordinary, whilst the great ocean of truth lay all undiscovered before me."

Sir Issac Newton (1642-1727), English mathematician, physicist. *Memoirs of Newton.*

1. CHAPTER 1

INTRODUCTION

1.1. Overview

The analysis of electric power networks requires a precise knowledge of the magnitude and duration of overvoltages that might occur in the system. Overvoltages appear mostly due to lightning discharges and switching operations [1]. The insulation level of transmission lines and terminal equipment, such as transformers and circuit breakers, must be able to withstand the stresses imposed by these overvoltages.

The most practical and effective way currently available to study the different types of overvoltages, their effects and the design of adequate insulation levels is through simulations with computer programs. The most widely known of these programs is the EMTP (Electro-Magnetic Transients Program) [2] which is a combination of mathematical models and solutions techniques representing the different components of the electrical network and their interrelationships. The EMTP models each component in the time domain through equivalent resistances and history current sources obtained from the mathematical models, once a given integration rule is applied. Finally, the whole electrical system is solved using numerical methods to solve the resulting simultaneous equations.

The modelling and simulation of travelling overvoltages is not an easy task. As waves propagate through transmission lines, they are subjected to attenuation and distortion,

which depend on the characteristics of the line and on the amplitude and shape of the waves themselves. The main sources of attenuation are the resistive losses in the conductors and in the ground, the losses caused by the occurrence of corona on the conductors and the insulator leakage losses. The main sources of distortion are the continuous process of energy reflection resulting from the series resistive losses and the changing shunt capacitance effect due to corona [1].

Transmission line models and methods to solve propagation waves in electric power systems have been developed for many years. Computer programs such as the EMTP possess very complete models [5] that take into account most of the sources of attenuation and distortion in the transmission lines. However, some limitations still exist in the actual models and the work presented in this thesis represents an advance in two specific areas of EMTP modelling: corona modelling and full frequency-dependent transmission line modelling.

1.2. Corona Modelling

A number of measurements have been taken and physical explanations have been formulated to better understand the corona characteristics in transmission lines [e. g. 3, 9, 10, 11, 12, 13, 15, 28, 34, 42]. However, the physical complexities of the phenomenon have made it difficult to formulate simple models that can be used in the context of general-purpose system-level transients simulations, as for example in the EMTP program.

Ideally, one should be able to derive some set of equations to describe the characteristics of the corona phenomenon from available line data and then formulate an

EMTP-type circuit model. This is the case, for instance, in normal (without corona) transmission line modelling [4], where relatively complicated equations (e.g., Carson's equations for the ground return) have to be translated into simple and computationally efficient circuit models. For corona, no general analytical expressions from basic line data are yet available and most descriptions are based on experimentally measured charge versus voltage characteristics (q-v curves). However, regardless of whether the physical description is derived analytically or measured experimentally, it still has to be translated into an efficient and practical circuit model for general-purpose transmission system simulation with the EMTP.

A main drawback of conventional circuit models for corona is their limitation in their ability to represent the phenomenon for a wide range of waveforms using the same set of circuit parameters. The model presented in this thesis overcomes this limited-bandwidth problem by formulating a circuit topology that more closely matches the topology of the actual physical system, and by including circuit components with higher-order dynamic responses.

The improved topology and dynamic response of the proposed model allow it to match, with a single set of circuit parameters, a wide range of surge waveshapes: from slow switching surges to very fast lightning strokes. In addition, the circuit model parameters obtained for a given conductor in a cage setup could be extrapolated for the more general case of the conductor above ground. In the latter case, the model can correctly respond to the changes in shape and rise time as surges propagate along the transmission line. A brief

review of corona phenomena and its modelling is presented in Chapter Two, together with the new proposed model and case-study simulations with the EMTP.

1.3. Full Frequency Dependent Transmission Line Modelling

Another element of importance in the accurate simulation of transmission lines with or without corona is the representation of the frequency dependence of the line propagation characteristics [3, 61, 62]. Currently used transmission line models in time domain simulations may not be totally accurate in the representation of asymmetrical line configurations. The main problem with these models is the frequency dependence of the transformation matrices (matrices of eigenvectors) that relate the modal and phase domains. Traditional multiphase transmission line and cable models in the EMTP ([4, 5, 45]) use Wedepohl's modal decomposition theory ([46, 47]) to decouple the physical system of conductors (phase domain) into a mathematically-equivalent decoupled one (modal domain). The main advantage of this approach is that each *natural* decoupled mode has its own propagation velocity. This is particularly important in the case of frequency dependence modelling by rational-function synthesis ([4, 45, 48]), where the time delay in the propagation functions can be easily extracted in modal domain synthesis while synthesis in the phase domain can be difficult due to the mixing up of time delays in the self and mutual waves.

The simplicity and elegance of modal decomposition analysis are lost in time domain simulations when the transformation matrix cannot be assumed constant. Two factors affect the validity of a constant transformation matrix assumption [49]: a) the degree of

asymmetry of the system of conductors, and b) the frequency dependence of the line parameters. To avoid the difficulties associated with frequency-dependent transformation matrices, a number of alternatives have been proposed recently to formulate the line model directly in phase coordinates [56, 57, 58, 60]. Some of these approaches use various fitting techniques to directly derive, in the phase domain, the coefficients of the discrete-time line representation. A major difficulty in these new approaches is to guarantee a numerically stable solution in the resultant time-domain representation.

A new transmission line model is proposed (z-line model) that combines the capability of including corona effects with a very accurate and absolutely stable frequency dependent line representation. The z-line model splits the representation of the line into two parts: ideal propagation and losses. The wave propagation in the line is visualized as a combination of *ideal propagation*, taking place "outside" the conductors in the external magnetic and electric fields, plus wave-shaping by the *losses* "inside" the conductors and ground in the resistance and internal inductance. This approach is similar to the one from [43] with two important differences: i) the losses in the z-line model include not only the resistance but also the internal inductance, and ii) the z-line model works entirely in phase coordinates and, therefore, does not require the use of frequency-dependent transformation matrices.

A limitation of the existing frequency dependent line models when applied to corona modelling is that they do not provide for space discretization. If the total line must be sectionalized to include some transversal phenomena between sections (as in the case of corona), the model becomes computationally inefficient. The proposed z-line model is

based on space discretization instead of time discretization and section subdivision takes the place of synthesis of the frequency dependent propagation function. Additional transversal phenomena such as corona can be placed at these sections directly without incurring into additional computational expenses in the line representation. The process of lumping the losses between line sections is similar to the technique used in the traditional constant-parameter line model in the EMTP [5] (cp-line), where the resistive losses are lumped into sections. The required number of sections is larger in the z-line model, however, because in addition to the resistance the internal inductance is also modelled as lumped. A major difference of z-line versus cp-line (in addition to the ability of z-line to provide a full frequency dependence representation) is that z-line does not need a transformation matrix while cp-line assumes a constant real transformation matrix.

The z-line model is presented in Chapter Three of this thesis with a brief background review and a theoretical description. Time simulations are shown for several cases and comparisons against the frequency dependent constant parameter fd-line model in the EMTP, and Dr. Wedepohl's frequency-domain solution technique are presented.

2. CHAPTER 2

CORONA MODELLING

2.1. Corona Characteristics and Literature Review

2.1.1. Physics of the Corona Phenomenon

The major difference between the breakdown in a uniform, or quasiuniform, field and that in a nonuniform field such as the one associated with corona is that the onset of a detectable ionization in the uniform field usually leads to the completion of the transition between non-ionized and ionized states and the establishment of a high energy plasma channel. In the nonuniform field this is entirely different and various visual manifestations of locally confined ionization and excitation processes can be viewed and measured long before the complete voltage breakdown between electrodes occurs. These manifestations have long been called "coronas" because of their similarity to the glow or corona that surrounds the sun.

In a power transmission line, a conductor produces corona discharges at its surface when the electric field intensity on that surface exceeds the breakdown strength of air. This corona phenomenon generates light, audible noise, radio noise, conductor vibration, ozone and other products, and causes a dissipation of energy that must be supplied by the power station [9]. Most corona effects encountered in high voltage transmission phenomena do not require, for their modelling in electrical power system analysis, an extensive background in

the theory of gaseous discharges [6], but some basic physics are presented here for a better understanding.

The basics of the mechanism of corona can be understood using the general laws controlling the gas discharge process. Electrical discharges are usually triggered by an electric field accelerating free electrons through a gas. When these electrons acquire sufficient energy from the electric field, they can produce fresh ions by knocking off electrons from atoms by collisions. This process is called ionization by electron impact. After one electron collides with an atom, another electron is liberated. Each of those electrons can then liberate two more electrons, a chain reaction causing the quantity of electrons to increase rapidly [6, 7, 8, 9].

The initial electrons that start the ionization process after the critical breakdown voltage gradient is reached are often created by photo-ionization. That is, a photon from some distant source imparts enough energy to an atom for the atom to break into an electron and a positively charged ion. During acceleration in the electric field, the electron collides with the atoms of nitrogen, oxygen, and other gases present. During most of these collisions the electron loses only a small part of its kinetic energy [6, 7, 8, 9]. Occasionally, an electron may strike an atom with sufficient force to cause excitation and consequently an atom shifts to a higher energy state. The orbital level of one or more of its electrons changes, and the impacting electron loses part of its kinetic energy. Later the excited atom may revert to its normal state, resulting in the radiation of the excess energy in the form of light (visible corona) and lower frequency electromagnetic waves (radio noise). A free electron may also collide with a positive ion, converting the ion to a neutral atom [6, 7, 8, 9].

During most of its travel the electron does not cause ionization but collides with the atoms in its path. With each collision the electron loses a small amount of energy and can experience another important kinetic energy loss - attachment. During attachment a neutral atom captures the electron, and the electron radiates its surplus energy. In air, an electron might make 2×10^5 collisions before capture. Some molecules have a high ability to capture electrons, for example, the halogens and water vapor. This is one reason that with increasing humidity the water vapor captures more ionizing electrons than during dry conditions. Once an atom captures an electron, a negative ion forms. Since this ion is a relatively immobile particle, it fails to ionize gases by collision except under extremely high-energy circumstances [6, 7, 8, 9].

Most of the literature divides the corona phenomenon into three main categories: negative or cathode corona, positive or anode corona, and ac corona [6, 8, 9]. When a steady negative dc voltage is applied to the electrode, as shown in Figure 2.1, most of the literature [e. g. 8, 9] describes the evolution of corona (as the voltage increases) through three stages: Trichel pulses, pulseless glow and negative streamers. These stages or modes and their descriptions are frequently based on a visual characterization of the corona phenomena. When a negative voltage pulse is applied, with very fast rise and decay times, the phenomenon does not develop the pulseless glow stage, because the time span is too short to allow the ions to move.

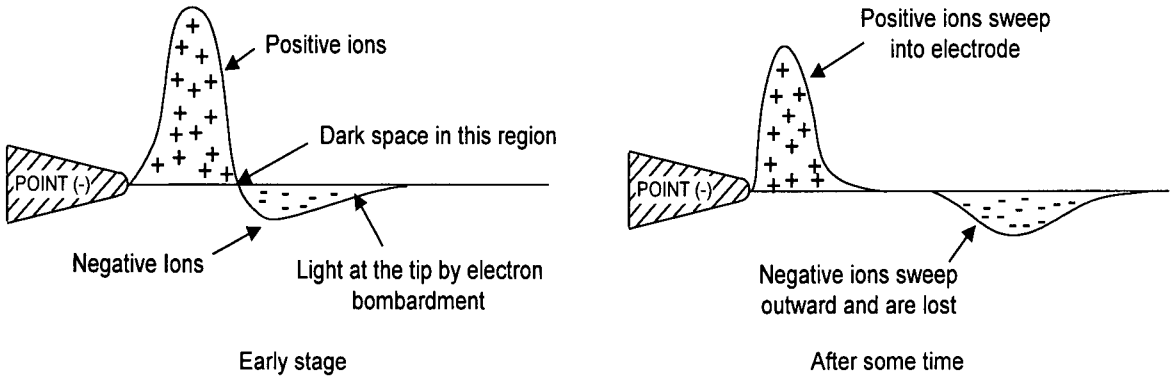

Figure 2.1. Suggested distribution of space charge in nonuniform field corona for a negative corona impulse [8].

For the case of steady positive dc voltage, shown in Figure 2.2, three similar stages are described in the literature: onset pulses, Hermstein's glow and positive streamers. In the case of a positive voltage pulse the glow stage does not develop.

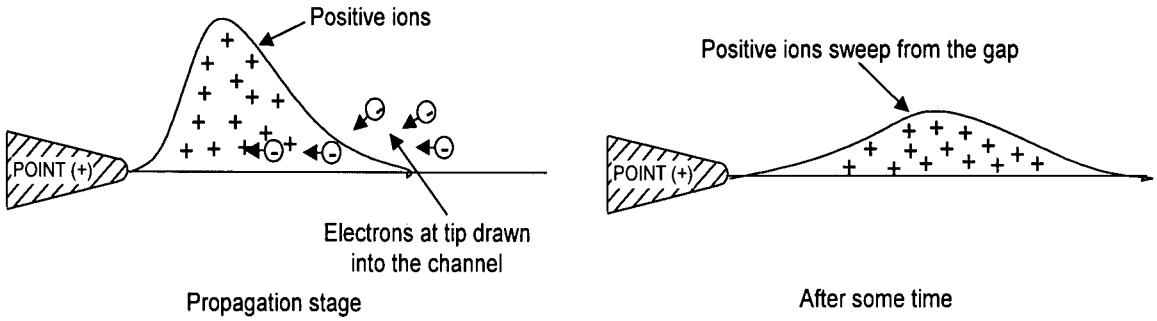

Figure 2.2. Suggested distribution of space charge in nonuniform field corona for a positive corona impulse [8].

2.1.2. Measurements

Since the pioneering work by Peek [10], laboratory and field tests have been used to examine the nature of corona and its effects on propagating surges along conductors. This

work has been of fundamental importance as much as it has enabled a basic understanding of the macroscopic mechanisms of the phenomena to be gradually obtained.

In 1954 and 1955 Wagner and Lloyd published two papers which were to become major sources of reference for corona work [11, 12]. Recordings of travelling impulses were taken on different practical conductors on a test site built for the Tidd 500 kV Test Project. Additionally, laboratory tests were also carried out with several conductors and measurements of their charge-voltage (q-v) curves were recorded. The effects of corona on a propagating wave were attributed to an increase in the shunt capacitance (which varies with the voltage) and the authors used the q-v curves to obtain parameters for this variable capacitance. These observations are today the basis for most mathematical and circuit corona models.

IREQ (Institut de Recherche d'Hydro-Québec) has made important contributions to the study of corona. In 1977 Maruvada et al published the results of tests performed on single and bundled conductors using a large outdoor testing cage [13]. The conductors were subjected to both lightning and switching surges and q-v curves were obtained. Later in 1989, IREQ published experimental results of the characteristics of conductor bundles under dynamic overvoltages [14]. Measurements of voltage and current in time were carried out in an outdoor test cage under conditions of fair weather and heavy rain, for steady 60 Hz voltages as well as dynamic overvoltages. This later study is one of the few analyzing corona in dynamic overvoltages.

Another important set of measurements was done by EDF (Electricite de France). These tests were reported by Gary et al in 1978 [15] and include laboratory tests carried out on several conductors to obtain their q-v curves. Additional field tests were made by applying very fast test surges (in the range of lightning phenomena) on an actual transmission line and recording the travelling surge at different points along the line, up to a distance of 10 km.

Another interesting study was performed at Central Research Institute of Electric Power Industry in Japan and reported by Inoue in 1978 [17]. Tests were performed on an experimental line having a single conductor, two 2-conductor bundles and two 4-conductor bundles and two ground wires. This report contains the only source currently available of oscillograms of propagation on bundles and also includes records of the induced surges.

Some early experimental work on corona characteristics was done using thin wires in cylindrical cages [18] mainly to study the possibility of using scale models for the study of corona. In 1981, Koster and Weck [20] reported measurements on a reduced model line, 180 m long, strung with a 7.5 mm diameter conductor, 1.75 m above the ground. This arrangement enabled the authors to measure the q-v characteristic in a section of the line and obtain the parameters for their model.

Similarly, Santiago et al described a study using a three-phase reduced-scale model line [21]. The parameters of the model line were such that it could be regarded as an approximate 1:10 scale model of 1 km of an actual three-phase line. The report presents q-v curves for different locations along the line and some current measurements.

2.1.3. Corona Models

In order to derive a model for the complicated physical processes of corona, a number of authors ([26, 33, 34, 35, 42, 39]) have proposed the so called "space-charge" model of the phenomenon. This model is based in some simplifying assumptions, among these:

- It is assumed that the mechanism of charge generation and diffusion is controlled, as a first approximation, by the electric field.

- Expressions for charge displacement under the influence of the electric field can be derived, on the basis of a particle description of the physical processes.

These models are able to represent the physical phenomena with great detail but fail to offer an easy representation of the macroscopic aspects of the corona and, therefore, are not well suited for travelling surge simulations in electric power system analysis.

In an effort to simplify the representation of the phenomena and concentrate on the aspects that have the most influence on wave propagation and distortion on a transmission line under corona, a number of simplified circuit models and mathematical descriptions have been proposed. Most of these models are based on q-v measurements which are then represented as close as possible by the model. A general approach in the modelling has been to represent corona as a lumped shunt branch, inserted between transmission line sections, using an equivalent circuit model. Except for the common approach of adding an extra capacitance above the corona onset voltage, there appears to be some disagreement

among different researchers with respect to the way to model the other aspects of the phenomenon.

Wagner and Lloyd proposed to use one or two additional capacitances which are switched onto the node only during those periods when the voltage is above a threshold voltage level (Figure 2.3) [11]. These models have been analyzed by some authors [3, 22] and the results show that they are not able to represent some aspects of the phenomena, such as the smooth transitions between operating regions and the continuous changing of the total capacitance value.

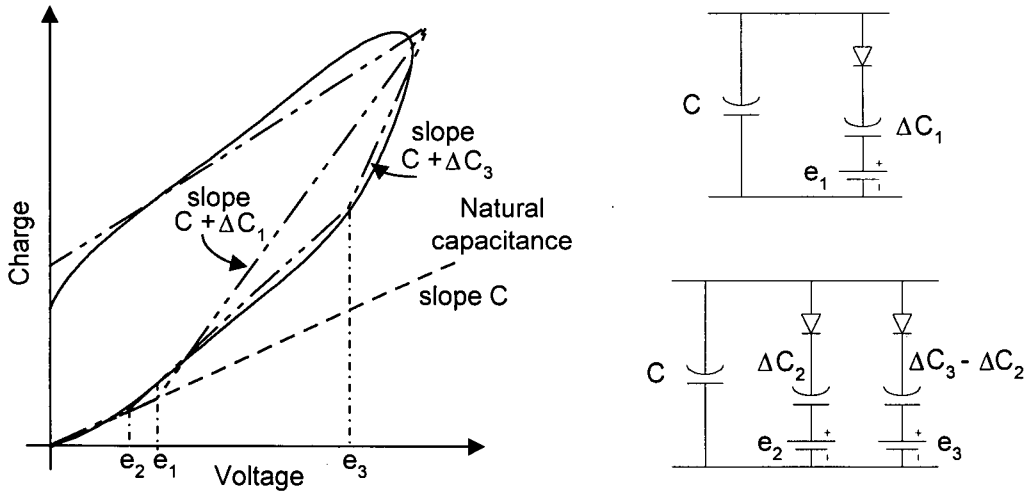

a. Typical Q-V curve.

b. Analogue circuit models

Figure 2.3. Circuit Corona Models and Their Response.

Christopoulos [23] used a circuit model based on the one proposed by Kudyan and Shih [24]. In this circuit, resistances are included in parallel with the capacitances to allow for a so-called "charge decay time constant". This circuit shows a small improvement over Wagner's model in the shaping of the curves. Similarly, Maruvada et al [13] introduced

additional switching elements to better represent the energy losses, and Comber et al [6] devised a circuit in which the corona capacitance is composed of two branches: the charge in one of the branches can return to the conductor, whereas the charge in the other will be lost through a conductance. This allows the representation of more corona processes and a better representation of the q-v curves.

Portela (Figure 2.4) [25] contends that series resistances R_1' and R_2' are necessary to reflect the energy dissipation when establishing corona while R_1, R_2, in conjunction with C_1 and C_2, can be used to represent the "attenuation of ionization, in the absence of transverse ionization current from the conductor". Elements D_1 and D_2 act similarly to diodes but also permit some current to flow in the reverse direction in order to account for some charges which may return to the conductor.

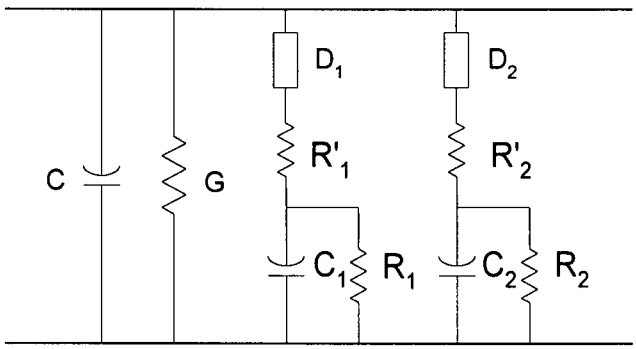

Figure 2.4. Circuit Corona Model.

Correia de Barros, having examined in some detail the mechanism of space charge generation and displacement for her space-charge model, proposed the scheme shown in Figure 2.5(a) as a reduced circuit model [26]. Two interesting features of this model are: the absence of conductances or resistances in the circuit and the series connection of the

capacitances. The former forces the model to produce q-v characteristics similar to the ones from Figure 2.3(b) and the latter one is praised by De Barros as an important conceptual difference with other circuit models. Santiago and Castellanos [22] proposed a circuit that includes a nonlinear resistance as shown in Figure 2.5(b). The addition of this nonlinearity allows for a better representation of the time constants associated with the electron avalanche and ion flows.

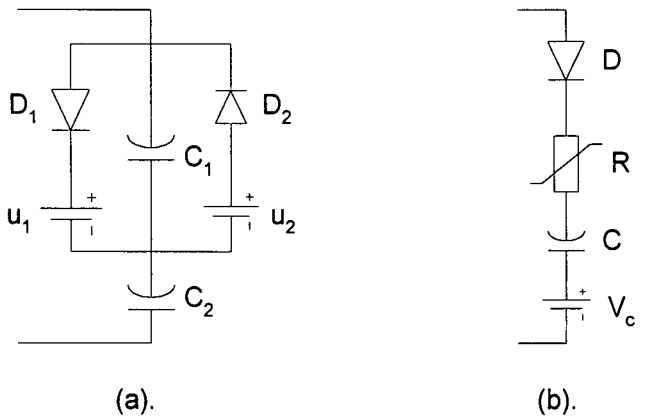

Figure 2.5. Circuit Corona Models.

The representation of corona with circuit models requires the use of several different elements which are connected through diodes. However, the switching of these elements may induce spurious numerical oscillations in the simulations. To avoid this problem and since these models are in fact based on linear or quasi-linear approximations of the q-v curve, it may be considered advantageous to use a mathematical function rather than a circuit model, and this is the procedure followed by some authors.

A first approximation to the corona nonlinearity is the piecewise linear representation proposed by Gary et al [15], which corresponds to the mathematical description of

Wagner's analog model. Suliciu and Suliciu [27] proposed a more complex mathematical model in which the path for the q-v curve, over the onset corona voltage, is described by a function of the derivative of the voltage at the wave-front. In this model, the area of the loop would ultimately depend on the steepness of the wave front. The model parameters are identified by fitting a set of measured q-v curves, ranging from lightning to switching surges. The results obtained match closely measured q-v curves and some authors [3, 29] have used this model in their surge propagation studies.

Several other researchers ([16], [17], [20], [30], [31], [32]) have opted for a different approach. They formulate empirical equations for the dynamic capacitance which provide continuous values for C along the ascending part of the q-v curve, thus avoiding numerical oscillations and improving some aspects of the modelling.

A main disadvantage of mathematical descriptions of the phenomena versus an equivalent circuit representation, for use in a transients solution program such as the EMTP is that the nonlinear function approach requires iterations at each step of the time solution. In the case of corona, where the transmission line has to be sectionalized into a large number of sections with corona lumped at each one of them, the iteration requirement at each corona branch would be very costly in terms of simulation times. On the other hand, circuit models with linear or piecewise linear elements do not require iterations. For this main reason, a circuit model approach was pursued in this work and it is presented in the following section.

2.2. Proposed Wide Band Corona Model

2.2.1. Q-V Curves and Conventional Models

As mentioned in the previous section, corona characteristics of transmission lines are usually obtained through experimental measurements. There are two basic types of measurements: 1) q-v curves, which are plots of charge versus voltage, and 2) measurements of voltage surges propagating along a transmission line. The q-v curves are obtained in cage set-ups such as the one in Figure 2.6, where an overvoltage is injected into the conductor. The voltage is measured in a voltage divider, and the charge is obtained as the integral of the current in a probe capacitance connected to the return circuit [13].

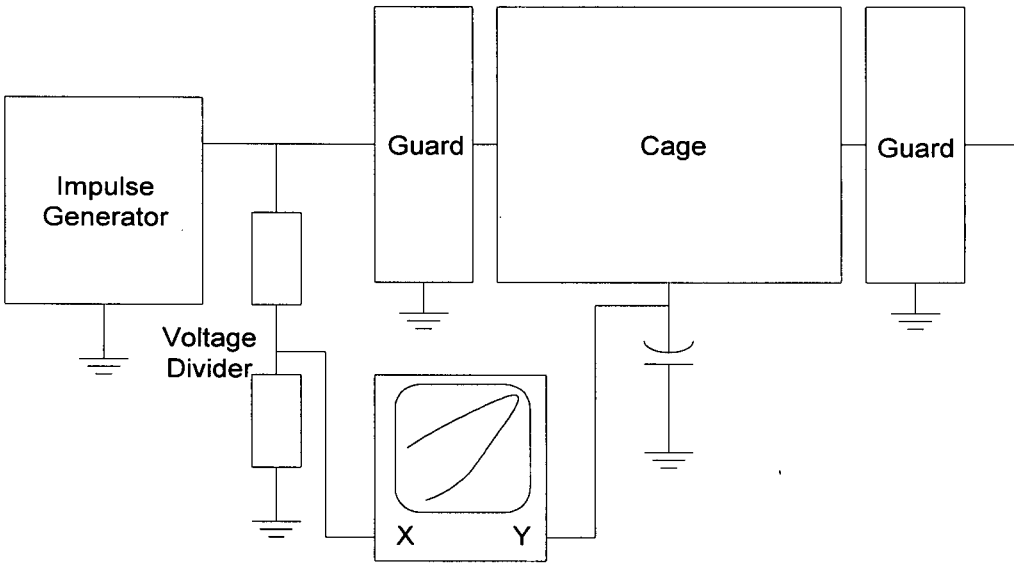

Figure 2.6. Experimental set-up for q-v curve measurements.

Typical measurements of q-v curves (reported in [13] and [21]) for single conductors of standard dimensions and for thinner conductors, for different applied voltage surges, are shown in Figure 2.7. From observation of the q-v curves, it is possible to conclude that the

main characteristics of one specific curve can be simulated by increasing the capacitance in the region between the knee point of the loop (apparent corona onset voltage E_{cor}) and the peak voltage, V_p. This type of representation has been used by previous researchers and it has been achieved with the basic model shown in Figure 2.8(a), where C_o is the geometric capacitance of the conductor, and C_{cor} is the capacitance introduced by the corona effect. The q-v curve obtained with this model is shown in Figure 2.8(b). Comparing this idealized curve with any of the measured ones, it can be observed that this type of model is limited in its ability to represent the smooth transitions between operating regions and the gradual increase of slope in the frontal lobe of the curve. In addition, since the q-v curve for a given conductor changes according to the shape of the surge, the parameters of the simplified circuit of Figure 2.8 have to be recalculated for different applied surges.

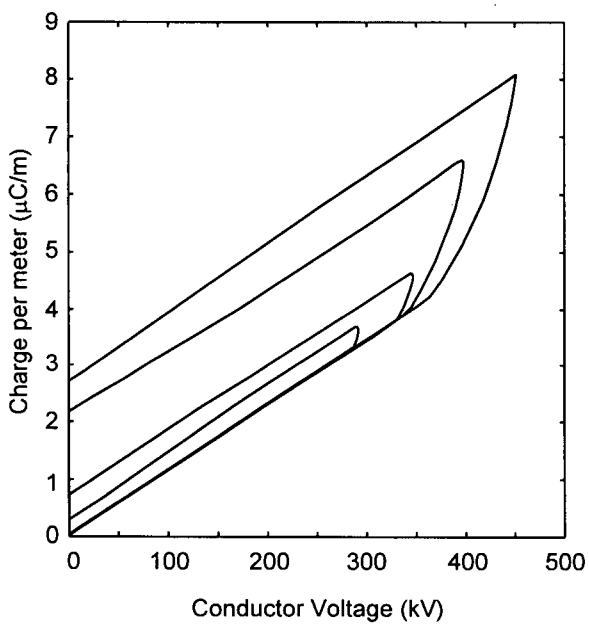

(a). Common single conductor (diam.1.2"), rise time 2.5 μs [13].

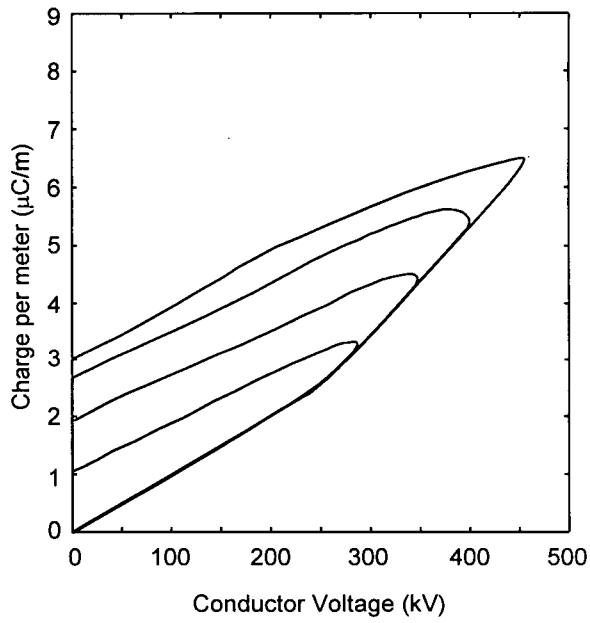

(b). Common single conductor (diam.1.2"), rise time 260 μs [13].

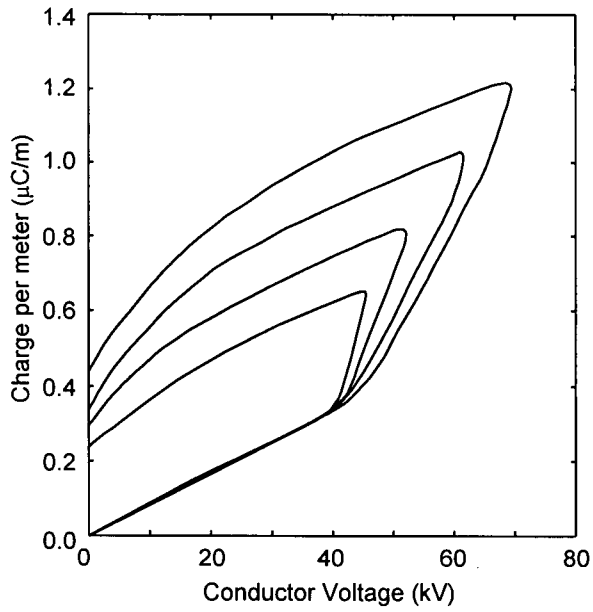

(c). Thin conductor (diam. 0.65 mm), rise time 0.12 μs [19].

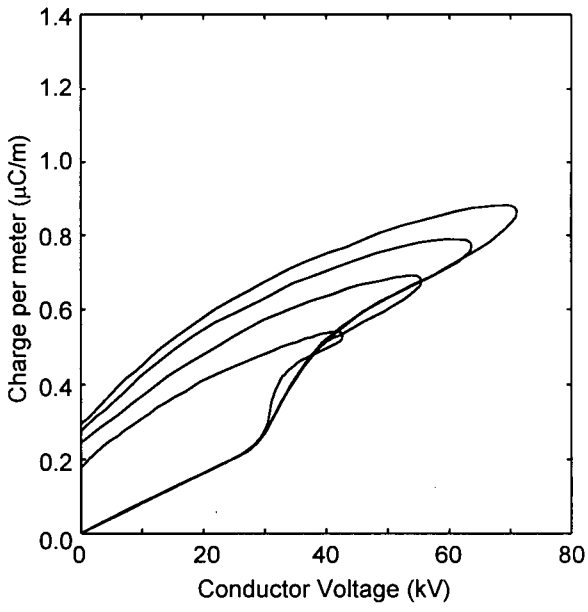

(d). Thin conductor (diam. 0.65 mm), rise time 1.2 μs [19].

Figure 2.7. Typical q-v curves.

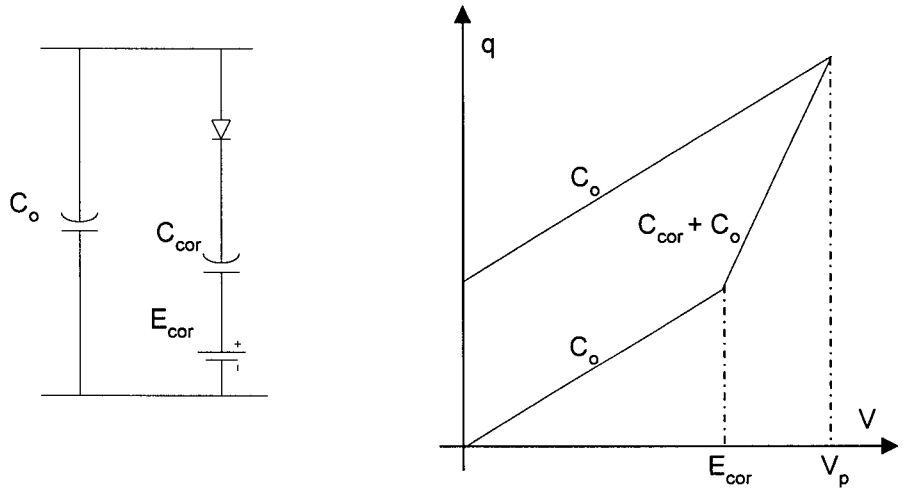

(a). Corona model. (b). Typical response of the model.

Figure 2.8. Basic corona model.

The basic circuit of Figure 2.8 can be improved by connecting to the circuit additional capacitances in parallel, additional corona branches in parallel, resistors in series or parallel, and other combinations. This methodology has been used by several researchers and some of their models were introduced in section 2.1.3. Comparative evaluations of some of these circuit models have been done using the EMTP and presented in [22] and [37].

Measurements of q-v curves for conductors in experimental cage arrangements are available from different references. Few of these references, however, have studied how the q-v curves are affected by the surge's frequency spectrum (e.g., switching versus lightning). Maruvada et al [13] have presented the most complete study until now covering different conductors subjected to switching and lightning surges of various magnitudes. Figure 2.7(a) and Figure 2.7(b) show some of these results. The following observations can be made with respect to these curves and the corresponding applied voltage surge:

1. The value of the corona onset voltage increases with the derivative of the voltage with respect to time. This increase is more pronounced for faster rise times.

2. The q-v curves present a smooth transition around the onset voltage. This is more noticeable in the case of slower rise times.

3. The portion of the q-v curve corresponding to the front of the surge after the onset voltage increases its slope as a function of the derivative of the voltage. This effect is more pronounced for faster rise times.

4. The portion of the q-v curve just after the turnaround at the voltage peak presents a slope that decreases as a function of the voltage derivative. This effect is more pronounced for faster rise times.

The above observations suggest that the corona effect is of a higher order than the simple first-order system of Figure 2.8(a). The strong dynamics of the phenomenon are particularly noticeable in thin conductors (curves in Figure 2.7(c) and (d)). The turning inwards of the slope in the characteristics of Figure 2.7(d) is another sign that strongly suggests a system of order two or higher.

In order to reproduce the various behaviours of the q-v curves under different shapes of surge functions, many researchers have opted for changing the value of the model parameters according to the type of surge applied. This approach can give satisfactory results when duplicating measured q-v curves by themselves, but it is not fully adequate for simulating travelling surges on transmission lines. During propagation, the shape of the surge gets distorted, and its rise time and frequency content change as the surge travels

down the line. This makes impossible to adjust the values of the circuit parameters for the different surge shapes along the transmission line.

Based on the foregoing analysis and observations, it is believed that a more general solution for a wide-band model of corona requires a higher-order circuit response and an improved topological representation of the geometry of the system of conductors. Another conclusion that can be extracted from the curves and observations of available data is that some of the corona dynamics are not that relevant if their time constants are smaller than those of the applied voltage surge, but become important for overvoltages having a short rise time to peak, as in the case of lightning. Results from lightning surges show that a time delay can be identified between the instant the corona onset voltage E_o is reached (which corresponds to the microscopic corona trigger) and the instant when the apparent onset voltage E_{cor} is reached (which corresponds to the macroscopic beginning of corona). A physical theory of the phenomenon considers the delay time as the sum of a statistical time delay, which corresponds to the time necessary for seed-electrons to appear, plus a formation time delay, which corresponds to the space-charge generation time [39].

2.2.2. Proposed Equivalent Circuit

The previous sections emphasized that one of the main obstacles in the modelling of corona is the difficulty in describing its physical characteristics. Several particle processes occur at the same time and a complicated electric field distribution surrounds the conductor. In spite of this, some basic assumptions can be made from a "practical" simulation point of view, many of which have been used by other researchers:

1. The corona effect can be pictured as a cylinder of ionized air. This cylinder is confined to a certain radius and surrounds the conductor, at its the center [11].

2. The main characteristics of the corona effect are related to three particle processes: first ionization, which produces free electrons and positive ions, second attachment, and third recombination, which produce negative ions [21, 22].

3. During the initial state of corona, the electron avalanche is the main component of the corona current. The corona current presents a fast rise time and a sharp drop (An even sharper drop occurs if the electron cloud has a very small spread in space as occurs for very fast surges) [21, 26, 39].

4. The electron avalanche time constant is very small compared with the time constants of the other processes [21, 22].

5. The corona onset voltage E_o is constant for a given conductor and physical setup of the transmission line. The apparent increase of the onset voltage is due to the dynamic characteristics of the avalanche process (Statistical time lag and the space charge formation time delay [38, 39]).

6. After a certain time, the corona current is caused mainly by the negative and positive ion flows [21, 22, 39].

7. The total capacitance of the ionized section increases as a result of the redistribution of particles [11].

The corona model proposed in this thesis is based on the previous assumptions plus the corona's macro-behaviour observable in the q-v curves. It achieves a wider frequency bandwidth than conventional models by using a second-order model and matching more closely the topology of the circuit to the topology of the actual physical system.

Circuit Derivation

The situation of a conductor above ground is shown in Figure 2.9. Under corona, the air surrounding the conductor is ionized from the conductor radius r to the border of the corona crown r_{cor}. The integral of the electric field from the conductor to ground, which equals the voltage applied between conductor and ground, is divided into two parts: from r to r_{cor}, under ionized air, and from r_{cor} to h, under normal air:

$$\int_r^h E \bullet dl = \int_r^{r_{cor}} E \bullet dl + \int_{r_{cor}}^h E \bullet dl \tag{2-1}$$

$$\int_r^h E \bullet dl = f(r, r_{cor}, \varepsilon_{cor}, q') + \frac{q}{2\pi\varepsilon_{air}} \ln\frac{2h}{r_{cor}} \tag{2-2}$$

$$\int_r^h E \bullet dl = V_{cor} + V_{air} = V \tag{2-3}$$

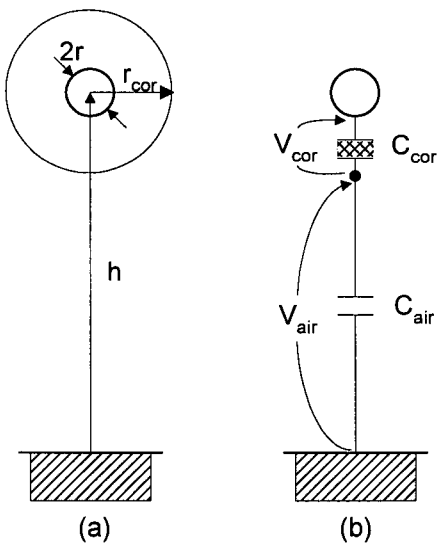

Figure 2.9. Conductor above ground and associated capacitances.

The particular form of $V_{cor} = f(r, r_{cor}, \varepsilon_{cor}, q')$ is not simple to define because depends on the permittivity ε_{cor} and the total charge q' inside the corona region, which are not easy to evaluate. Nonetheless, it can be seen from (2-1) and (2-3) that there are actually two capacitances, C_{cor} and C_{air}, connected in series between conductor and ground (Figure 2.9(b)). As discussed next, this simple observation brings out an important topological difference between the physical system and most of previously proposed circuit representations (e.g., Figure 2.8(a)).

The newly proposed circuit representation of a conductor above ground and under corona is shown in Figure 2.10. This model is composed basically of two parts connected in series, as described previously: the electric field in the ionized air under corona surrounding the conductor and the field outside the corona radius.

The upper part of the circuit of Figure 2.10 (corona part) represents the dynamic high-order processes of corona during the nonlinear ascending and descending branches of the q-v curve characteristic. During the initial linear part of the q-v curve, before the applied voltage $v(t)$ reaches the ideal corona onset voltage E_o, branches C_{cor}-L_h-R_h and R_g in the circuit of Figure 2.10 are open. The air capacitance C_{a1} (between the conductor radius r and the distance r_{cor}) and the air capacitance C_{a2} (between r_{cor} and ground) are connected in series, and their combined value equals the total geometric capacitance C_o between the conductor and ground with no corona. The ideal corona onset voltage E_o depends only on the conductor and line geometry and it is a constant value for different type of surges.

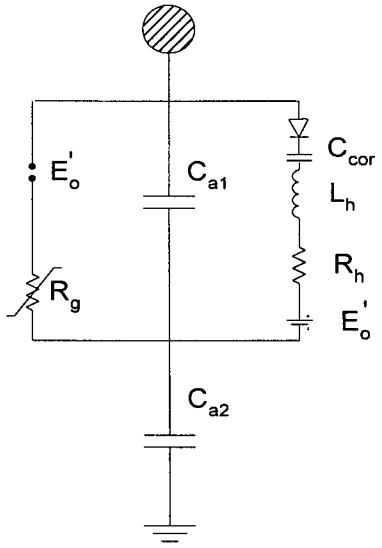

Figure 2.10. Proposed corona model.

When the surge voltage *v(t)* reaches the ideal corona onset voltage E_o, the corona process starts, with a time delay given by the statistical time lag [38] (statistical time needed by a seed electron to start the corona discharge plus the formation time delay). After this time lag, which depends on the rate of rise of the surge, the electron avalanche process proceeds very rapidly and the air surrounding the conductor becomes ionized. In the proposed circuit of Figure 2.10, when the voltage across the corona branch reaches the DC source value of E'_o the diode begins to conduct and the capacitive corona branch C_{cor}-L_h-R_h "clicks in". At the same time, the corona discharge branch R_g also "clicks in" through a spark gap with a breakdown voltage E'_o.

Therefore, when the surge voltage *v(t)* reaches the ideal corona onset voltage E_o, the two corona branches start conducting. Due to the much larger permittivity of the ionized air under corona, the capacitance C_{cor} becomes dominant and the circuit consists essentially of the capacitive corona branch C_{cor}-L_h-R_h in series with the normal air capacitance of the non-

ionized region C_{a2}. (By contrast, in the conventional circuit of Figure 2.8(a), the capacitance C_{cor} is not limited to the ionized region but extends all the way from the conductor to ground).

The diode in the proposed circuit of Figure 2.10, or in the simplified conception of Figure 2.8(a), stops conducting when the surge voltage reaches its peak value V_p. With the capacitive corona branch isolated from the circuit by the diode, the capacitance corresponding to the descending branch of the q-v loop is again the total air capacitance C_o, from conductor to ground, in both the conventional and newly proposed circuit. In the more realistic proposed circuit, at the moment the diode stops conducting, the voltage split between capacitances C_{a1} and C_{a2} is not at their non-ionized air value (ratio of the capacitive voltage divider C_{a1}-C_{a2}) because capacitance C_{a2} was charged to a much higher value during the time the capacitive corona branch C_{cor}-L_h-R_h was clicked-in by the diode.

To restore the natural voltage ratio between capacitances C_{a1} and C_{a2}, a path must be provided for the charges to redistribute themselves. In the proposed circuit this path is provided by the resistance R_g. This resistance is switched into the circuit at the ideal inception voltage E_o by an air gap. Since the air gap does not cease to conduct until the voltage across its contacts comes down to zero, R_g remains in the circuit during the entire descending part of the q-v characteristic. As the cycle proceeds along this descending branch, the voltage ratio across capacitances C_{a1} and C_{a2} returns to its natural value (value without corona) at a rate determined by the time constant of the circuit formed by C_{a1}, C_{a2} and R_g.

Summarizing, the elements in the upper part of the proposed circuit represent various aspects of the corona dynamics: C_{cor} represents the increase in capacitance due to the ionization of the air surrounding the conductor, R_h the additional conduction losses due to the avalanche process, and R_g the additional losses due to the attachment and recombination processes. The combination of L_h and R_h in the capacitive branch provides the total time delay to simulate the statistical time delay, corresponding to the space-charge generation time [39]. This time constant has practically no effect on slow surges.

A better understanding of the effects of the different circuit elements can be drawn by examining the diagram of Figure 2.11. The changing capacitance in the proposed model represents the increase in capacitance due to the ionization of the air surrounding the conductor and the change of slope from C_o to C_1, R_h the additional conduction losses and shaping in the frontal lobe of the q-v loop, and R_g the additional losses and shaping in the tail of the loop.

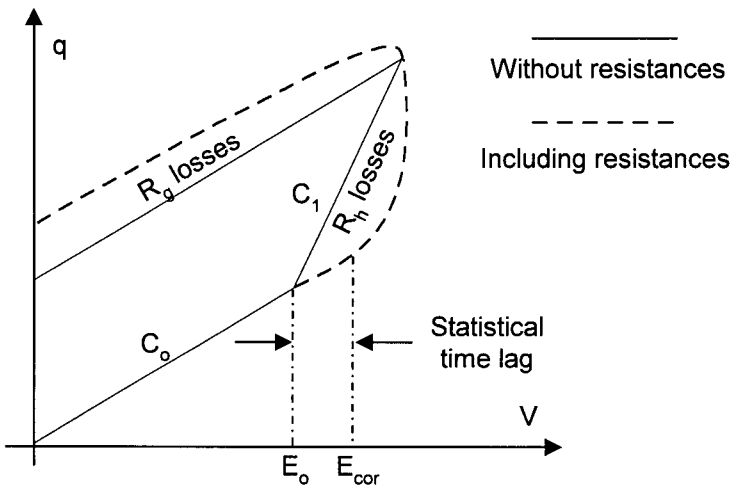

Figure 2.11. Shaping of the q-v loop.

An interesting point to notice with respect to the shape of the q-v loop is that the slope at the tip of the loop (transition from ascending to descending branches) can be negative. This behaviour, which has been observed in experimentally measured q-v curves (Figure 2.7), has been of some concern in the past. Some authors [e. g. 54] have interpreted this negative slope as corresponding to a negative capacitance, which is difficult to explain from a physical point of view.

The association of a negative slope in the q-v loop to a negative capacitance probably arises from interpreting the q-v characteristic as a plot of charge versus voltage on a capacitance. In this connection, it should be emphasized that the experimental q-v curves are not obtained from a direct measurement of the charge but from integration (with a probe capacitance) of the current in the ground return circuit. If the phenomenona were not purely capacitive, this integral would not give exactly the charge.

The circuit model proposed in this thesis provides an explanation of the negative slope at the tip of the q-v loop that does not require the concept of a negative capacitance. As shown in Figure 2.11 and section 2.3.1, the proposed circuit is able to duplicate the negative slope in the transition between ascending and descending branches using conventional circuit elements of positive value. When only capacitances are considered in the circuit (before R_h and R_g are added), the slope of the q-v loop is always positive. It is when resistances R_h and R_g are added to the equivalent circuit that their shaping effect results in a negative slope at the corner of the loop.

2.2.3. Equivalent Circuit Parameters

In spite of all the research in corona, the measurements available to build a complete model for electric power transients constitute only a very limited set and include only a few variables. As discussed in section 2.1.2, the main measurements available are q-v curves and travelling surges. The reduced amount of quantities measured during these corona tests creates limitations on the models used to represent the phenomenon. More complete models could be developed if additional variables (e.g. current, time) were to be measured during the q-v tests. These measurements could provide a more complete picture. Due to this lack of more extensive measurements, some of the proposed circuit parameters have to be found through an iterative fitting process on sets of curves for fast and slow surges.

Cage Setup

The situation of a conductor in an experimental cage setup is similar to the one shown in Figure 2.9(b). In the cage setup case, the ground is surrounding totally the conductor in a circular shape. This results in a more symmetrical field distribution than for the actual case of a conductor above a ground plane. Despite this difference between experimental and actual conditions, the form of the proposed model permits direct use of the experimental measurements.

The measured q-v curves of slow and fast surges provide asymptotic conditions that allow to define the various circuit parameters of the proposed model. Therefore, a set of q-v curves, for fast and slow surges, is needed to tune the proposed circuit model.

The first parameter that can be easily calculated or measured from any of the q-v curves is the total geometric capacitance of the cage setup C_o. Next, capacitances C_{a1} and C_{a2} can be calculated. Their values depend on the maximum corona radius, r_{cor} which, in spite of the complexity of the electric field surrounding the conductor, can be approximated under the following assumptions presented in [44]:

- The electric field at the surface of the conductor is equal to Peek's critical field E_{peek} [10].
- Streamers (charge movement) develop nearby as long as the electric field in front of them is not lower than a critical field E_{cri} [41].
- The electric field inside the ionization cloud can be approximated by the electric field due to the conductor charges.
- The space charges are located within a corona of radius r_{cor} (to the end of the streamers) and have the same polarity as those located on the conductor.

The electric field E_r at a radial distance r from a charge q can be expressed as

$$E_r = \frac{1}{2\pi\varepsilon_o}\left(\frac{q}{r}\right) \tag{2-4}$$

and the geometric capacitance of a conductor of radius r in the center of a cylindrical cage setup of radius R as

$$C = \frac{2\pi\varepsilon_o}{\ln\left(\frac{R}{r}\right)} \tag{2-5}$$

It then follows that the voltage peak V_p applied to a conductor of radius r at the center of a cylindrical cage of radius R can be calculated as:

$$V_p = E_{cri} \cdot r_{cor} \left[\frac{E_{peek} \cdot r}{E_{cri} \cdot r_{cor}} \ln\left(\frac{r_{cor}}{r}\right) + \ln\left(\frac{R}{r_{cor}}\right) \right] \tag{2-6}$$

To determine the maximum radius r_{cor} of the corona charge, equation (2-6) can be solved by a Newton Raphson method for a given voltage peak V_p. With this value, capacitances C_{a1} and C_{a2} can be calculated. Figure 2.12 and Figure 2.13 show the calculated corona radius and the associated capacitances for the case of R = 2.25 m and r = 1.5 cm.

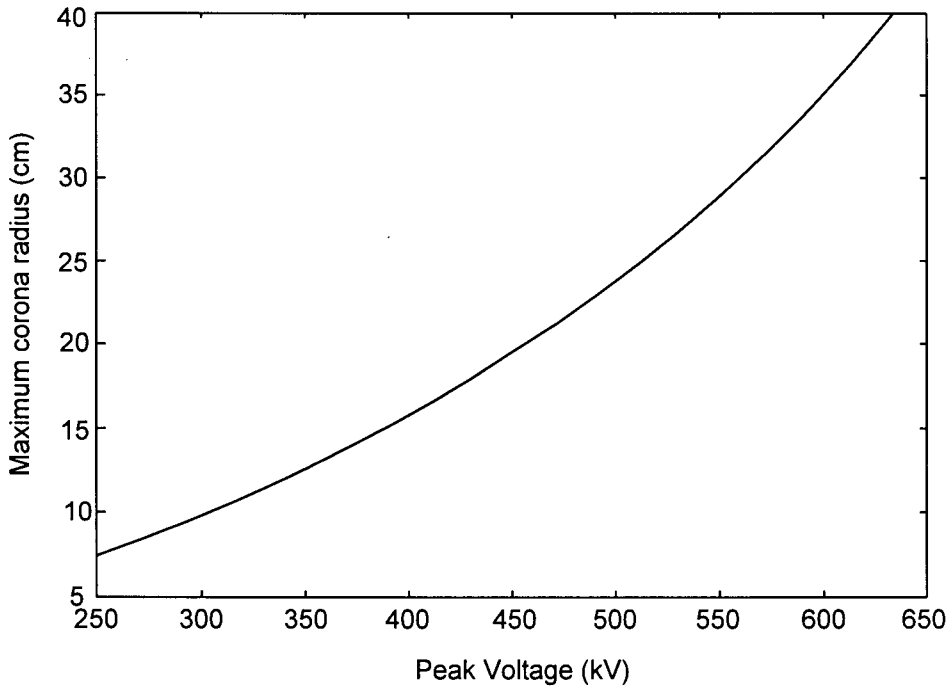

Figure 2.12. Maximum corona radius for a cage setup.

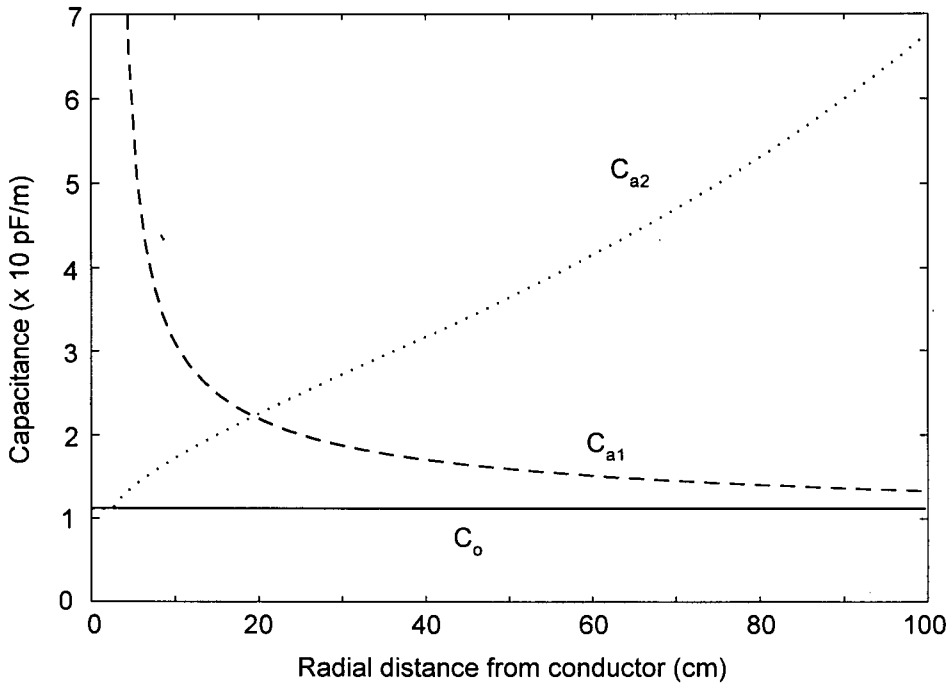

Figure 2.13. Air capacitances for a cage setup.

Next, from the q-v curves for slow surges it is possible to measure the corona onset voltage E_{cor} and the slope (capacitance) after corona C_{dyn}. These quantities can be related to the DC source E'_o and C_{cor} in the proposed circuit model of Figure 2.10 through the following equations,

$$E'_o = E_{cor}\frac{C_{a2}}{C_{a1}+C_{a2}} \tag{2-7}$$

$$C_{dyn} = (C_{a1}+C_{cor})\frac{C_{a2}}{C_{a1}+C_{a2}+C_{cor}} \tag{2-8}$$

The rest of the parameters of the proposed circuit (i.e., R_h, R_g) are found through an iterative fitting process on the q-v curves, of both fast and slow surges assuring that the additional energy added to the process by these elements is matched with the energy in the

q-v curve. This process can be explained with the help of the diagram of Figure 2.11. The full curve (dotted line) is built on top of the piece-linear curve (solid line) by the effect of resistances R_h and R_g in shaping the lobe and the tail of the cycle, and by the time delay in the lobe of the curve provided by the time constant of the L_h-R_h combination.

Q-V curves of slow surges, where the shaping of the tail of the curve is more pronounced, are used to fit the R_g resistance (associated with the attachment and recombination process). The fitting of L_h and R_h is better accomplished with the use of q-v curves for fast surges, where the shaping of the lobe of the curve is more pronounced (associated with the total time delay and the electron avalanche process). From experience, it is better to approximate first L_h and to fit R_h afterwards. (A first approximation to R_h could be calculated from the total time delay $t \approx 2 \cdot L_h / R_h$.)

Using the previous methodology it is possible to find the values of the proposed circuit model parameters from a set of q-v curves for fast and slow surges with peak voltage value V_p for a given conductor and cage setup. If different values of peak voltage are used then average values for the parameters can be calculated and the model will still give good responses as long as the range of peak voltage values produces small variations in the values of capacitances C_{a1} and C_{a2}.

Voltage Propagation along the Line

Another experiment used to obtain corona characteristics of transmission lines is the measurement of voltage surges propagating along a transmission line. Very few of these

tests are reported in the literature probably because of the complexity in setting up the experiments, but they are vital to validate corona models on transmission lines.

Because of the space-distributed nature of corona along the transmission line, it is very difficult to establish a clear relationship between the parameters in the proposed circuit model and the voltage waveshapes at different distances along the line. However, it is possible to calculate the total capacitance C_o from the geometry of the conductor configuration, and to calculate the maximum corona radius r_{cor} from an expression similar to the one developed for the cage setup (Equation 2-6). Then, the values for C_{a1} and C_{a2} in the model can be determined. Figure 2.14 shows the calculated air capacitances for the reported Tidd line [12]. One noticeable aspect is the "flatter" behaviour of the capacitances ratio compared with the cage setup case shown in Figure 2.13. This characteristic translates into small variations in the air capacitance values for a large range of r_{cor}. This implies than an average value of the model parameters can be derived for longer ranges of peak voltage than for the cage setup case.

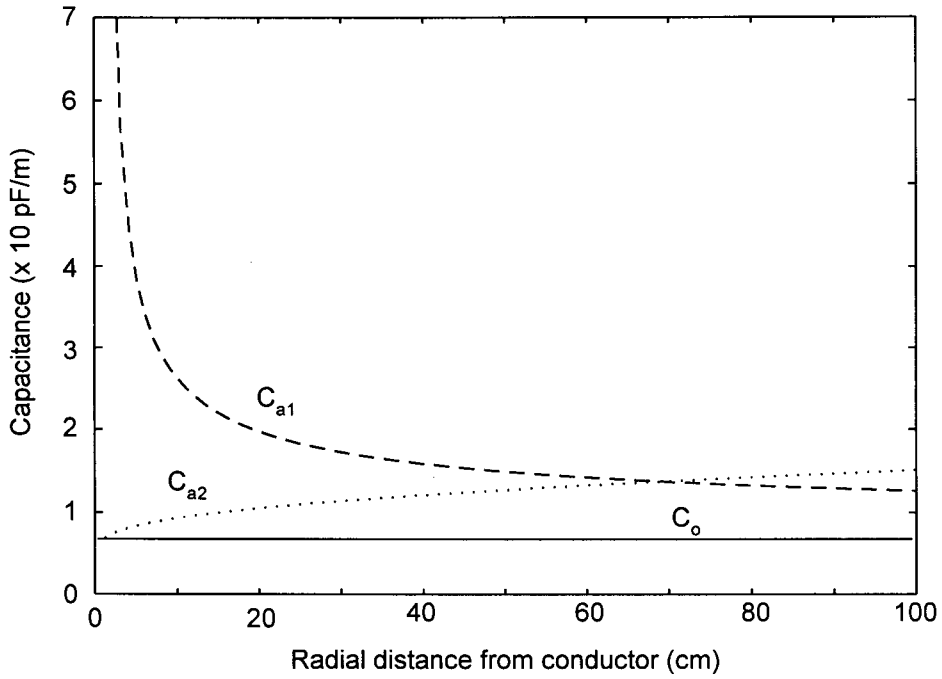

Figure 2.14. Air capacitances for Tidd line case.

From Figure 2.10, showing the proposed corona model, it is possible to observe that if the model parameters have been found from a set of q-v curves for a conductor in a cage setup, the upper part of the model (the ionized area surrounding the conductor) will not change for the same conductor on a transmission line setting as long as the calculated C_{al} for the cage test is very close to the calculated C_{al} for the transmission line. This is based on the fact that the electric field distribution between r and r_{cor} is very similar for both cases (for small r_{cor}). In this case it is possible to take the upper part of the model, calculated from the q-v curves in the cage, and add it to the external capacitance C_{a2} corresponding to the transmission line.

The described way of relating the model parameters for the cage setup and overhead conductor is possible because the circuit topology of the proposed model matches closely

the actual topology of the physical system. This represents a big advantage compared with previous models for which it is not easy to relate the representations for the cage test with the representation for the overhead conductor and one must use different parameters in the two cases.

The link between cage and overhead conductor model parameters is very important because it allows the use of q-v tests data to obtain a corona model for an arbitrary overhead line configuration. A review of the existing bibliography has shown that this is the first time such a relationship has been proposed.

2.3. Incorporation of the Corona Model in the EMTP

2.3.1. Simulation of Q-V curves

To validate the proposed circuit model and the methodology to obtain the parameters, "reverse-engineering" simulations in which the q-v curves are derived from the model were performed using the EMTP program. The methodology explained in the previous section was used to obtain the average parameters for a set of measured q-v curves for surges varying from switching (260/2700 μs) to lightning (2.5/60 μs), with peak values between 275 kV and 450 kV, applied to the single conductor of 3.04 cm of diameter and a total length of 61 m reported in [13]. Figure 2.15 and Figure 2.16 compare some of the q-v curves derived from the proposed model of Figure 2.10 against the measured ones. All the simulated curves of Figure 2.15 and Figure 2.16 were obtained with a single set of circuit parameters, shown in Table 2.1.

CIRCUIT PARAMETER	PARAMETER VALUE
C_{a1}	21 pF
C_{a2}	21 pF
C_{cor}	140 pF
L_h	23 mH
R_h	3 kΩ
E_o	125 kV
R_g	90 MΩ (0-50 kV)
	45 MΩ (50-125 kV)
	9 MΩ (125 kV and up)

Table 2.1. Circuit parameters for Q-V simulations (3.04 cm diameter conductor).

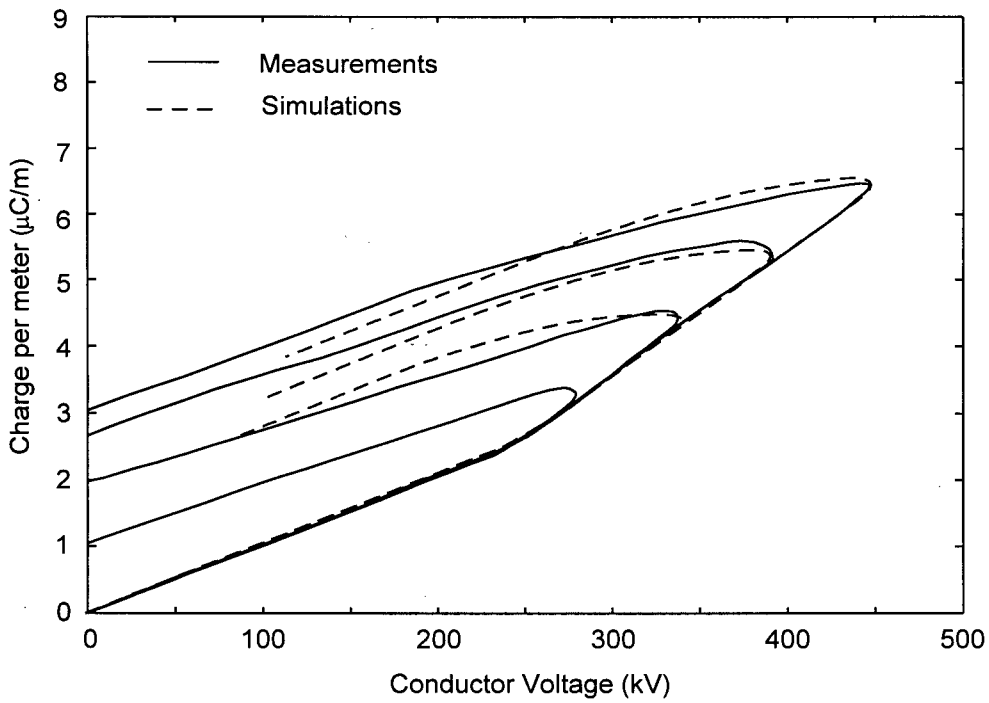

Figure 2.15. Comparison between model-derived and measured q-v curves for switching surges (3.04 cm diameter conductor).

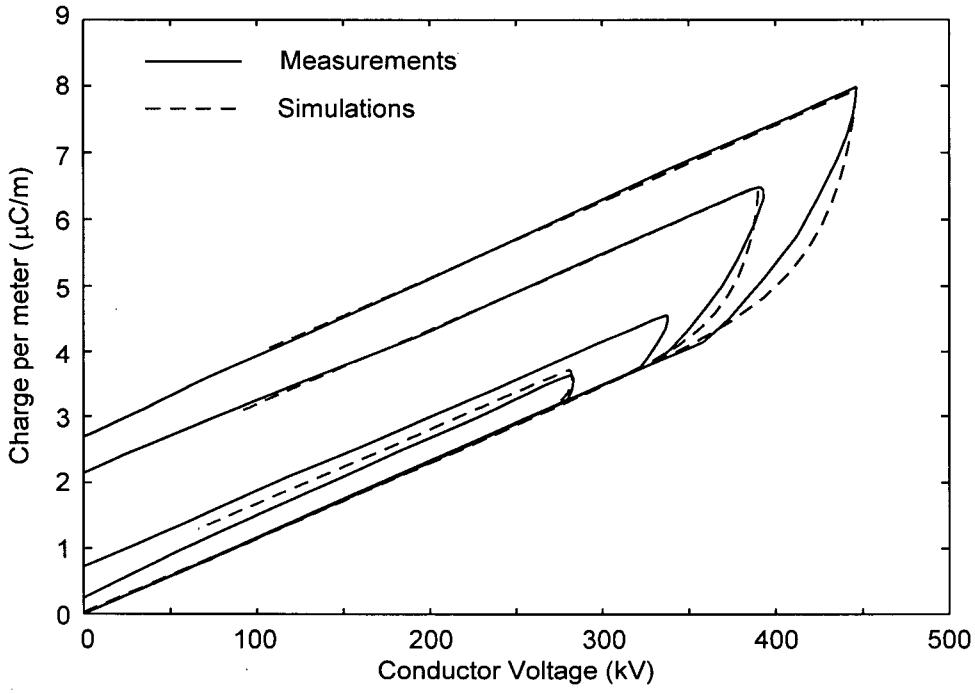

Figure 2.16. Comparison between model-derived and measured q-v curves for lightning surges (3.04 cm diameter conductor).

From the results of Figure 2.15 and Figure 2.16, it can be seen that the main characteristics of the experimental tests, particularly in the ascending part of the q-v loops, are reproduced accurately by the proposed constant-parameter model.

The following general observations can be made in connection with the results shown in Figure 2.15 and Figure 2.16:

1. The rise portion of the simulated q-v curves (corresponding to the dynamic capacitance) matches the experimental results very well for a variety of fast and slow surges.

2. The increase of the onset voltage E_{cor} for faster surges is reproduced by the proposed circuit by the dynamics of the R_h-L_h-C_{cor} branch using a constant value of DC source

voltage E'_o(single microscopic corona insertion voltage). The ability of the circuit to simulate this effect is more clearly observed in the fast surges of Figure 2.16.

3. The proposed circuit can reproduce the negative slopes observed (in some of the measured q-v curves) at the tip of the loop. This is achieved by the dynamic behaviour of the proposed second-order circuit model and does not require the concept of a negative C in the circuit. This effect is more noticeable in the slow surges of Figure 2.15.

4. The descending part of the simulated q-v curves does not fit exactly the measured ones. This effect is more noticeable in the slow surges of Figure 2.15.

Figure 2.17 and Figure 2.18 show simulated q-v curves for the case of thin conductors. All the simulated q-v curves were obtained with the same constant set of circuit parameters shown in Table 2.2. These simulations emphasize the capability of the model in reproducing the unusual dynamics observed in experimental measurements with thin conductors (Figure 2.7(c) and (d)).

CIRCUIT PARAMETER	PARAMETER VALUE
C_{a1}	16 pF
C_{a2}	16 pF
C_{cor}	100 pF
L_h	0.3 mH
R_h	30 Ω
E_o	117 kV
R_g	3 MΩ (0-117 kV)
	0.03 MΩ (117 and up)

Table 2.2. Circuit parameters for Q-V simulations (thin conductor).

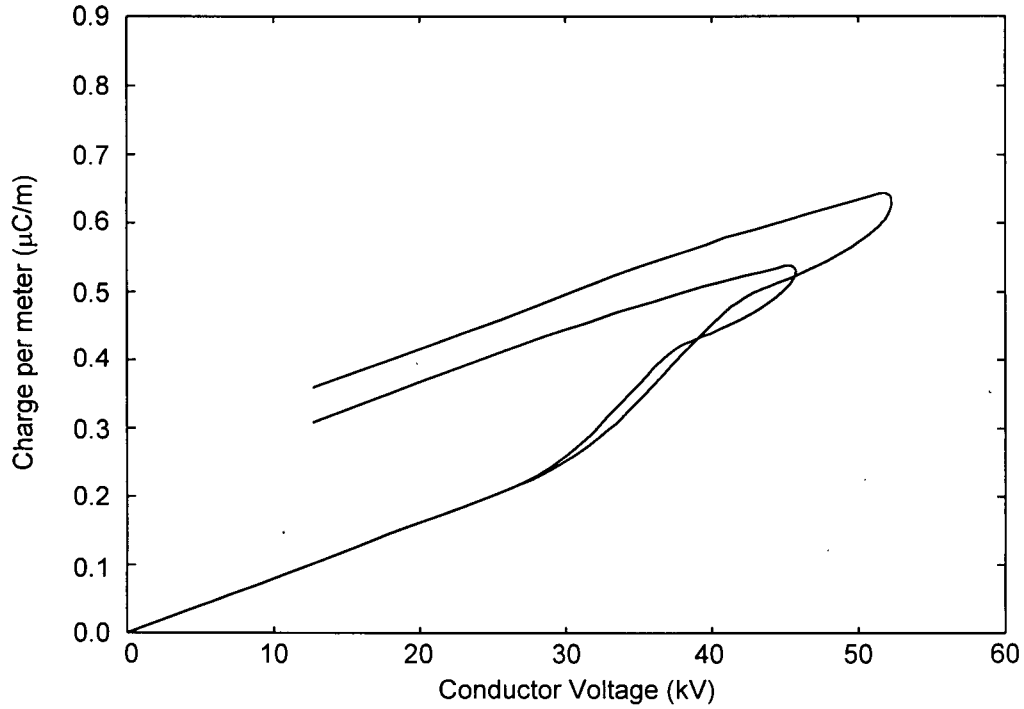

Figure 2.17. Model-derived q-v curves for thin conductor (0.65 mm- rise time 1.2 μs).

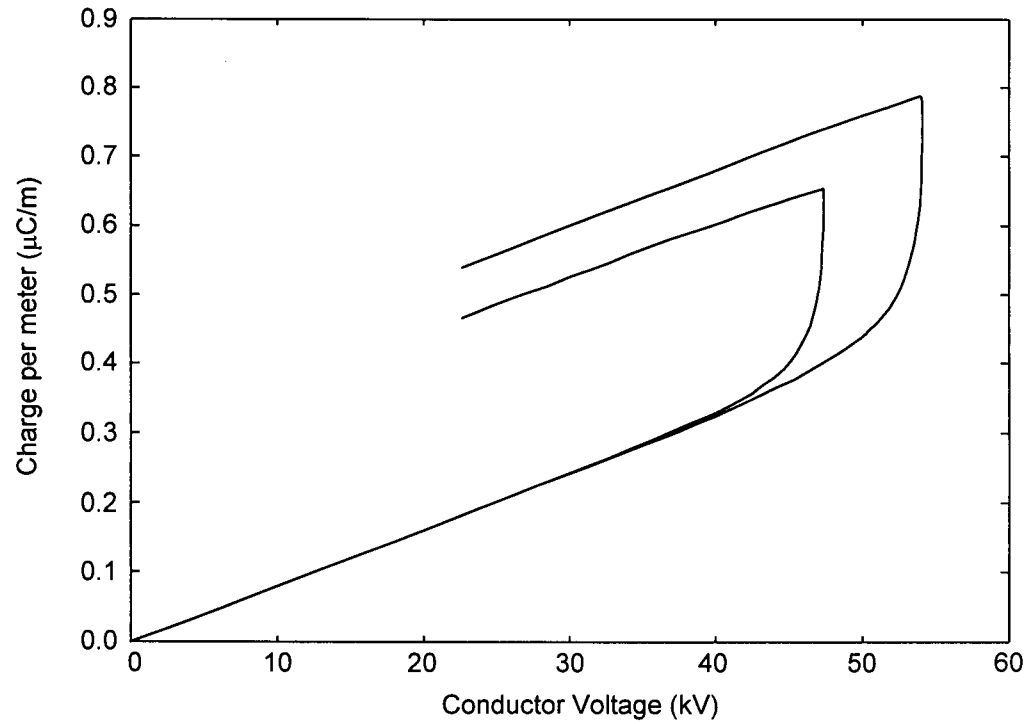

Figure 2.18. Model-derived q-v curves for thin conductor (0.65 mm-rise time 0.12 μs)

Comparing the model-derived q-v loops of Figure 2.17 and Figure 2.18 against the field measured curves of Figure 2.7(c) and Figure 2.7(d), the following general observations can be extracted:

1. The rise portion corresponding to the dynamic capacitance of the model-derived q-v curves follows very well the shape of the experimental results for different type of surges.
2. The increase of onset voltage E_{cor} for faster surges is realized in the proposed circuit by a constant value of DC source voltage, E'_o. This property is clearly observed in Figure 2.18.
3. The proposed circuit can reproduce the negative slopes observed at the tip of the loops.
4. The complex behaviour of the rise portion of the measured curves is followed closely by the proposed model with a constant set of parameters.
5. The descending part of the simulated q-v curves does not fit too well the measured ones. The changing slope in this section of the loops is not reproduced well by the proposed model.

In general, the proposed corona model matches very closely the main characteristics of the q-v curves for a wide range of fast and slow surges, with a constant set of circuit parameters [19].

2.3.2. Simulation of Surge Propagation

A set of simulations were performed for the propagation of voltage surges along a transmission line. In order to test the proposed model using standard EMTP components, the line was subdivided into short segments, with the corona model connected between them. In the case of surges with rise times in the range of lightning, a segment length of 50 m is normally considered adequate [3]. The transmission line part of the line segment was represented using the distributed parameters line model. Since the corona model already includes the geometric capacitance of the line, and since this capacitance is also included in the distributed parameters line model, it is necessary to connect at each corona section a negative capacitance of the same magnitude, in order not to count it twice. This part of the modelling has been previously suggested in [19, 36, 40, 42, 43]. Figure 2.19 shows the general scheme of one section of the modelled transmission line.

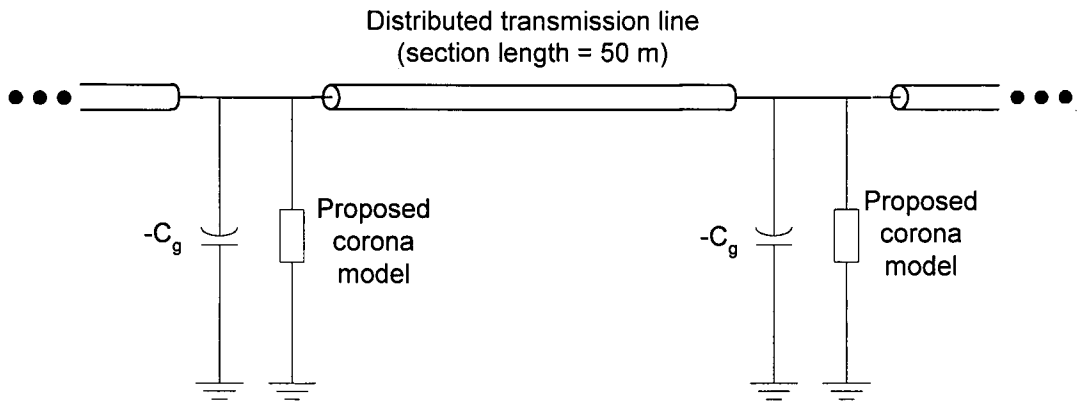

Figure 2.19. Transmission line simulation.

To test the dynamic behaviour of the proposed corona circuit and its ability to simulate a measured case of surge propagation, an equivalent circuit was set up to duplicate the

results reported in [12] for the Tidd line. The data for this experimental case is shown in Table 2.3.

Conductor type	ACSR 2.35 cm diameter
Average conductor height	18.9 m
Applied impulse voltage	1650 kV peak, 0.7 μs rise time
Points of voltage measur.	0, 0.62, 1.28 and 2.22 km
Load impedance	484 Ω
Total length	2.5 km

Table 2.3. Transmission line data for Tidd line case [12].

The parameters of the corona model (with the exception of the air capacitances which were calculated directly) were found through the iterative fitting process explained earlier in this chapter and the obtained values for a 50 m section are listed in Table 2.4. For the simulation of the Tidd line the piecewise linear resistance R_g has only one value given that the main interest of the simulation is on the rise of the surge.

CIRCUIT PARAMETER	PARAMETER VALUE
C_{a1}	0.81 nF
C_{a2}	0.6 nF
C_{cor}	1.5 nF
L_h	0.04 mH
R_h	150 Ω
R_g	1.8 MΩ
E_o	110 kV

Table 2.4. Corona circuit model parameters for the Tidd line case.

A comparison of the simulated and measured results is shown in Figure 2.20. This figure presents the applied voltage at one end of the line and three voltage measurements

along the transmission line. The following general observations can be made based on the experimental results:

1. The surge's amplitude decreases as the surge travels.
2. The apparent onset voltage decreases as the surge travels.
3. The steepness of the surge decreases as the surge travels.

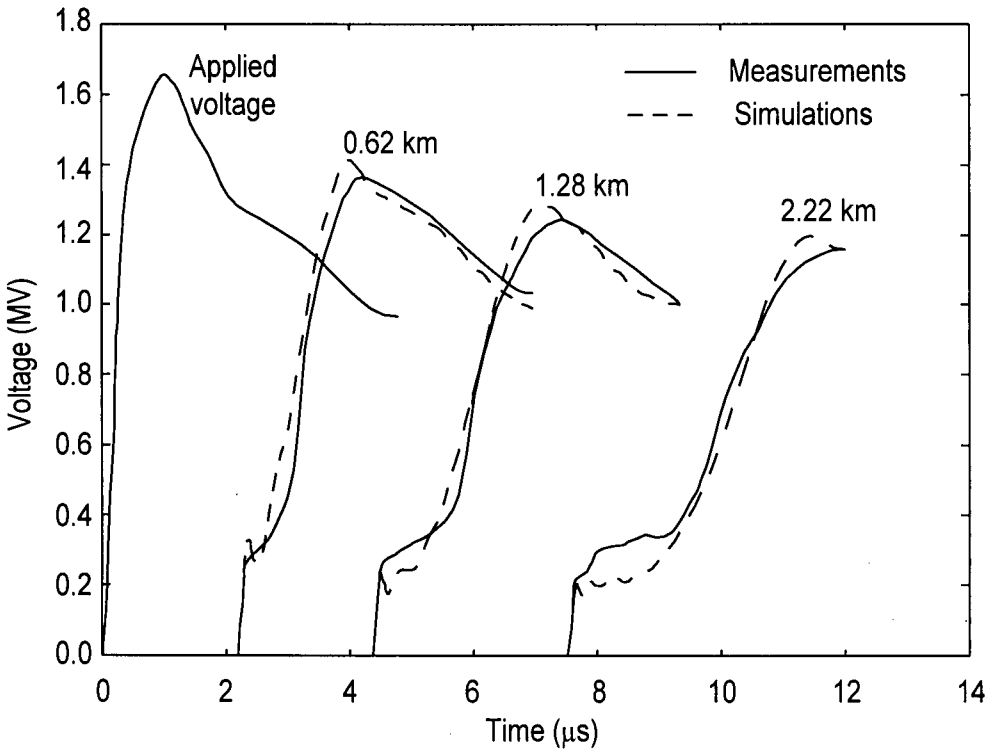

Figure 2.20. Simulation and experimental results for a travelling surge.

Comparing the simulation and test results, it is seen that the proposed model is capable of following very well the changes in magnitude, apparent corona onset voltage, and steepness of the surge as it travels along the transmission line. This very good agreement is noticeable even for distances as long as 2.2 km from the surge injection point. This agreement was obtained despite the possible accumulated error of cascading more than

forty line and corona sections in the EMTP model. Another limitation of this simulation was the use of a constant-parameter line model, as opposed to a frequency-dependent line model. The constant-parameter line model was calculated at 60 Hz. Better results could be obtained if a frequency-dependent line model were to be used [61, 62]. Existing frequency dependent line models, such as fd-line, however, require very large amounts of computer memory and calculations for the representation of the large number of sections used in this type of simulation. A full frequency-dependent transmission line model more suited for this type of studies (the z-line model) is developed in the second part of this thesis.

The simulated results present small oscillations around the apparent onset value of corona, which do not appear in the measured ones. These oscillations can be explained in the circuit by the dynamics of the corona inception branch C_{cor}-L_h-R_h in Figure 2.10. Some results presented in the literature [12, 15] for other voltages and conductors have shown similar oscillations, but at this point, we do not have a definitive conclusion about the reason for this behaviour.

The results obtained with the proposed model can be also compared with results obtained for simulations with other corona models shown in [3] for the Tidd line measurements. These comparisons are shown in Figure 2.21 which shows waveforms at the relatively far away measuring point of 1.28 km for the Tidd line field test described earlier. Figure 2.21 shows that the proposed model matches much more closely this field measurements than the previous models.

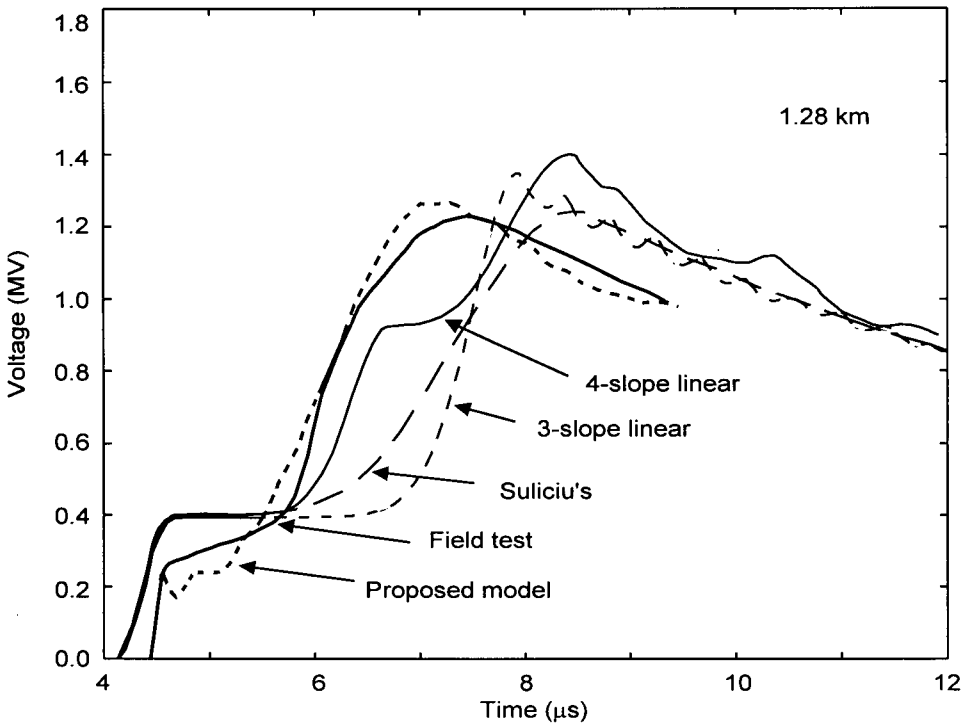

Figure 2.21. Comparison between analytical methods and the proposed model.

2.4. Summary

The first part of this thesis proposes a corona model that can closely match, with a constant set of circuit parameters, the q-v characteristics of a wide range of fast and slow surges. Conventional models require different sets of parameters for different waveshapes. The proposed model achieves the required wide frequency response with a single set of parameters closely matching the topology of the circuit model to the topology of the actual physical system of conductors, and by using a circuit model with a second-order dynamic response. To summarize, some of the highlights and conclusions of this work are as follows:

1. To our knowledge, this is the first time in the reported literature that an equivalent circuit model can represent a wide range of fast and slow surges of different voltage magnitude with a single set of circuit parameters.

2. The proposed model is capable of simulating the apparent increase in the corona inception voltage for faster surges without changing the value of the DC voltage source E'_o in the equivalent circuit.

3. Due to its second-order dynamic characteristics, the model can also reproduce the negative slope at the upper tip of the q-v loop with normal positive values for the circuit parameters.

4. The q-v response of the model matches very closely the experimentally measured q-v response of the conductors in the ascending branch of the loop for a wide range of fast and slow surges. This region includes the statistical time lag needed to initiate the electron avalanche process.

5. The results obtained with the proposed model are not totally satisfactory in the representation of the descending branch of the q-v loops and further research is needed to better model this region. This region, however, is less critical in overvoltage studies.

6. The dynamic characteristics of the model allow it to represent the unusual behaviour of the q-v curves measured for thin conductors.

7. Previous dynamic models, such as Suliciu's, are not directly realizable with simple circuit elements and require the solution of a system of differential equations to achieve a dynamic adaptation of the model to the changing q-v characteristc. The proposed model is much simpler than Suliciu's and is based on standard circuit components available in the EMTP, making it very easy to implement in any EMTP-type program.

8. The simulation of travelling surges for the Tidd line case shows that the proposed model can match the general behaviour of the phenomenon considerably better than previously published comparisons. The Tidd line test, however, has a number of uncertainties regarding the accuracy of the data and of the measurements. A more thorough assessment of the proposed model in terms of surge propagation would probably require a fresh set of experiments with well-known line data and more accurate measurements.

9. The values of the parameters for the proposed model can be calculated from a set of measured q-v curves measured in a cage setup and can be used for a general overhead line configuration. This is a very important and novel quality of the proposed model. Previous models required complicated (and not exact) data conversions according to the particular line configuration.

The main obstacle encountered in developing the proposed model was the lack of more measurements. The q-v curves alone do not contain information on the evolution in time of the corona effect and the time constants related to the physical phenomenon cannot be evaluated directly. This could be improved by evaluating the total current flowing through the cage, which could be obtained by differentiating the total charge or substituting the measuring capacitor C_m (in the cage setup) by a resistance.

The second part of this thesis develops a full frequency dependent transmission line model that is appropriate, in terms of simulation times and memory requirements, for inclusion of corona branches. Even though originally aimed at providing support for corona modelling, the developed new line model is very efficient, and numerically stable, and is

fully adequate as a stand-alone general purpose line model, even when corona is not included.

3. CHAPTER 3

MULTIPHASE TRANSMISSION LINE MODELLING

3.1. Transmission Line Modelling and Literature Review

The differential equations for a distributed parameter transmission line are

$$-\frac{\partial v}{\partial x} = Ri + L\frac{\partial i}{\partial t}$$
$$-\frac{\partial i}{\partial x} = Gv + C\frac{\partial v}{\partial t} \qquad (3\text{-}1)$$

where R, L and G, C are, respectively, the series and shunt parameters of the line.

If the solution to the above equations is to be found when the line is subjected to overvoltages, allowance must be made for the fact that the series parameters R, L are dependent on the frequency and the shunt parameter C is affected by corona. Under these circumstances, the equations become time-dependent and nonlinear and can only be solved numerically. Their solution requires discretization in both time and space.

Such a solution, which combines both discretizations, can be implemented in programs such as the EMTP, which contain frequency-dependent line models and solve the resulting system of equations at discrete time steps [5] one step at the time. Space discretization can be introduced by considering the line divided in sections of suitable length, connected in cascade. In this approach, at every node or point of interconnection between sections, a

shunt branch is added to represent the nonlinear corona effect, and the rest of the line section can be treated using standard linear techniques.

Some authors [11, 17, 23, 24] have adopted a simple model in which the line is composed of very small (3 to 8 m long) lossless sections, thus enabling each section to be dealt with as a lumped parameter circuit. This approach neglects the losses associated with the conductors and ground return and which represent an important factor in the attenuation of the surge. But even if the losses were included in each section, the small length of the sections used in this approach makes it practical only for very short lines as the number of sections (and variables) considerably increases for normal line lengths.

Instead of using very small lumped lengths to introduce space discretization and to include corona, other authors have chosen a hybrid approach of lumped/distributed combinations. This approach presents the following characteristics:

- It treats each section as a linear distributed-parameter transmission line.
- Models corona as lumped between sections.
- It is easy to interface with existing EMTP-type programs.
- Frequency dependence of the line parameters can be introduced using a number of techniques.
- Fewer number of sections and computer operations are required.

The technique used to introduce the corona effect in the line modelling depends on the way the corona itself is modelled. Lumped circuit models of corona are very

straightforward to interface, the only requirement being that the elements of the selected circuit can be represented as external components and connected to each interconnecting node. This approach has been adopted by several authors [6, 22, 23, 3, 43]. A disadvantage of the approach is the increase in computer memory requirements and the numerical problems that may arise from wave reflections at the junctions.

When the corona model is based on mathematical relations such as in piecewise linear representations or in space charge models, different procedures have been used. For example, Lee [31] rewrote the line equations as:

$$-\frac{\partial v}{\partial x} = L\frac{\partial i}{\partial t}$$

$$-\frac{\partial i}{\partial x} = C\frac{\partial v}{\partial t} + C_{dyn}\frac{\partial v}{\partial t} + (vi_r)v \qquad (3\text{-}2)$$

where C_{dyn} and vi_r are functions of the radius and height above ground of the conductor, the corona onset voltage, the instantaneous voltage and some "corona loss constants". The above equations can then solved by the compensation method (Thevenin Equivalent) and have been incorporated in a special version of the EMTP.

Gary et al [30] expand the above equations including losses and frequency dependence. They express the transmission line equations as:

$$-\frac{\partial v}{\partial x} = l_o\frac{\partial i}{\partial t} + \frac{\partial}{\partial t}\int_0^t r(t-t')i(x,t')dt'$$

$$-\frac{\partial i}{\partial x} = C_{dyn}\frac{\partial v}{\partial t} + qv \qquad (3\text{-}3)$$

where C_{dyn} is the dynamic corona capacitance and where the convolution term enables frequency dependence of the parameters to be accounted for. After some manipulations, these equations are discretized using finite-difference techniques and solved in the time domain.

A similar solution technique is presented by Naredo [54]. Naredo represents the transmission line by a system of first order quasilinear partial differential equations, which are solved on a characteristic system of coordinates by applying interpolation techniques. Additionaly, the transmission line equations incorporate the corona model proposed by Gary et al [16]. Although the results obtained with finite-difference solution techniques are very reliable, their integration into time-domain solutions, such as the EMTP, is difficult and they are not use in this thesis.

Semlyen and W.G. Huang [42, 43] presented one of the few models available for three-phase transmission lines. Their model divides the transmission line into segments, each with a small travel delay, a lumped longitudinal block for the modelling of frequency dependence, and a lumped transversal model for the nonlinear effect of corona. The computations are performed in the modal domain for the longitudinal phenomena and in the phase domain for the transversal branches which include corona in each phase. The corona phenomenon is modeled with a simplified space-charge model. The travel delay effectively decouples the nodes and the calculations for the corona branches, thus permitting the representation of each line segment by Norton equivalents at each end. This model can then be easily included into an EMTP-type program.

Semlyen and Huang's model shows good results. However, some of its shortcomings are: first, the use of a relatively simple corona model which does not allow for a more complete description of the corona phenomenon. The use of a space-charge corona description imposes a heavy cost in terms of computer time and memory, making it difficult to add other particle processes. Second, the use of modal decomposition introduces the errors associated with a constant modal transformation matrix [53, 60].

Guillier et al [50] presented a three-phase model where the current injected at one of the line conductors is divided into a number of samples. The corona effect is considered linear per section from the moment the onset voltage is reached. Therefore for each sample k of the current wave there corresponds a capacitive coupling matrix and a conductance matrix. The system is solved by decomposing each sample k into a Fourier series and superimposing, for a given point in the line, the modal components of the Fourier series. Finally the solution is converted into the phase domain and a solution in time is obtained. The frequency-domain approach of this solution makes it difficult to interface with time-domain solutions of the electrical network. Additionaly, the corona model is a simple piecewise representation making it difficult to simulate a wide variety of conductors and surges.

As mentioned earlier, the most generic and common way of solving the transmission line equations including the corona effect is using space discretization. Carneiro et al [61, 62, 63] have developed efficient recursive schemes to implement this technique in the EMTP program using the frequency-dependent transmission line model (fd-line) to include the frequency dependence of the line parameters. Although the fd-line model is a good

model, it is not the best suited for use in conjunction with space discretization. The fd-line model uses rational functions to fit the line propagation function [$\mathbf{e}^{-\gamma(\omega)x}$] and the characteristic impedance [$\mathbf{Y}_c(\omega)$]. In the case of space discretization each line segment uses a relatively large number of poles and zeros in the rational function approximations and the total amount of calculations increases tremendously.

Additionally, fd-line and most of the current transmission line models manifest problems associated with the transformation matrices used to connect the modal (mathematical) domain to the phase (physical) domain. These line models consider these transformation matrices to be constant when in reality they are frequency-dependent. This makes these models inaccurate for asymmetrical configurations. This shortcoming has been addressed by researchers from different directions with a number of new models [53, 56, 57, 58, 59, 60], which suggests that the state of the art in full frequency dependent line and cable modelling is improving.

3.2. Proposed Transmission Line Model

The initial motivation for the proposed new line model is that space discretization (instead of the traditional time discretization) would allow the (nonlinear) corona model developed in the first part of this thesis to be used in conjunction with an efficient full frequency dependent model. Mathematically, space discretization instead of time discretization can be used to synthesize the modelling of the propagation matrix [$\mathbf{e}^{-\gamma(\omega)x}$] in the line equations. Physically, at each space-discretized section the wave distortion due to the resistance and internal inductance of the line conductors and ground can be grouped into

one (frequency-dependent) lumped impedance matrix in phase coordinates [$\mathbf{Z}^{loss}(\omega)$], while the ideal wave propagation (at the speed of light) in the medium due to the external magnetic field [$\mathbf{L}^{ext}$] and capacitance [**C**] can be represented by an ideal-line segment. Since for ideal propagation all modes travel at the same speed (speed of light), the equations for this part of the model can be formulated directly in phase coordinates without concern for mixed-up travelling times as in the lossy case. This separation between the ideal section and the losses defines a very clean cut in the model between the parameters that are frequency dependent and those that are constant and dependent only on the geometry of the line configuration.

Basic Transmission Line Theory

The modelling of transmission lines is based on the travelling wave equations, which can be expressed, for a given frequency ω as

$$\frac{d^2\mathbf{V}}{dx^2} = [\mathbf{ZY}]\mathbf{V}$$
$$\frac{d^2\mathbf{I}}{dx^2} = [\mathbf{YZ}]\mathbf{I}, \tag{3-4}$$

where [**ZY**] and [**YZ**] are full matrices that couple the propagation of voltage and current waves in all phases. The series impedance matrix [**Z**] is a full matrix with elements of the form

$$Z_{ij} = R_{ij} + j\omega(L_{ij}^{ext} + \Delta L_{ij}), \tag{3-5}$$

here R_{ij} contains the resistance of the conductor and the effect of the common ground return for the self terms ($i = j$) and contains the effect of the ground return for the mutual

terms ($i \neq j$), ω is the frequency, L_{ij}^{ext} is the inductance related to the external flux outside the conductors and ground, and ΔL_{ij} is the inductance related to the internal flux inside the conductors and ground return. Matrix [**Z**] can thus be rewritten as

$$[\mathbf{Z}]=[\mathbf{Z}^{loss}]+j\omega[\mathbf{L}^{ext}],$$

$$[\mathbf{Z}]=[\mathbf{Z}^{loss}]+[\mathbf{Z}^{ext}], \tag{3-6}$$

$$\text{with } Z_{ij}^{loss}=R_{ij}+j\omega\Delta L_{ij}$$

The shunt admittance matrix [**Y**] can be written (assuming conductance $G \approx 0$) as

$$[\mathbf{Y}]=j\omega[\mathbf{C}], \text{ with } [\mathbf{C}]=[\mathbf{P}]^{-1}, \tag{3-7}$$

where [**P**] is the Maxwell coefficients matrix. For up to about 1 Mhz frequencies, the [**Y**] matrix does not require any correction for ground return and its elements depend only on the external capacitances (geometry) of the system. With equations (3-6) and (3-7), [**YZ**] can be written as

$$\begin{aligned}[\mathbf{YZ}]&=j\omega[\mathbf{C}]([\mathbf{Z}^{loss}]+j\omega[\mathbf{L}^{ext}]),\\ [\mathbf{YZ}]&=j\omega[\mathbf{C}][\mathbf{Z}^{loss}]-\omega^2[\mathbf{C}][\mathbf{L}^{ext}].\end{aligned} \tag{3-8}$$

Equation (3-8) shows how the product [**YZ**] can be expressed as the combination of two main components: the first one related to the internal losses and ground effect corrections and the second one related to the ideal propagation in the external field. Additionally, the second term representing the ideal propagation can be expressed as

$$[\mathbf{C}][\mathbf{L}^{ext}]=\mu_o\varepsilon_o[\mathbf{I}]=\frac{1}{c_o^2}[\mathbf{I}] \tag{3-9}$$

where μ_o is the permeability of free space, ε_o is the permittivity of free space, c_o is the speed of light and [**I**] is the identity matrix.

The elements of $[\mathbf{Z}^{loss}(\omega)]$ are frequency dependent due to the skin effect. However, neglecting the proximity effect, they are very little affected by the geometry of the system of conductors. In the space-discretized model, $[\mathbf{Z}^{loss}(\omega)]$ is represented as lumped and its elements are synthesized in phase coordinates as frequency-dependent functions. These functions are very well-behaved and simpler to synthesize (fewer poles needed) than $[\mathbf{e}^{-\gamma(\omega)x}]$ and $[\mathbf{Y}_c(\omega)]$ in the traditional time-discretized models [4].

The line parameters associated with the external magnetic and electric fields $[\mathbf{L}^{ext}]$ and [**C**] (second term in equation 3-8) depend only on the line geometry and are, therefore, constant and independent of frequency. This part of the model corresponds to the ideal line component of the discretized space segment. Since in the ideal line segment all modes travel at the speed of light and there is a single time delay, the model for this part of the circuit is identical to the model for a single-phase ideal line, just replacing single voltages and currents by vectors. Since the model is exact for this ideal line, any arbitrarily asymmetrical configuration of conductors is exactly represented without the need for frequency dependent transformation matrices.

If we assume that, overall, the effect of considering the losses as lumped versus distributed in each discrete-length segment is of second order as compared to being able to model propagation in the ideal line segment exactly the circuit model shown in Figure 3.1

can be postulated. This assumption is met, for a given frequency, when the length of the section is "small" compared with the wavelength of the propagating waves.

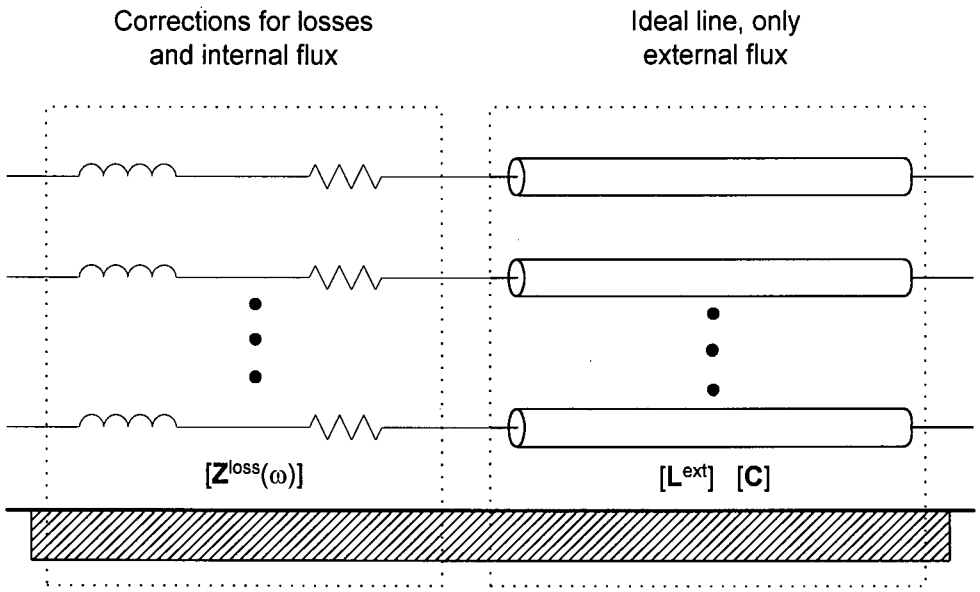

Figure 3.1. Separation of basic effects in the Z-line model.

The line-parameters matrices $[\mathbf{Z}^{loss}(\omega)]$ in the line must be evaluated for a wide range of frequencies and, then, processed to generate the components of the model. This has been accomplished introducing modifications to the EMTP line-constants program which calculates the electrical line parameters based on the geometry and physical properties of the conductors.

3.3. Phase-Domain Modelling of the Ideal Line Section

Once the impedance corrections ($[\mathbf{Z}^{loss}(\omega)]$) are extracted from the total transmission line parameters, the solution in the time domain for the multiphase ideal line section can be formulated directly in phase coordinates. Since the travelling time τ is the same for all the modes, Dommel's lossless line equation [2] for the time-domain single-phase case can be

used directly for the multiphase ideal line case. This is illustrated in Figure 3.2, where the current and voltage variables are now vectors and the impedances are matrices. From the circuit, the terminal voltage vectors $\mathbf{v}_k(t)$ and $\mathbf{v}_m(t)$ can be expressed as functions of the terminal current vectors $\mathbf{i}_k(t)$ and $\mathbf{i}_m(t)$, the characteristic impedance matrix $[\mathbf{Z}_c]$, and the history source vectors $\mathbf{e}_{kh}(t)$ and $\mathbf{e}_{mh}(t)$. The history source vectors are calculated at each time step as functions of past values, through the expressions

$$\begin{aligned} \mathbf{e}_{kh}(t) &= \mathbf{v}_m(t-\tau) + [\mathbf{Z}_c]\mathbf{i}_m(t-\tau), \\ \mathbf{e}_{mh}(t) &= \mathbf{v}_k(t-\tau) + [\mathbf{Z}_c]\mathbf{i}_k(t-\tau), \\ \text{with } [\mathbf{Z}_c] &= [\mathbf{Y}]^{-1}\{[\mathbf{Y}][\mathbf{Z}^{ext}]\}^{1/2} \end{aligned} \tag{3-10}$$

In this case, the characteristic impedance matrix $[\mathbf{Z}_c]$ represents the coupled system in the phase domain and is a full matrix but it can be easily calculated as

$$[\mathbf{Z}_c] = \frac{1}{j\omega}[\mathbf{P}]\, j\frac{\omega}{c_o}[\mathbf{I}] = \frac{1}{c_o}[\mathbf{P}] \tag{3-11}$$

with $[\mathbf{P}]$ the matrix of Maxwell coefficients, making $[\mathbf{Z}_c]$ a unique constant matrix for the given line geometry. This characteristic impedance matrix $[\mathbf{Z}_c]$ is calculated by the modified EMTP line-constants mentioned in the previous section.

As in the case of the single-phase lossless line model if the integration step Δt of the time domain solution is an exact multiple of the travelling time τ, then the multiphase ideal line model is independent of the integration rule, and represents an exact solution of the line equations. Notice that this is not possible to achieve in traditional multiphase models because different propagation modes have different travelling times. In that case there is an

interpolation process required in the history vectors which limits the accuracy of the model and forces Δt to be many times smaller than τ. In the present case of the z-line model Δt can be as large as the τ of the section and still have an exact solution.

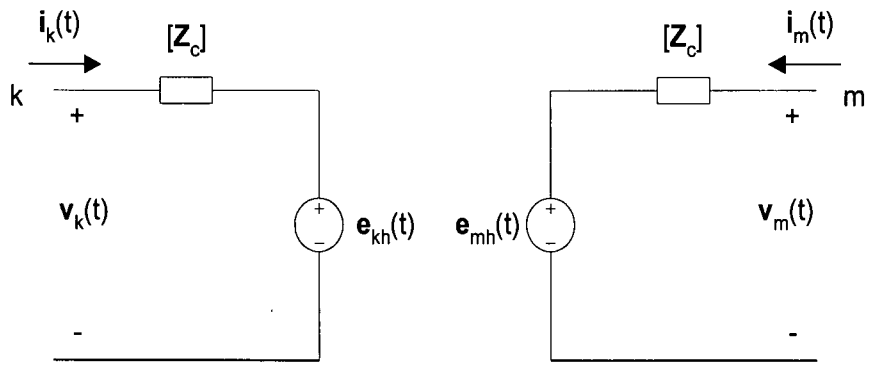

Figure 3.2. Multiphase ideal transmission line model in the time domain.

3.4. Phase-Domain Modelling of the Frequency-Dependent Lumped Loss Section

Theoretically, the solution in the time domain of frequency-dependent functions can be obtained through numerical convolution integrals. These numerical convolutions can be avoided if the frequency-dependent functions can be first synthesized with rational functions. In this case very efficient discrete-time recursive techniques can be applied [4, 5, 65]. These recursive techniques are used in the present fd-line model in the EMTP and have proved to be excellent tools.

The elements of the matrix $[\mathbf{Z}^{loss}(\omega)]$ are in general frequency-dependent functions. In principle, an accurate modelling of $[\mathbf{Z}^{loss}(\omega)]$ could be achieved by fitting each element of the matrix with a rational function approximation (similarly to the methodology used for the modal-domain EMTP frequency-dependent line models [4, 45]). Mathematically, however, one has to be very careful when synthesizing coupled systems (as opposed to

modal-domain decoupled systems). During the development of this thesis a number of examples were found where fitting each element of $[\mathbf{Z}^{loss}(\omega)]$ independently with stable poles (and using very accurate procedures) produced unstable solutions in the time responses.

From network synthesis theory, there are a number of conditions regarding the relationship among poles and zeros of the elements of a system's matrix that need to be met to assure the stability of the resulting synthesis [51]. In general, these conditions will not be met if each element of the matrix is synthesized independently of the other elements. A new synthesis procedure was implemented in this work that achieves a simultaneous or coordinated synthesis of all elements of the matrix together and maintains realizability and stability of the matrix at all frequencies. This procedure is general and can be used not only for the present $[\mathbf{Z}^{loss}(\omega)]$ synthesis but also for other cases of frequency-dependent coupled systems, such as, transformers, generators, motors, coupled loads, etc.

The synthesis functions used in the proposed z-line model have the following form:

- The basic fitting block is the first-order function $\frac{sK}{(s+p)}$ (where $s=j\omega$). This function corresponds to a parallel *R-L* block in the continuous time domain.
- Each element of $[\mathbf{Z}^{loss}(\omega)]$ is expressed as a sum of several of these blocks (total number of blocks = m), plus an additional resistance term, R_{iio}, in the diagonal elements to satisfy the dc condition ($R_{iio} = R_{ii}$ @ dc). With subscript f indicating "fitted" function we have:

$$Z_{fii}^{loss}(\omega) = R_{ioo} + \sum_{l=1}^{m} \frac{sK_{ii(l)}}{s + p_{ii(l)}} \quad \text{Diagonal elements} \tag{3-12}$$

$$Z_{fij}^{loss}(\omega) = \sum_{l=1}^{m} \frac{sK_{ij(l)}}{s + p_{ij(l)}} \quad \text{Off - diagonal elements} \tag{3-13}$$

- The same number of blocks (m) is used for each one of the elements in the $[\mathbf{Z}_f^{loss}(\omega)]$ matrix.

The concept of coordinated fitting is realized as follows. Assume a particular frequency ω_1. Constants $K_{ii(1)}$, $K_{ij(1)}$, and poles $p_{ii(1)}$, $p_{ij(1)}$ in (3-12) and (3-13) are calculated for each entry of the matrix $[\mathbf{Z}_f^{loss}(\omega)]$ to exactly match the transmission line data at this frequency $[\mathbf{Z}^{loss}(\omega_1)]$. This gives the first *R-L* block for each element of the matrix. The procedure is now repeated for the next frequency ω_2. A second set of matching of *R-L* blocks in (3-12) and (3-13) is obtained which is independent of the previous set. The procedure is then repeated for m frequency points to obtain m matching sets of first-order blocks. The addition of the m different *L-R* blocks for each element of $[\mathbf{Z}_f^{loss}(\omega)]$ results in the total expressions shown in equations (3-12) and (3-13). Notice that the equivalent impedance network $[\mathbf{Z}_f^{loss}(\omega)]$ resulting from this procedure can be interpreted as m impedance matrices, each of order one, connected in series.

Once a synthesis network is obtained with the procedure outlined above, a second pass of fitting optimization is performed using a linear least square technique. The procedure minimizes the error between the real part of each function in $[\mathbf{Z}_f^{loss}(\omega)]$ and the corresponding original one of $[\mathbf{Z}^{loss}(\omega)]$. Since the original functions $[\mathbf{Z}^{loss}(\omega)]$ are minimum phase, fitting any one complex coordinate (real part, imaginary part, magnitude or angle)

assures that the approximated function will fit the original function on both of its complex coordinates. The optimization routine minimizes the error by adjusting the values of the constants $K_{ij(m)}$ in equations (3-12) and (3-13). This optimization procedure operates on the real part of the functions in order to enable the use of linear iterative techniques. Non-linear iterative techniques would be needed to fit, for example, the magnitude function. This would increase the calculation process and introduce possible convergence problems.

Finally, the fitting procedure delivers the approximated functions $[\mathbf{Z}_f^{loss}(\omega)]$. Figure 3.3 and Figure 3.4 show some typical fitting curves calculated with 9 *R-L* blocks, as well as the original data from $[\mathbf{Z}^{loss}(\omega)]$. The approximated curves basically superimpose the original data. By experience, the average number of blocks needed for a close fit is about one block per decade of frequency, making the total number of blocks usually less than ten. However, still very good approximations can be obtained with only 5 blocks or less.

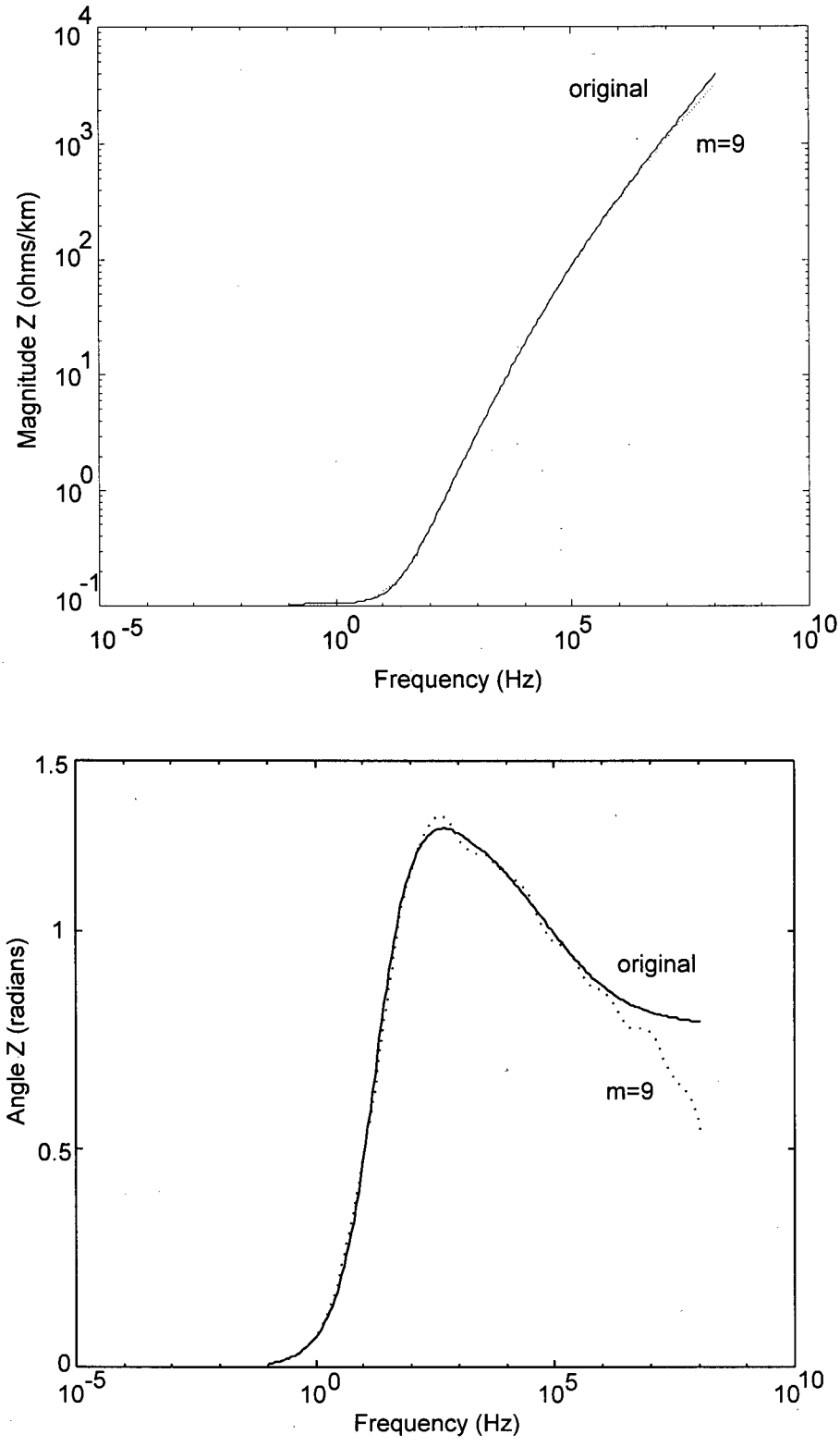

Figure 3.3. Typical [$\mathbf{Z}^{loss}(\omega)$] diagonal element and fitting functions.

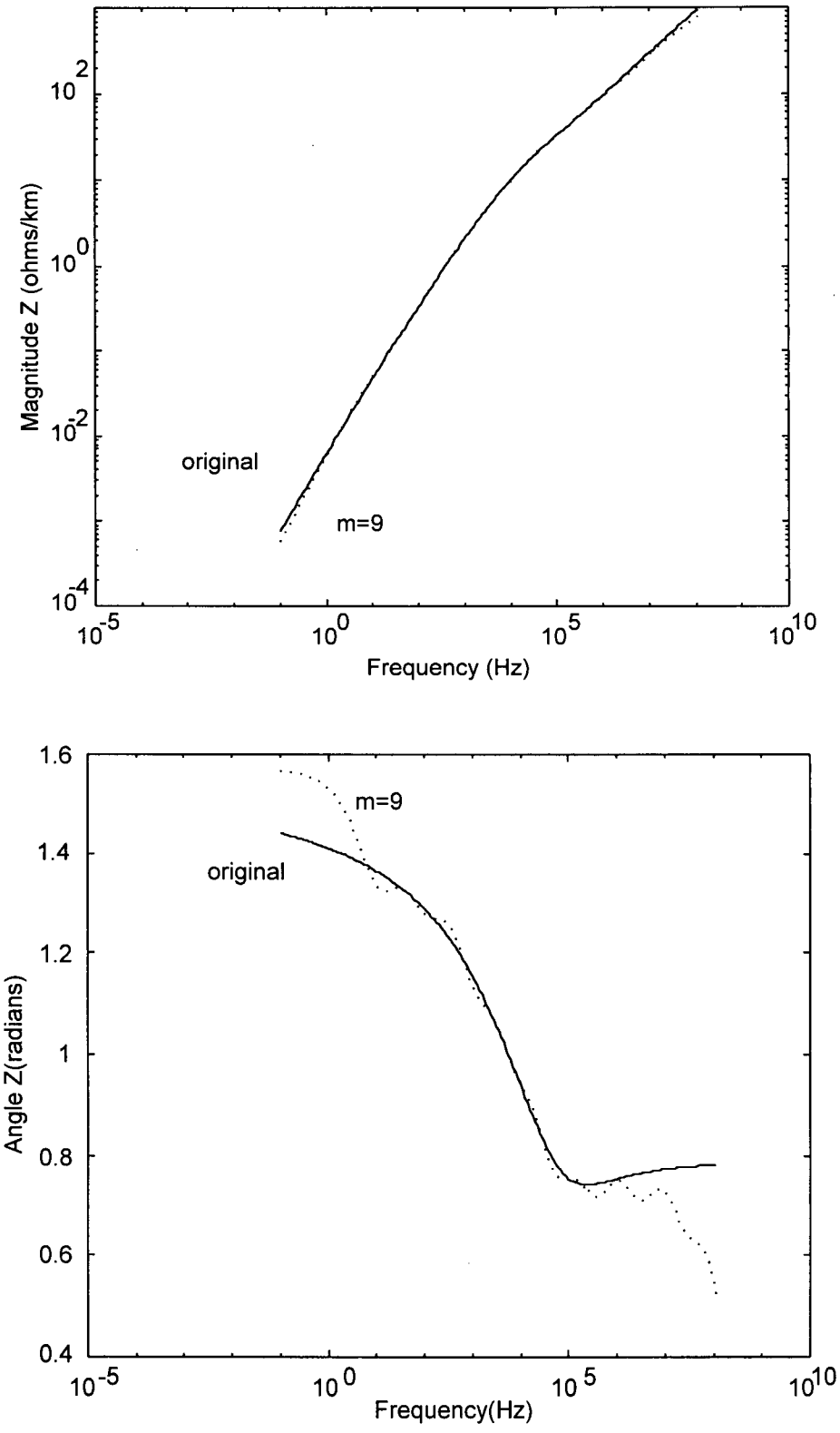

Figure 3.4. Typical [$\mathbf{Z}^{loss}(\omega)$] off-diagonal element and fitting functions.

Numerical Stability

The stability of the approximated set of functions can be studied from the point of view of input-output control theory. In this case the state-variable equation

$$\dot{\mathbf{x}} = [\mathbf{P}] \cdot \mathbf{x} + [\mathbf{B}] \cdot \mathbf{u} \qquad (3\text{-}14)$$

becomes

$$\dot{\mathbf{i}} = -[\mathbf{L}]^{-1} \cdot [\mathbf{R}] \cdot \mathbf{i} + [\mathbf{L}]^{-1} \cdot \mathbf{v} \qquad (3\text{-}15)$$

with **i** the state vector, **v** the input vector and with the companion matrix [**P**] equal to the product $-[\mathbf{L}]^{-1}[\mathbf{R}]$.

In a stable system, the eigenvalues of [**P**] are real and negative and represent (with opposite sign) the time constants of the system. The eigenvalues can be evaluated at different frequencies and their behaviour in the frequency spectrum of interest plotted, such as in Figure 3.5.

This figure compares three of the eigenvalues of the original matrix $[\mathbf{Z}^{loss}(\omega)]$ and its fitted values $[\mathbf{Z}_f^{loss}(\omega)]$ for a double circuit line composed of a flat circuit and a vertical circuit. This case is relatively prone to instability because of its highly asymmetrical configuration and it is reported in more detail in section 3.6.

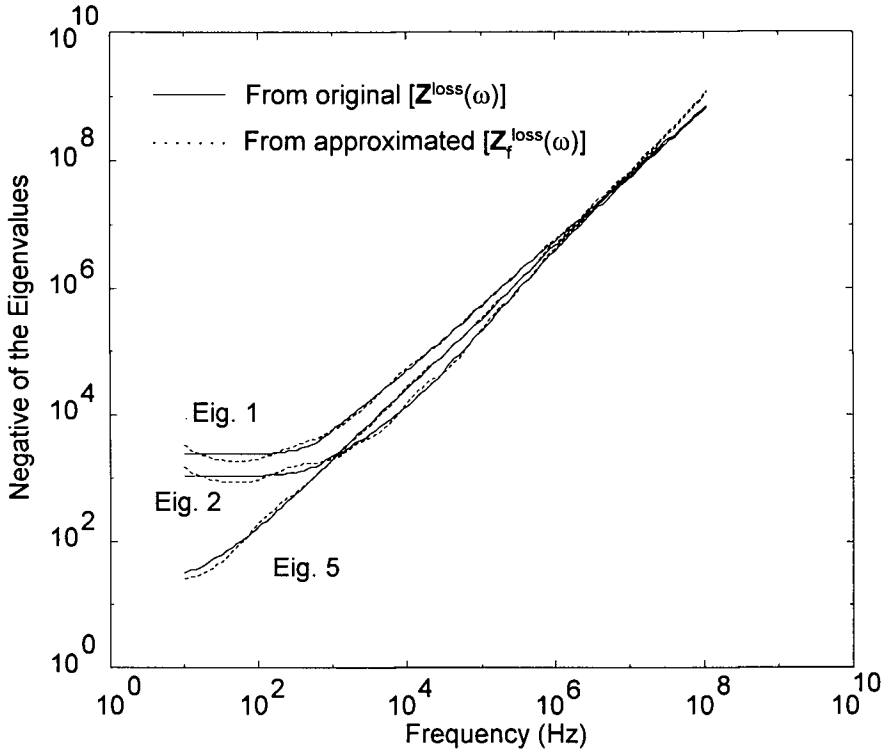

Figure 3.5. Eigenvalues for stability analysis.

As can be observed in Figure 3.5, the eigenvalues of the approximating functions match very closely the eigenvalues of the original functions and are always negative, thus assuring numerical stability. The eigenvalues of the fitting functions match exactly the original ones at the specific frequencies where the *R-L* blocks of the model are calculated.

A minimum realization model can be obtained with only one block (m=1). This is a particular option of the program and corresponds to a single-frequency approximation. In terms of computational efficiency, the model resulting from this option (one parallel *R-L* block per self and mutual term) is equivalent to the constant-parameter line model in the EMTP (one series *R-L* per self and mutual term). As shown in [53], however, the accuracy

of the one-block z-line model is much higher. An equivalent representation of this special case is presented in Appendix A.

Once the $[\mathbf{Z}_f^{loss}(\omega)]$ synthesis functions are obtained, the general system of equations for the voltage-drop across the multiphase lumped-loss component can be formulated in the discrete time domain for a recursive solution using the trapezoidal rule of integration. The general system $\Delta\mathbf{V} = [\mathbf{Z}_f^{loss}(\omega)]\mathbf{I}$ in the frequency domain can be solved in the discrete-time domain as:

$$\Delta\mathbf{V}(t) = [\mathbf{A}]\mathbf{I}(t) + \mathbf{Eh}(t) \tag{3-16}$$

with [**A**] representing the equivalent resistance matrix of the system with elements given by:

$$A_{ii} = R_{iio} + \sum_{l=1}^{m} \frac{\dfrac{2K_{ii(l)}}{\Delta t}}{\dfrac{2}{\Delta t} + p_{ii(l)}} \tag{3-17}$$

and

$$A_{ij} = \sum_{l=1}^{m} \frac{\dfrac{2K_{ij(l)}}{\Delta t}}{\dfrac{2}{\Delta t} + p_{ij(l)}} \quad \text{for } i \neq j \tag{3-18}$$

The equivalent history-source vector **Eh**(t) is given by

$$\mathbf{Eh}_i(t) = \sum_{j=1}^{n}\sum_{l=1}^{m} heq_{ij(l)}(t) \tag{3-19}$$

with n the number of conductors, and

$$heq_{ij(l)}(t) = -\frac{\frac{4K_{ij(l)}p_{ij(l)}}{\Delta t}}{\left(\frac{2}{\Delta t}+p_{ij(l)}\right)^2} I_j(t-\Delta t) + \frac{\frac{2}{\Delta t}-p_{ij(l)}}{\frac{2}{\Delta t}+p_{ij(l)}} heq_{ij(l)}(t-\Delta t) \qquad (3\text{-}20)$$

The system equation (3-16) follows the typical EMTP representation of elements: an equivalent system resistance matrix [**A**], in series with an equivalent history-voltage source **Eh**(t). Notice that for this case the equivalent history voltage source is composed of several history voltage sources connected in series. Each one of these individual history voltage sources corresponds to one of the *R-L* blocks.

3.5. Phase-Domain Transmission Line Solution

The model for a short line section is obtained combining the solution of the ideal line segment and the solution of the $[\mathbf{Z}^{loss}(\omega)]$ network. To combine the lumped $[\mathbf{Z}^{loss}(\omega)]$ model with the distributed ideal-line model, $[\mathbf{Z}^{loss}(\omega)]$ is divided into two halves, and each half is added at the ends of the ideal line segment, as shown in Figure 3.6. The solution for a full transmission line is accomplished by connecting several of the z-line short-section models in cascade. The cascaded sections are ordered in such way that the full matrix of the line is a block-diagonal matrix. The resulting diagonal submatrices are independent of each other due to the decoupling delay introduced by the travelling time in the ideal line sections. Using this technique, the solution of a full line is coded without actually building the total matrix but working at the diagonal submatrices level. Notice that the power network connected at the line ends sees only the first and last line segments during the power system solution. The internal line segments are solved "by themselves" together with a possible shunt branch (e.g., a corona branch) added in-between sections. The entire line solution is

thus computationally very efficient. Indeed, from a computational point of view, the solution of m line sections of z-line (without an external transversal branch) is equivalent to the solution of a one-segment frequency dependent line model when n poles are used to synthesize each element of the propagation function $[e^{-\gamma(\omega)x}]$. The availability of the nodes between sections in the z-line model can be useful in a number of situations, as for example, for measuring the voltage or current profile along the line, connecting ground wires to ground at specific points, and, as indicated previously, for connection of transversal elements to the line, such as corona models.

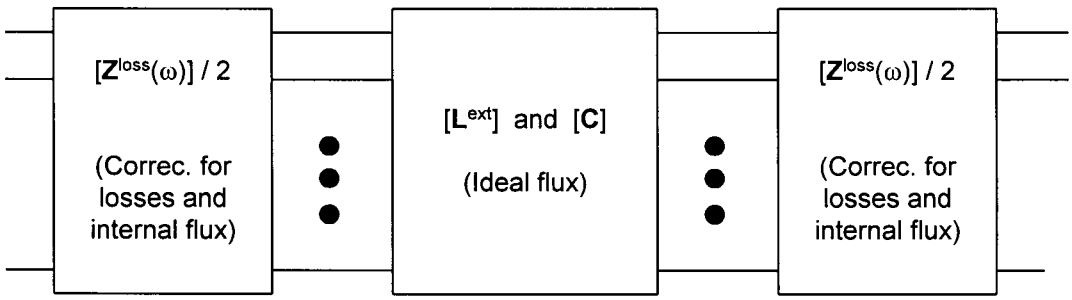

Figure 3.6. Proposed line-section for the z-line model.

In order to asses the effect of lumping the losses, a number of tests were conducted to obtain a relationship between the maximum section length of the model and the maximum frequency of interest in a study. The transmission line used for these tests was a fully balanced three-phase line. The base case is shown in Figure 3.7 and consists of one sinusoidal source attached to node *a* at the sending-end of the line and different resistance terminations at the other sending- and receiving-end nodes. The parameters of the model were calculated at the frequency of the source. The steady-state time domain response of the z-line model was then compared against the solution obtained with the constant-

parameter (cp-line) line model of the EMTP. For a fully balanced line and small Δt, cp-line gives an exact response for a single-frequency simulation. An average error of 3% was allowed in the results. By repeating this process for several frequencies an empirical relationship between the length of the line-section and the frequency of the analysis was established. The results of these tests are shown in Figure 3.8 and can be used as guidelines for other studies.

It is important to note that the section length will determine the largest Δt that can be used in the simulation. The maximum Δt to use for the z-line model corresponds to the travel time τ of the ideal line section. Looking at the graphic of Figure 3.8 it is possible to conclude that the Δt restrictions imposed by the line sectionalization (space discretization) do not differ too much from the ones imposed by the distortion introduced by the integration rule in the time discretization. For example, a maximum distortion of about 3% using the trapezoidal rule to discretize an inductance or capacitance requires a Δt of one tenth or less of the inverse of the maximum frequency of interest in the transient (This follows from the maximum sampling rate $f_{Nyquist} = \frac{1}{2\Delta t}$ and allowing the frequency to reach up to $\frac{1}{5} f_{Nyquist}$ to limit the distortion of the trapezoidal rule to 3%). For a given frequency of interest it is possible then to find the Δt required based on the integration rule distortion and the one based on the z-line space discretization. In general, the time step imposed by the sectionalization is about 50% smaller than the time step required by the trapezoidal integration rule.

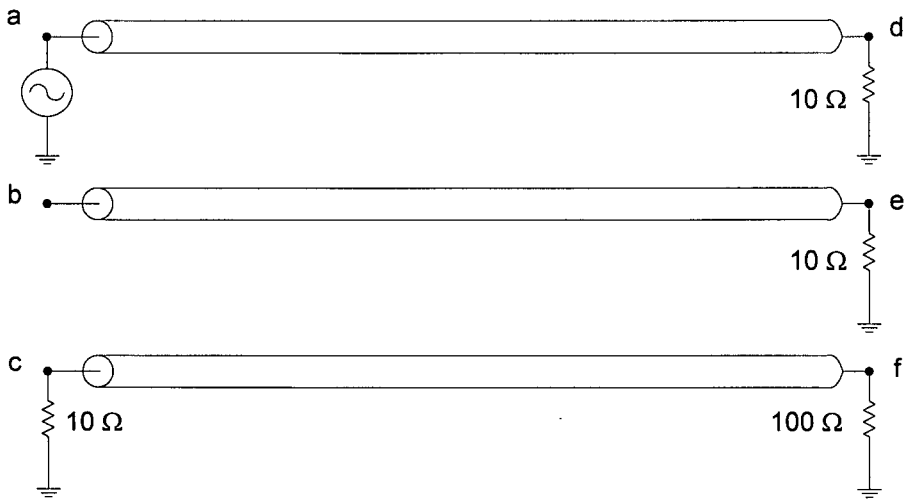

Figure 3.7. Base case for analysis of the z-line model.

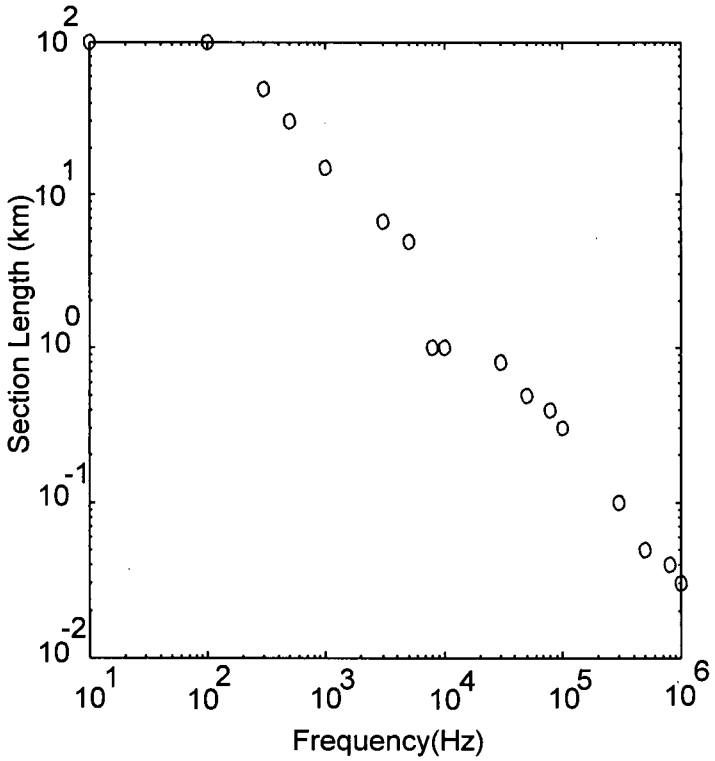

Figure 3.8. Z-line maximum section length vs. maximum frequency of interest.

High-Frequency Truncation

The approximation of $[\mathbf{Z}^{loss}(\omega)]$ by rational functions in the frequency domain and its translation into the discrete time domain introduce some special considerations. Even though the frequency response of the approximating functions $[\mathbf{Z}_f^{loss}(\omega)]$ is practically identical to the original $[\mathbf{Z}^{loss}(\omega)]$, the frequency response considering the effect of the finite Δt is meaningless beyond certain frequencies. This behaviour is due to two factors:

- From the Sampling Theorem in Signal Analysis Theory, the discrete sampling at Δt intervals in the time domain results in a repetition of the spectrum of the signal. For a given Δt, the maximum frequency that can theoretically be represented (and actually exist in the time domain) is $0.5/\Delta t$ (Nyquist frequency).

- In order to transform the rational functions from the frequency domain to the time domain a recursive discretization technique is used. From recursive equation (3-20) it can be observed that the second coefficient becomes negative for poles larger than $2/\Delta t$.

The first of the above factors means that it is wasteful in terms of computational time to have poles beyond the Nyquist frequency of $0.5/\Delta t$. The second factor introduces numerical oscillations (ripples) in the time-domain solution. These oscillations eventually decay and the final answer converges to the correct solution. However, the oscillations can take some time to die out, depending on the Δt, and they can propagate, especially in the case of cascade sections.

Following the analysis above, the fact that the response of the rational functions in the time domain does not have any meaning beyond the Nyquist frequency and that poles higher than $2/\Delta t$ will cause mathematical oscillations suggests that the fitting functions should be truncated to avoid these problems and at the same time save valuable computation time. A truncation procedure has been implemented that is performed just before the transient simulation is started, when the Δt is known. The truncation procedure evaluates the poles of the functions in $[\mathbf{Z}_f^{loss}(\omega)]$ and discards the blocks which poles are beyond the cut-off frequency $2/\Delta t$. To compensate for the distortion introduced by dropping these poles, the last block of the remaining poles is readjusted.

The code for the development and testing of the proposed z-line model was written in a stand-alone program using the ADA-95 object-oriented language. A number of simulations were performed [55, 66] for highly asymmetrical line configurations and system conditions and the results were compared against line models in the EMTP and against the FDTP (Frequency Domain Transients Program [52]).

3.6. Simulations and Validation

Simulation results to validate the proposed z-line model are presented next. The results obtained with z-line are compared with those obtained with the frequency-dependent model (fd-line) in the EMTP and the FDTP. The fd-line model [4] is a full frequency dependent line model but imposes the restriction of using a constant transformation matrix to relate modal domain and phase domain quantities. The FDTP program solves the power network in the frequency domain (using an inverse Fourier transform to obtain the time-domain

waveforms) and, therefore, its accuracy is not affected by issues of frequency dependence of the line parameters or degree of asymmetry of the line configuration.

The transmission line configuration used in the following studies is shown in Figure 3.9. The line is highly asymmetrical given that it is untransposed and composed of a flat and a vertical circuit at some distance from each other. The total length of the circuits is 100 km. The transformation matrix for the fd-line model was calculated at 1200 Hz.

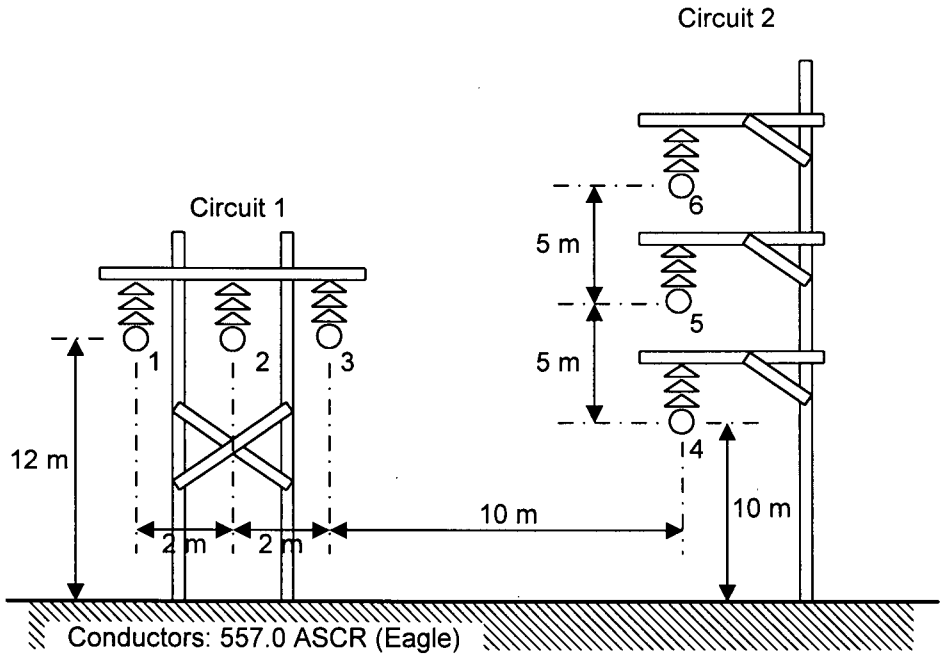

Figure 3.9. Line configuration of the double-circuit case.

The transmission line was modelled with the z-line model using 40 sections of 2.5 km each, for a bandwidth, according to Figure 3.8, of about 8 kHz. The time step Δt of the simulations was chosen as 8.339 μs to match exactly the travelling time of the ideal sections. For the L and C elements of the network (including the L's in $[\mathbf{Z}^{loss}(\omega)]$), a Δt = 8.339 μs gives a bandwidth of about 12 kHz for a distortion of about 3% with the

trapezoidal rule of integration ($f = \frac{1}{5} f_{Nyquist} = \frac{1}{10\Delta t}$). As mentioned before, the sectionalization requirements of the model (number of sections and size of $\Delta t = \tau_{section}$) to achieve a certain bandwidth of accurate modelling are, therefore, not too different from those imposed by the distortion of the integration rule on L and C components: 8 kHz for sectionalization versus 12 kHz for distortion in this case.

Nine *R-L* blocks were used to fit the $[\mathbf{Z}^{loss}(\omega)]$ functions over an extended frequency range. The pole truncation algorithm was then applied to discard those poles close and beyond the Nyquist frequency. This truncation procedure reduced the number of *R-L* blocks used in the transient simulation to only four per function, with no sacrifice in the accuracy of the synthesis. For the case studied the z-line model was about seven times slower in terms of computer time than the fd-line model. In general, experience with a variety of cases indicates that the model is about N to 2N times slower than the fd-line line model, where N is the number of phases of the line (i.e., N=3 for a single-circuit line, N=6 for a double-circuit line, etc.). The current code, however, is development code and, therefore, not yet optimized.

The simulation results presented for the transmission line of Figure 3.9 correspond to the middle phase of the first circuit (phase 2) at the receiving end and all three phases of the second circuit (phases 4, 5 and 6) at the receiving end. The latter ones measure the ability of the model to accurately represent the frequency-dependency of the coupling effect among the different conductors including the important ground return. The main goal was to

observe the voltages induced in the second circuit (vertical one) by the highly asymmetrical coupling with the first circuit (horizontal one).

The results are presented in two time scales: a large scale that permits the observation of the fundamental frequency of the system and a small scale that permits the observation of the transient period. The different curves are marked with the labels: f = fd-line model, w = FDTP and z = z-line model.

3.6.1. Open Circuit Test

For the open circuit test, the configuration shown in Figure 3.10 was used. A three-phase balanced voltage source of 1.0 p.u. was connected at time zero, energizing phases 1, 2 and 3. The receiving end of these phases was left open, while the other phases (4, 5 and 6) were grounded at both ends through 10 Ω resistances.

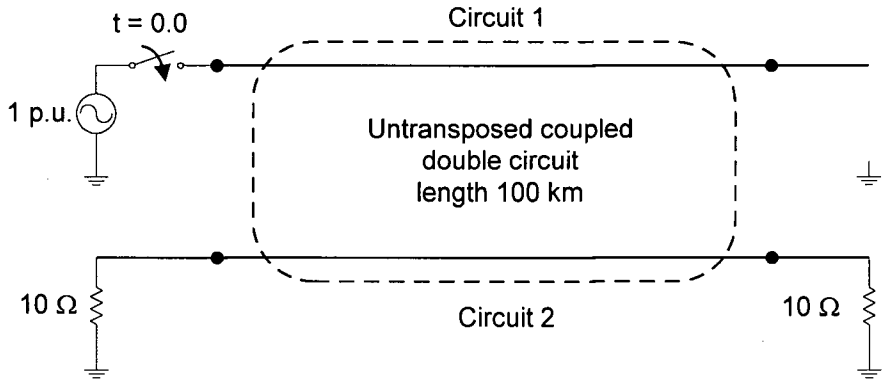

Figure 3.10. One-line diagram of the open-circuit test.

As can be observed in the results, the three models agree quite well for the case of the open circuit test. The fd-line model tends to deviate from the other models especially as the height of the conductor from ground increases.

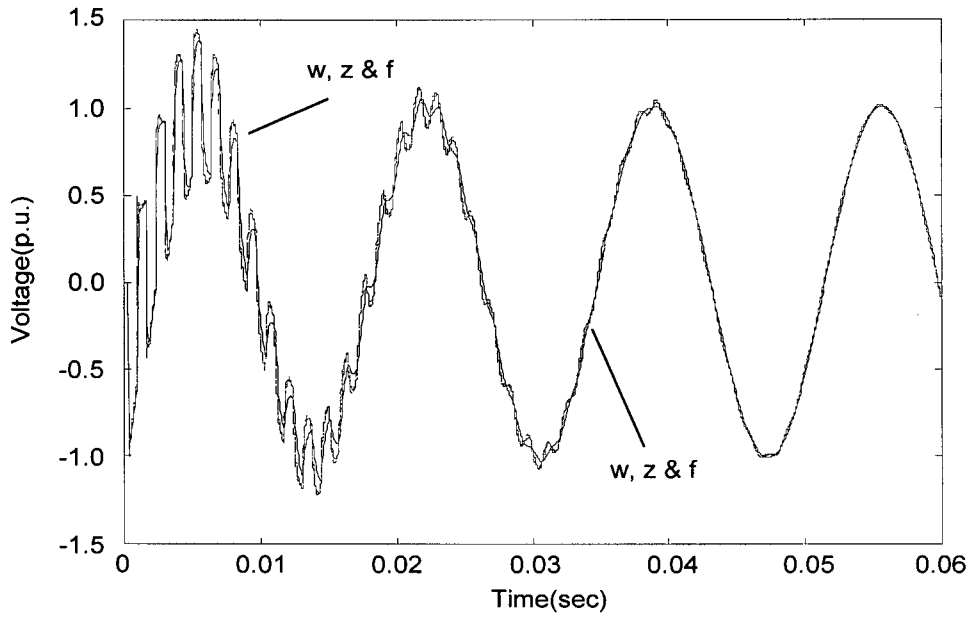

Figure 3.11. Receiving end voltage phase 2.

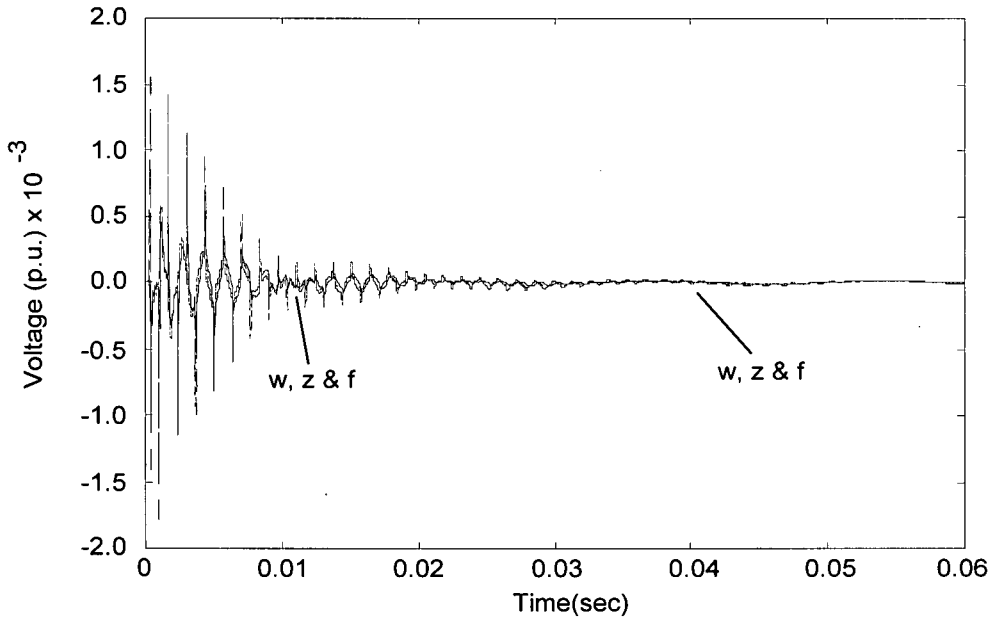

Figure 3.12. Receiving end voltage phase 4.

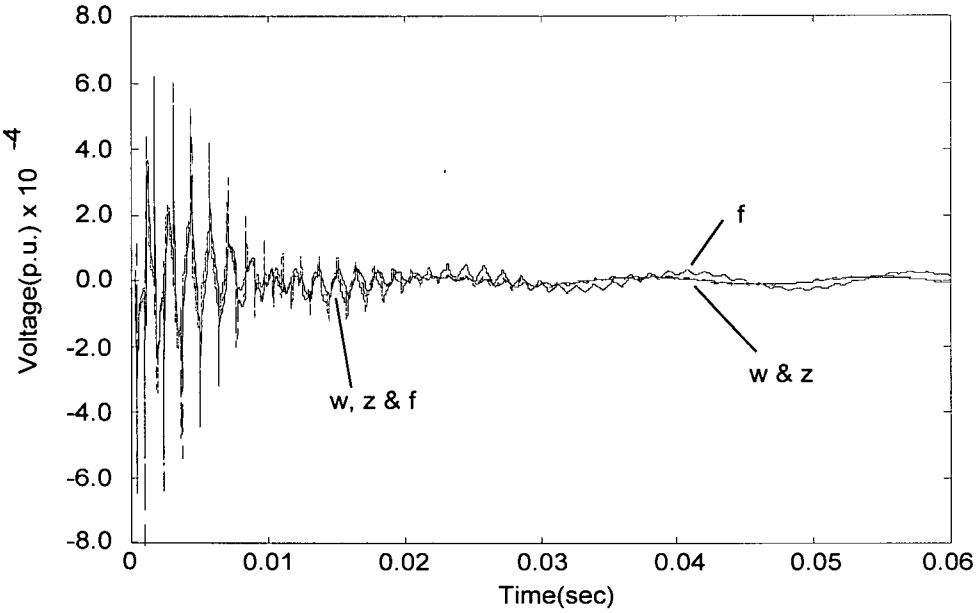

Figure 3.13. Receiving end voltage phase 5.

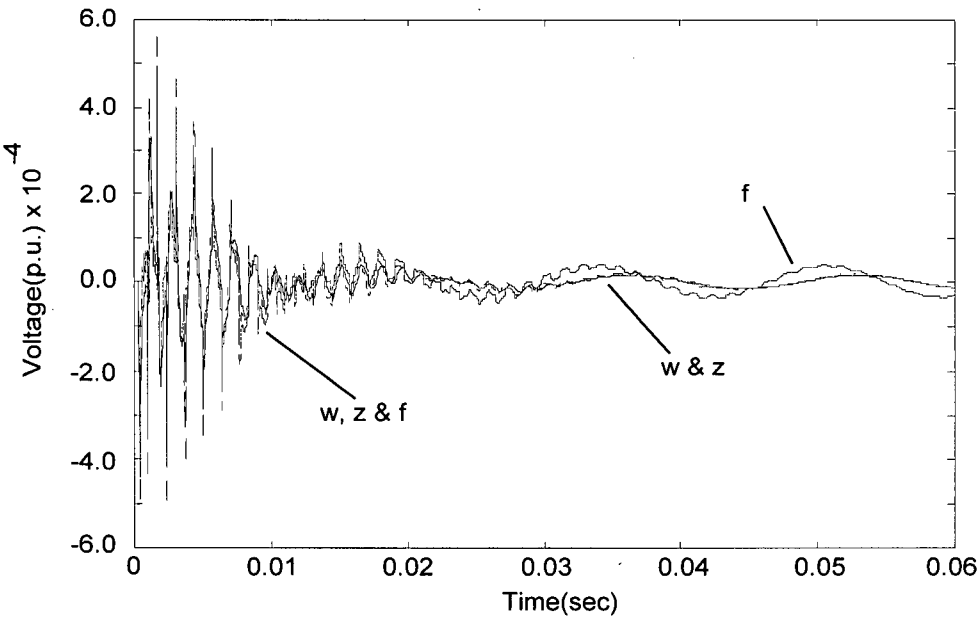

Figure 3.14. Receiving end voltage phase 6.

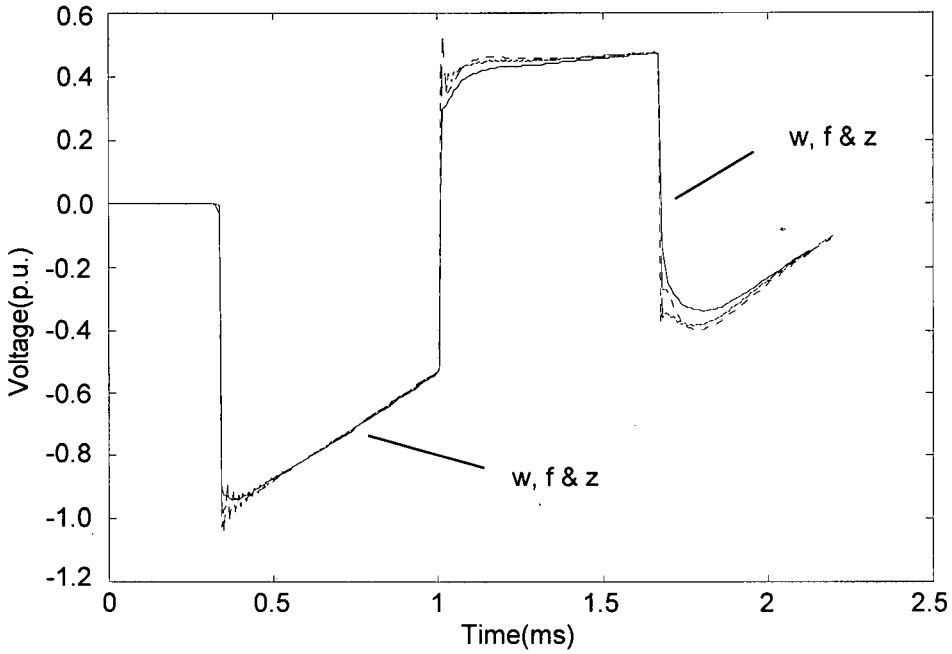

Figure 3.15. Initial transient on receiving end voltage phase 2.

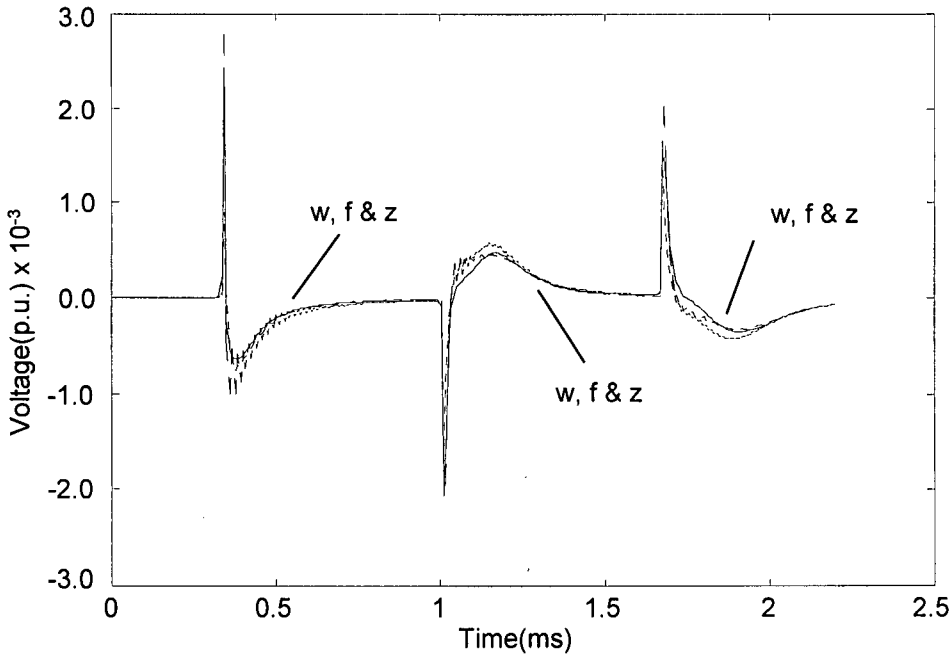

Figure 3.16. Initial transient on receiving end voltage phase 4.

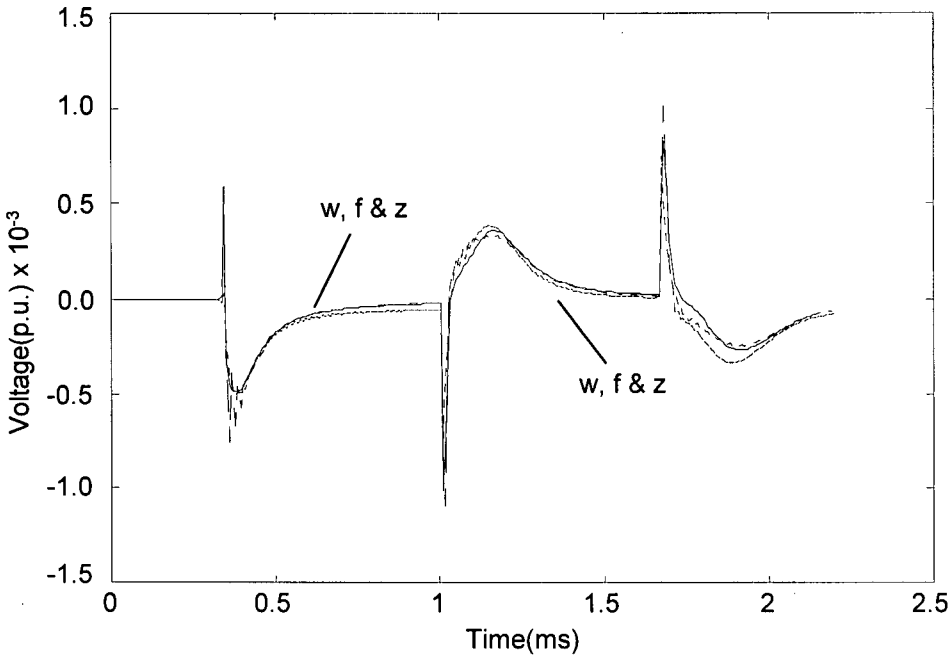

Figure 3.17. Initial transient on receiving end voltage phase 5.

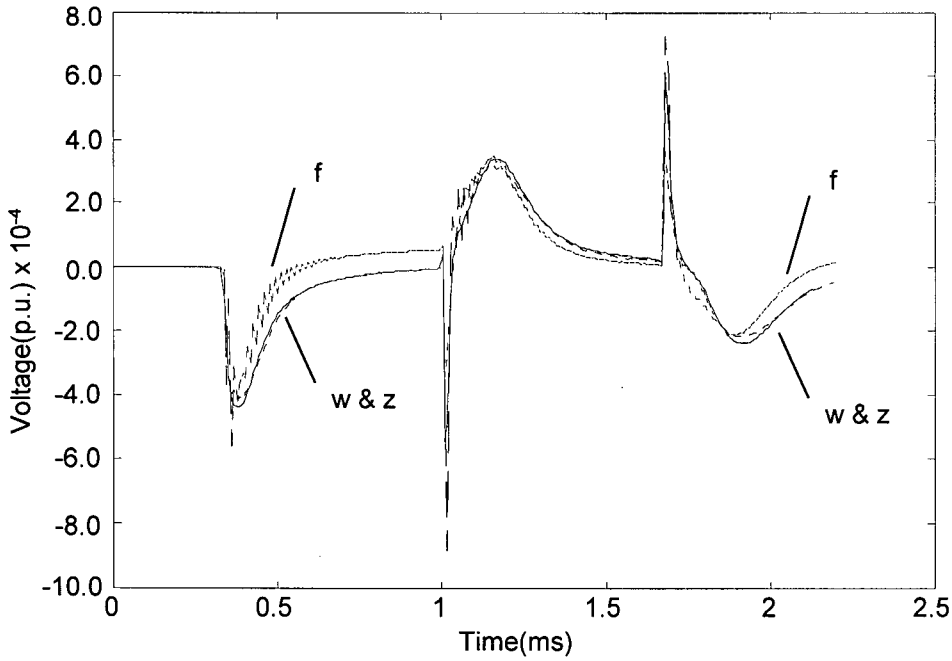

Figure 3.18. Initial transient on receiving end voltage phase 6.

3.6.2. Short Circuit Test

The system configuration for the short circuit test is shown in Figure 3.19. A three phase balanced voltage source of 1.0 p.u. was connected at time zero, energizing phases 1, 2 and 3. The receiving end of these phases was grounded through 10 Ω resistances, as well as the two ends of the second circuit.

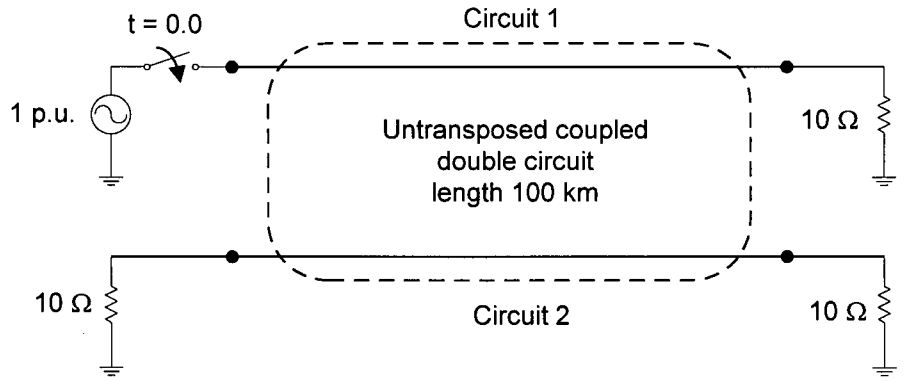

Figure 3.19. One-line diagram of the short-circuit test.

The results for this case present a more drastic difference between line models than the ones for the open circuit. The fd-line model differs from the other models for some of the variables by margins higher than two. Not only the magnitude is affected, but phase shifting is visible as well. The z-line model closely agrees with the results of the FDTP.

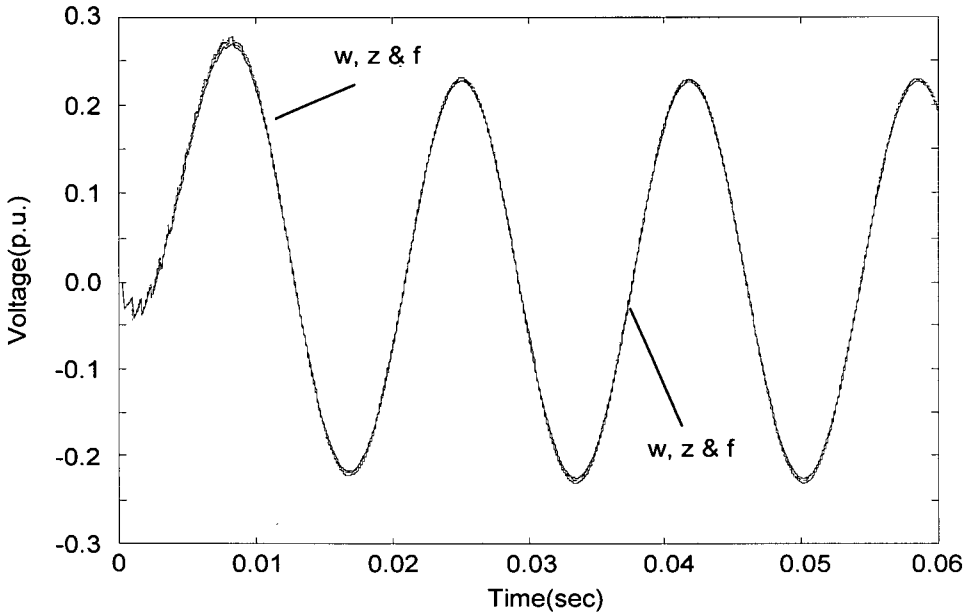

Figure 3.20. Receiving end voltage phase 2.

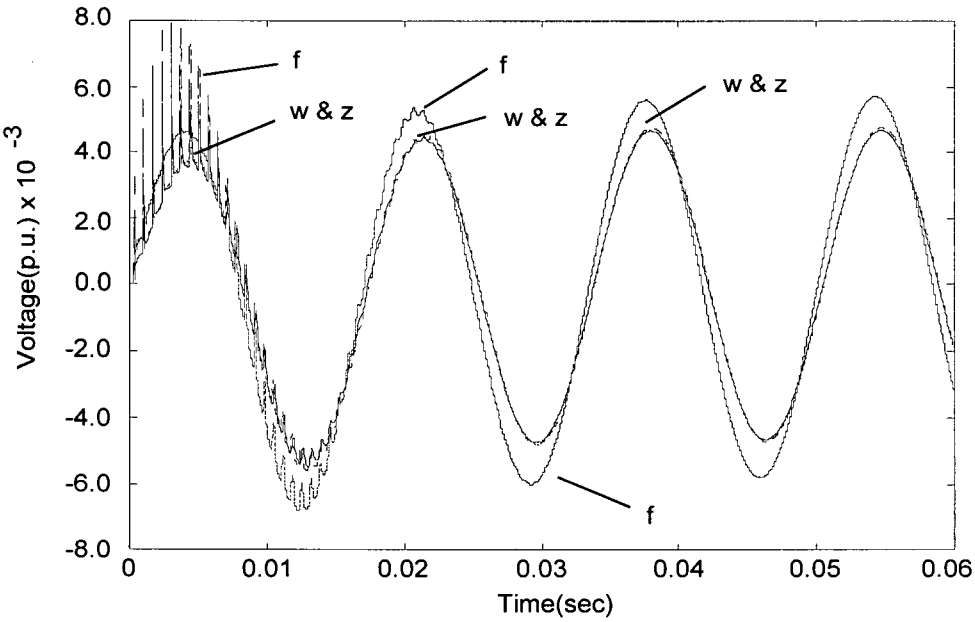

Figure 3.21. Receiving end voltage phase 4.

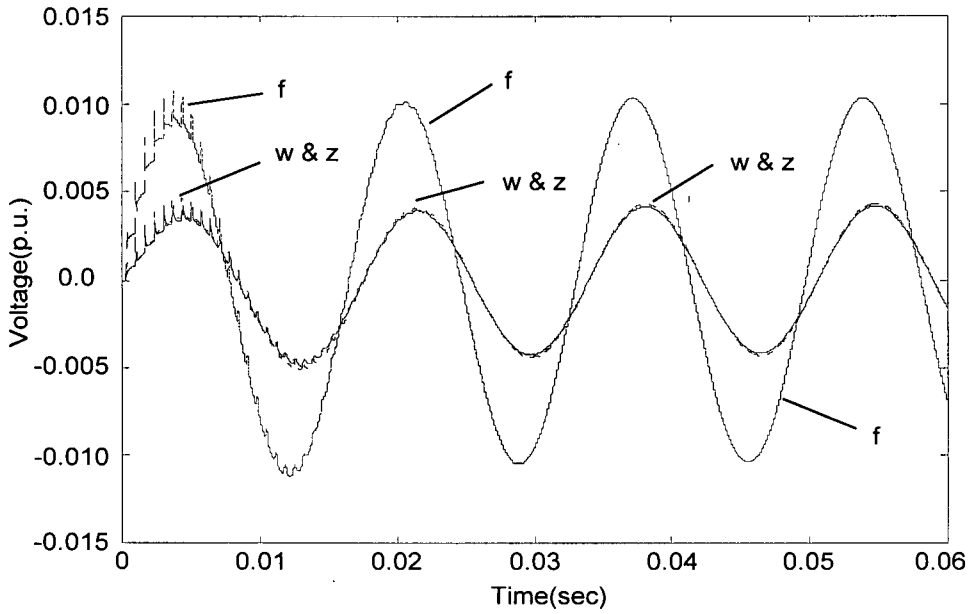

Figure 3.22. Receiving end voltage phase 5.

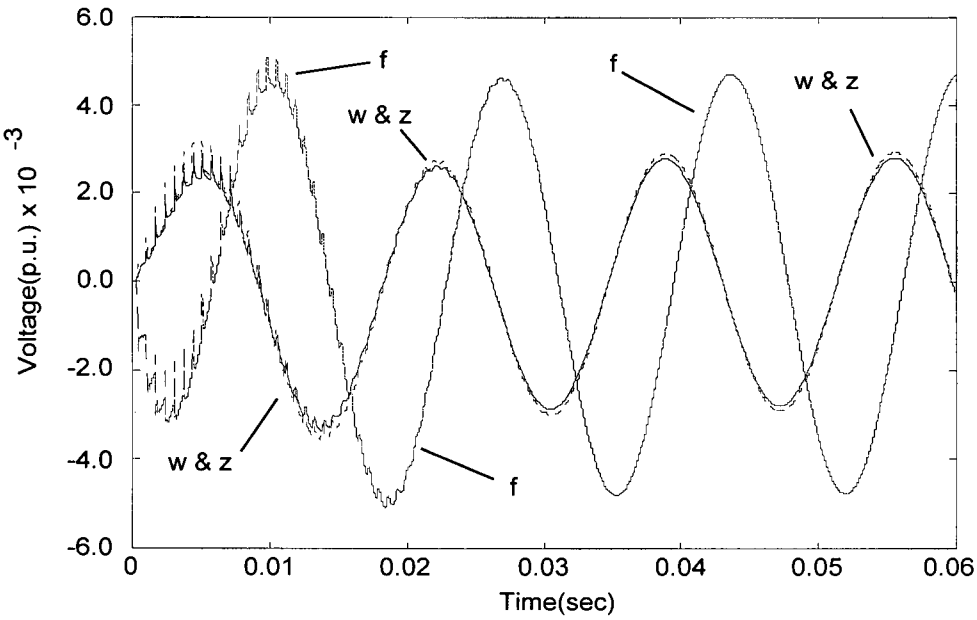

Figure 3.23. Receiving end voltage phase 6.

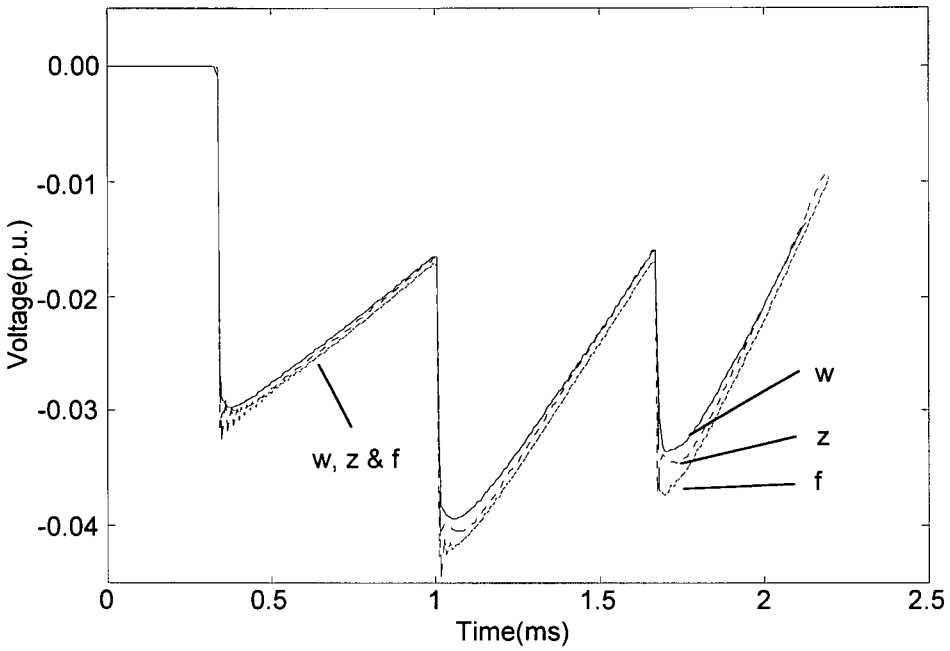

Figure 3.24. Initial transient on receiving end voltage phase 2.

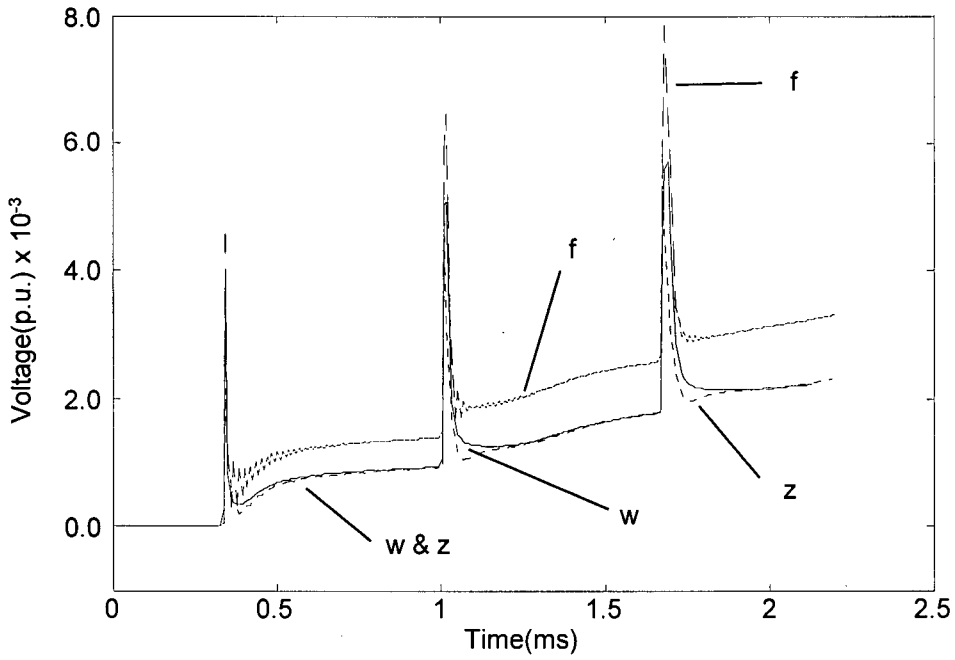

Figure 3.25. Initial transient on receiving end voltage phase 4.

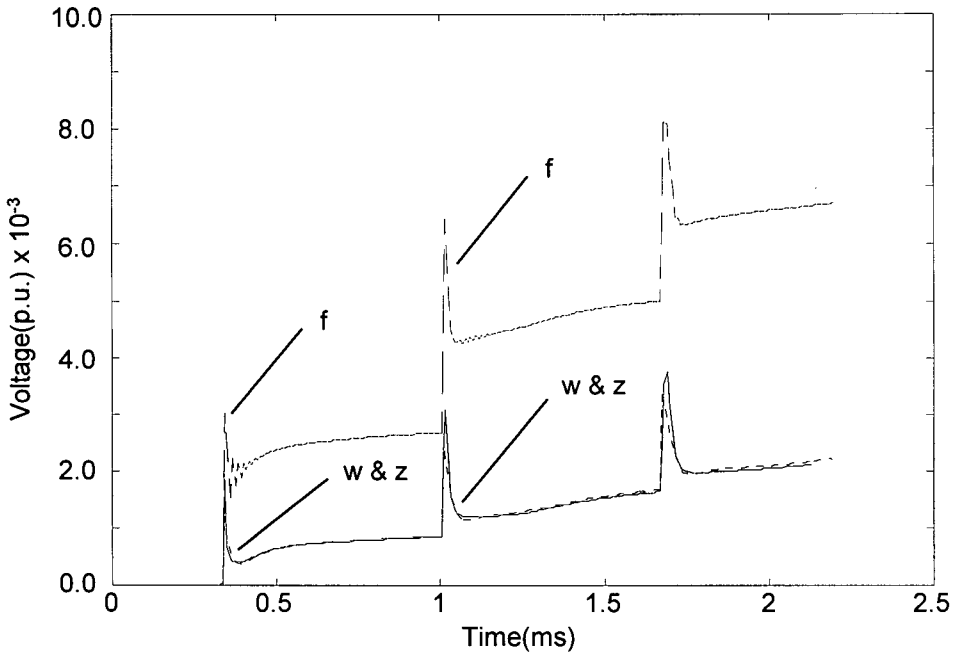

Figure 3.26. Initial transient on receiving end voltage phase 5.

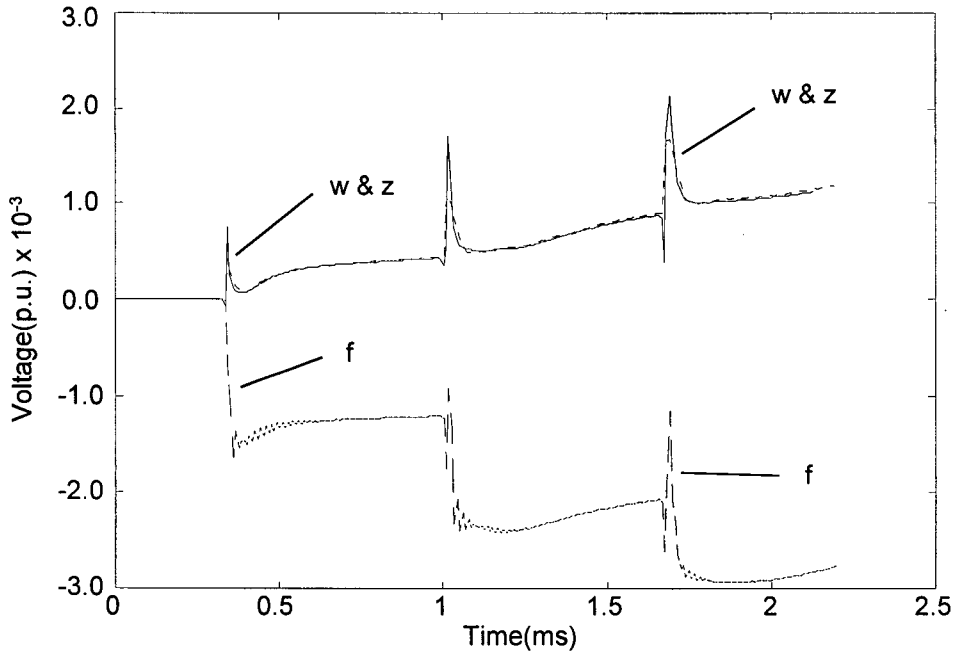

Figure 3.27. Initial transient on receiving end voltage phase 6.

3.6.3. Load Test

In this test, shown in Figure 3.28, circuit 1 is energized at the beginning of the simulation ($t = 0$) with a three-phase sinusoidal voltage source with a peak value 1 p.u. The receiving end of circuit 1 is connected to a three-phase Y-connected resistive load of 500 Ω/phase. The second circuit is connected to ground at the sending end through a small three-phase Y-connected resistive path of 10 Ω/phase.

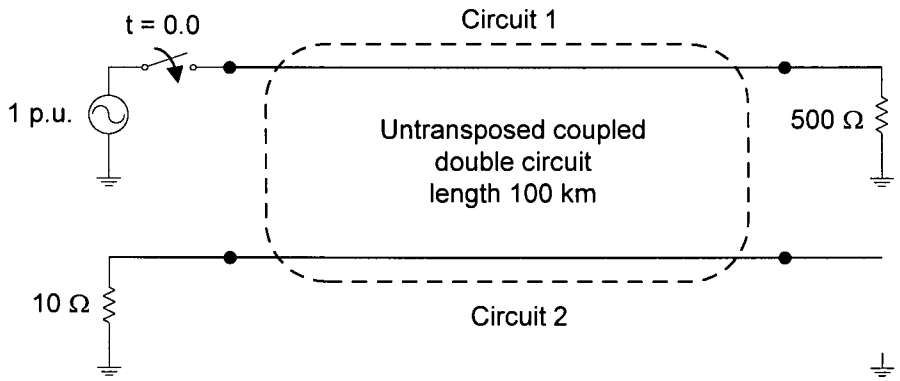

Figure 3.28. One-line diagram of the general study case.

The results show a noticeable difference in magnitude and phase for the simulations with the fd-line model versus the FDTP and z-line models. It is believed that those differences are mostly due to the fact that the imaginary part of the transformation matrices is neglected for the fd-line model. The imaginary component is important in this case where the conductors are located at different heights, which results in a strong asymmetrical configuration. As seen in some of the results, the use of a constant and real transformation matrix in fd-line introduces errors not only in the magnitude and phase of the output, but also distorts the time constants associated with the transients duration and decay. The z-line

model, on the other hand, presents a very good agreement with the FDTP solution over the whole time span.

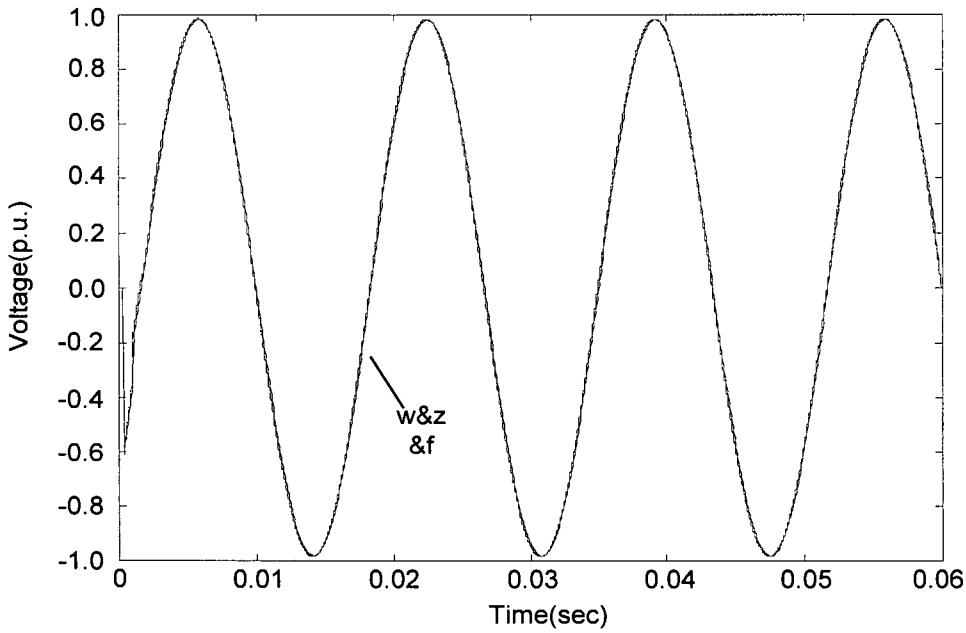

Figure 3.29. Receiving end voltage phase 2.

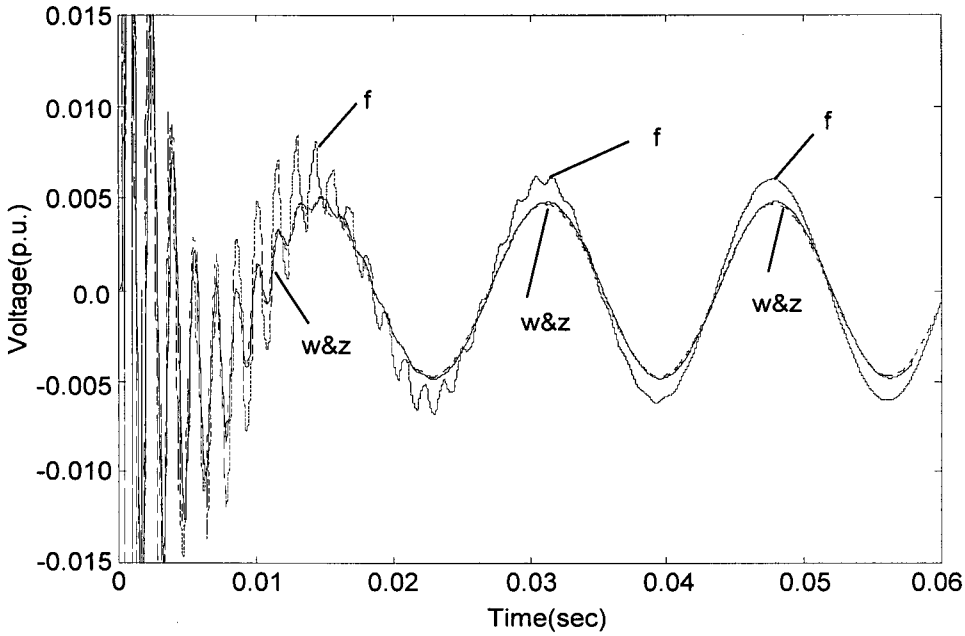

Figure 3.30. Receiving end voltage phase 4.

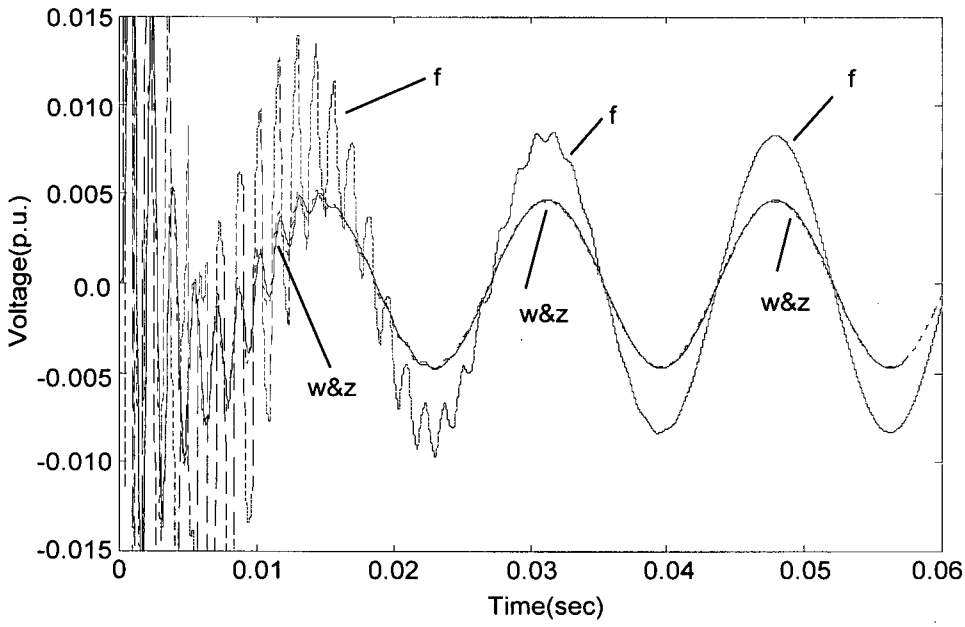

Figure 3.31. Receiving end voltage phase 5.

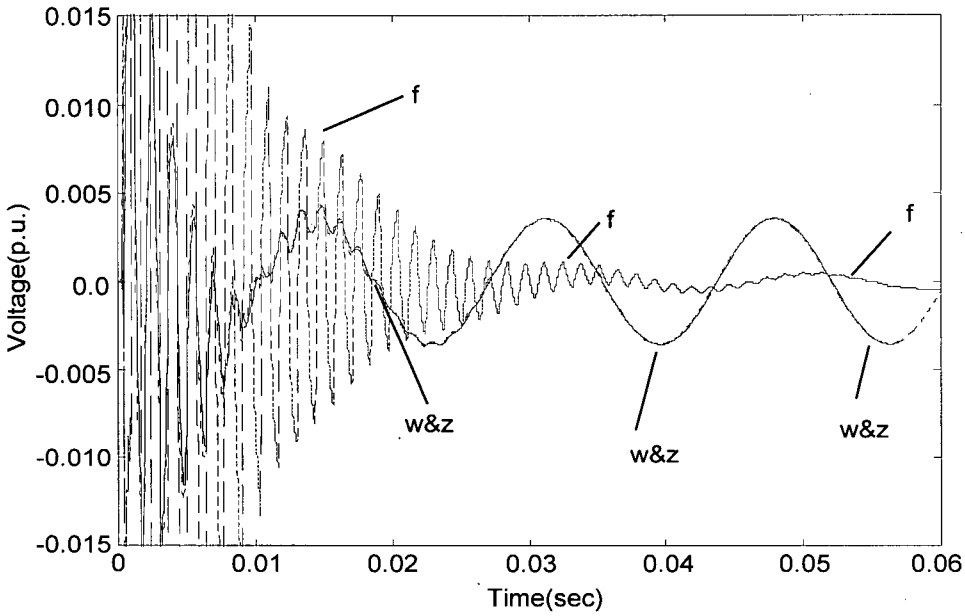

Figure 3.32. Receiving end voltage phase 6.

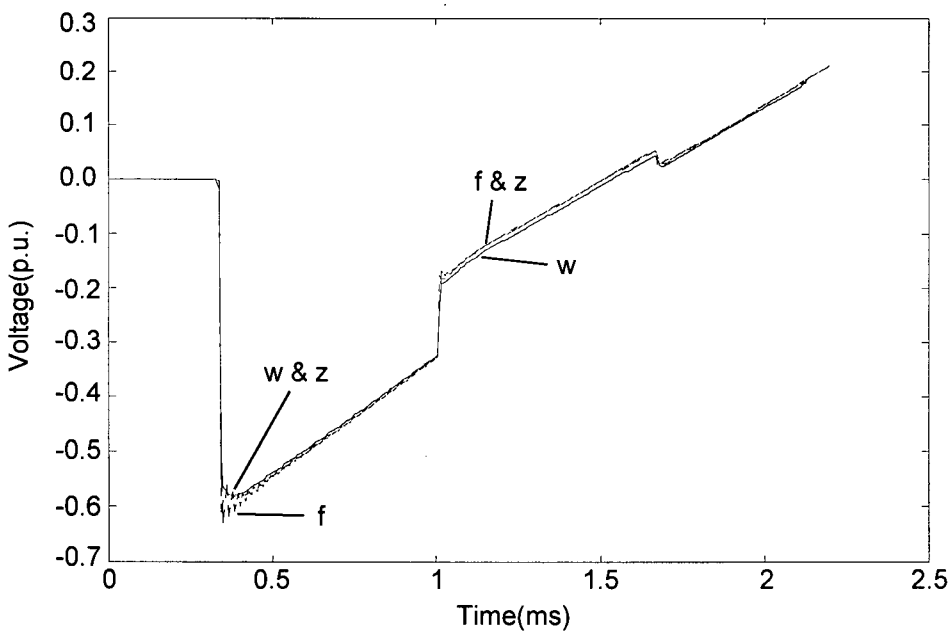

Figure 3.33. Initial transient on receiving end voltage phase 2.

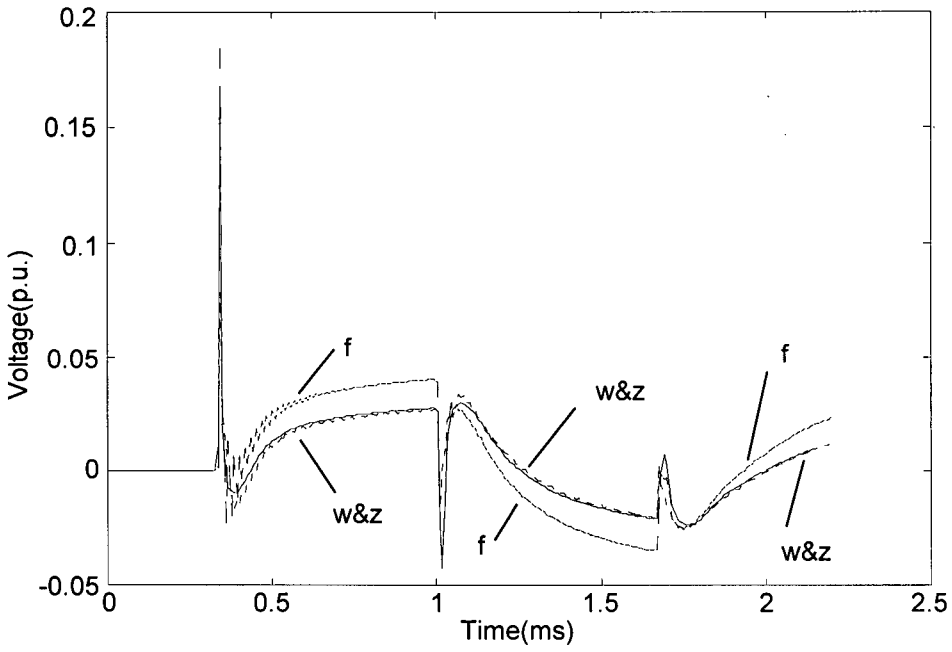

Figure 3.34. Initial transient on receiving end voltage phase 4.

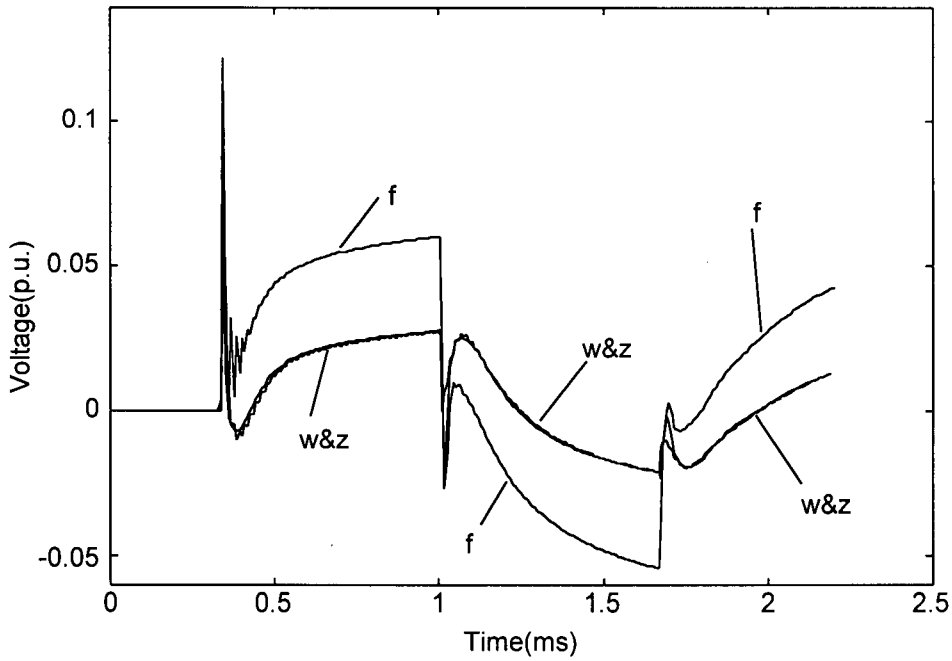

Figure 3.35. Initial transient on receiving end voltage phase 5.

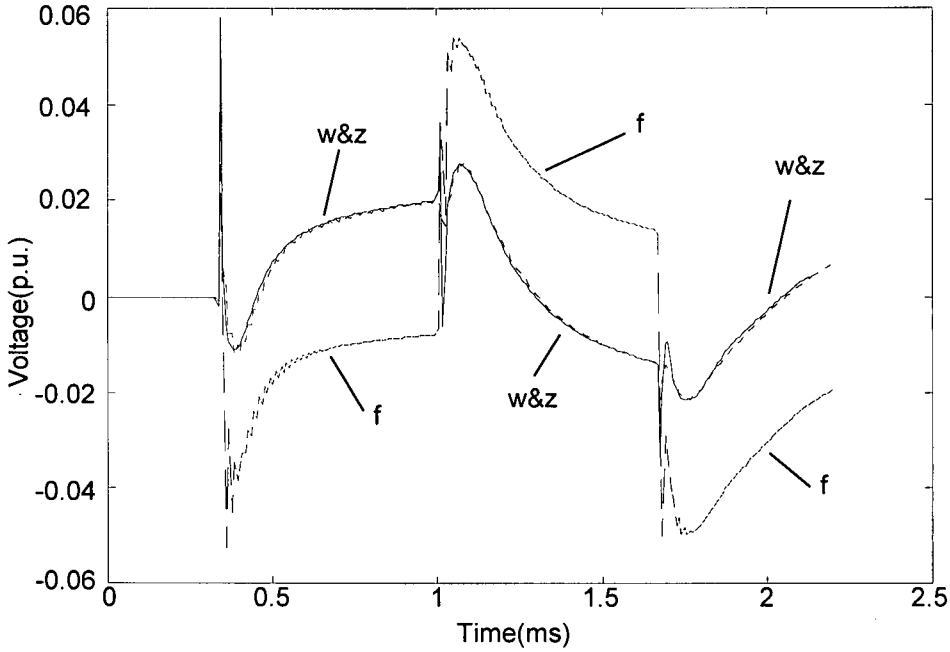

Figure 3.36. Initial transient on receiving end voltage phase 6.

3.6.4. Z-line Model and Corona Model

The Tidd line simulation test of Figure 2.20 presented in the first part of this thesis was repeated modelling the transmission line sections with the new full frequency dependent z-line model. The number of sections used for the simulation was the same as for the one with the cp-line representation. Each $[\mathbf{Z}^{loss}(\omega)]$ section was represented by nine *R-L* blocks. The results of the simulation are shown in Figure 3.37. The results show the effect of frequency dependence modelling in reducing the peak value of the surge - bringing it closer to the field test - and in improving the phase response. Also, the small ripples observed with the cp-line model in the initial step at the level of corona inception on the wave are smaller with z-line.

Overall, even though the results that were obtained with cp-line were quite good, the results with z-line are closer to the original field test measurements.

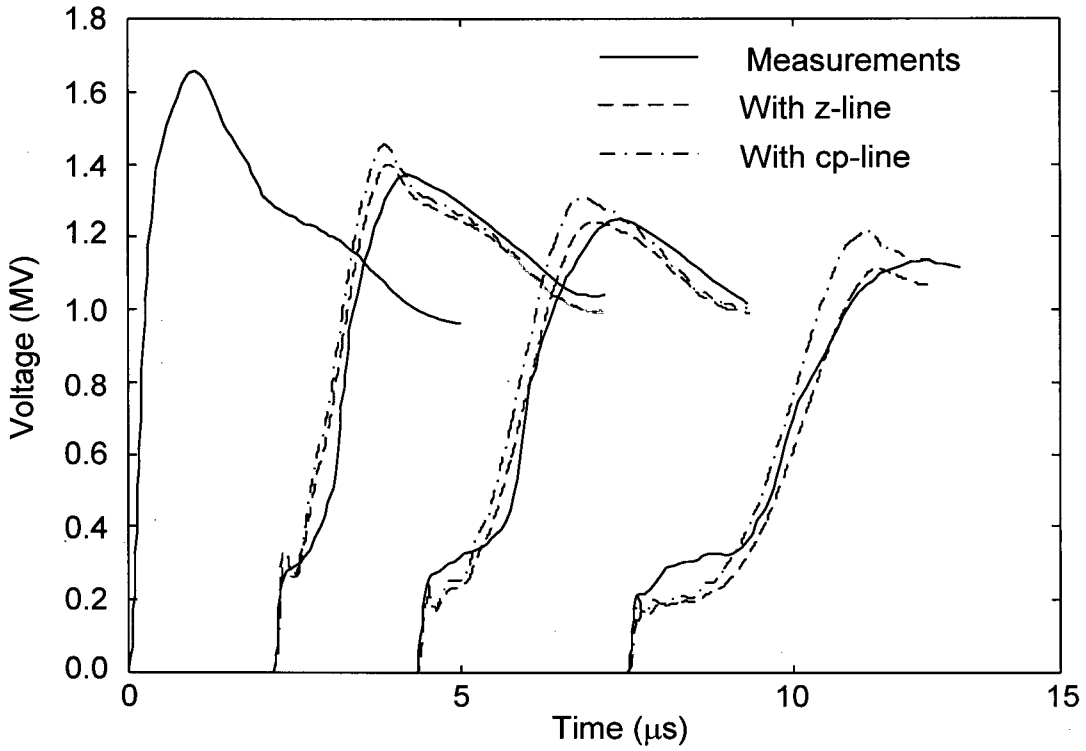

Figure 3.37. Simulation and experimental results for the Tidd line case.

3.7. Summary

The major difficulty in frequency-dependent transmission line modelling for time domain solutions has been the frequency dependence of the transformation matrices connecting modal and phase domains. The importance of this factor increases with the degree of asymmetry of the line configuration.

The z-line model presented in this thesis is formulated directly in the phase domain and can very accurately represent any arbitrary asymmetrical configuration.

The model is based on space discretization instead of time discretization and on separating the characteristics of the wave propagation along a discrete-length transmission line segment into two parts: constant ideal propagation at the speed of light in the external electromagnetic field ($[\mathbf{L}^{ext}]$ and $[\mathbf{C}]$) and frequency-dependent distortion due to the losses (resistance and internal inductance) inside the conductors and ground, $[\mathbf{Z}^{loss}(\omega)]$. The model separates the external geometry and propagation media from the internal ones. This property allows the model to represent *exactly* the geometry of strongly asymmetrical configurations (mostly an external effect). In this regard, the new model is particularly suited for cases involving multiple circuits in parallel or circuits coupled with near-by pipes or other elements. Since the model is based on space discretization, it is also particularly suited for the modelling of very short lines where full-length models based on the synthesis of $[\mathbf{e}^{-\gamma(\omega)x}]$ tend to have problems. These problems are due to the fact that $[\mathbf{e}^{-\gamma(\omega)x}]$ tends to the unit matrix for very short line lengths and the dynamics of the propagation function tend to be numerically lost.

A new coordinated fitting procedure is introduced to fit all the elements of the loss impedance matrix $[\mathbf{Z}^{loss}(\omega)]$ simultaneously. This procedure avoids the numerical stability problems associated with independently fitting each element of a fully-coupled system matrix. Even though the model was developed initially under the precept of sections discretization for corona modelling, in the end it turned out to be a very good model for general line modelling even when corona is not included.

The approach of replacing the synthesis of the line propagation function $[\mathbf{e}^{-\gamma(\omega)x}]$ by space sectionalization resulted in a model which is very accurate, computational efficient,

and numerically stable. Tests performed indicate that in cases of strong line asymmetry the new model is much more accurate than the frequency-dependent constant-transformation matrix fd-line model in the EMTP.

Compared to other full frequency dependent line models (not restricted to a constant transformation matrix as fd-line), as for example the models in [45] and [60], z-line is very competitive in terms of computer solution times and is totally robust in terms of numerical stability for any arbitrary asymmetrical configuration of the line conductors.

4. CHAPTER 4

FUTURE RESEARCH

The work presented in this thesis has been possible thanks to the accumulated research and work of many previous researchers and engineers, as the bibliography clearly reflects. New contributions are usually based on previous ones. This thesis is not an exception and it is hoped that its contributions can be used as the basis of future research in several areas, some of which are suggested here:

- Corona tests measuring a larger number of variables are very important for the future development of corona models. The tests should attempt to collect information about the time constants of the different processes involved in the phenomenon.

- The corona model presented in this thesis was developed to represent effects under unidirectional surges (positive or negative). A next step would be to extend the model to bipolar surges. This is of special interest for switching transients and dynamic overvoltages, as pointed out in [14].

- The extension of the corona model to a three-phase transmission line. This should be easier to achieve than with previous models, given the concept of limiting the corona model to a cylindrical surface around the conductors. Some

research must be done in clarifying the influence of corona among conductors, an aspect upon which many researchers do not totally agree [43, 63, 64].

- The representation of the descending part of the corona loop is not totally satisfactory and further research is needed to model this region. This is more critical in the case of thin conductors, where the dynamics of the corona phenomena seem to be more complicated.

- The efficiency of the z-line model can be improved by the use, where possible, of a common set of poles for all the elements in the approximation of the $[\mathbf{Z}^{loss}(\omega)]$ matrix, as suggested in [60]. This will reduce the amount of calculations considerably.

- To implement the z-line model in a general version of the EMTP.

5. CHAPTER 5

CONCLUSIONS

This thesis reports the work developed in two areas of time-domain modelling of electric power systems: corona modelling and full frequency-dependent transmission line modelling.

The developed corona model achieves several improvements over existing models by representing more closely the physical topology of the phenomenon. The proposed model is the first model that matches closely, with a constant set of circuit parameters, the q-v characteristics of a wide range of fast and slow surges as well as measured travelling wave distortion in test lines. The model can accurately represent the apparent changes in the corona inception voltage and the different slopes (including negative) in the corona active region of the q-v curves.

The proposed corona model can be easily implemented in the EMTP. Simulations of q-v curves and travelling surges show very good agreement with measured results. The parameters of the model can be calculated from a set of cage-measured q-v curves and can be extrapolated for an arbitrary overhead line configuration. The portability of cage results to the overhead line model is of vital importance for the practical use of corona models in transmission line transients analysis.

The z-line model developed in this thesis is formulated directly in the phase domain and is able to represent the full frequency dependence of the line parameters. The model is based on the synthesis of the frequency-dependence of the basic circuit parameters **[R]**, **[L]**, as opposed to most models that represent the frequency dependence of the line propagation functions. The model separates the part of the parameters affected by skin effect inside the conductors and ground (resistance and internal inductance) from the part of the parameters which is constant (external inductance and capacitance). This separation allows the model to be practically exact in its representation of the geometry of the line, which is associated with the external (constant) parameters. The model can then represent with high accuracy highly asymmetrical multiple circuit configurations.

The developed z-line model has extended the concept of rational-functions fitting procedures to coupled systems by solving the problem of numerical stability. The number of rational fractions used to approximated the frequency dependent functions is about half or less than of the fd-line model. The new z-line model has proved to be a more accurate model that fd-line and has shown to be stable and computational efficient.

BIBLIOGRAPHY

[1] A. Greenwood, Electrical Transients in Power Systems. Second Edition. John Wiley and Sons. USA. 1991.

[2] H. W. Dommel, "Digital Computer Solution of Electromagnetic Transients in Single and Multiphase Networks", IEEE Trans. PAS, Vol. 88, p.p. 388-399, April 1969.

[3] S. Carneiro, J. Martí, "Evaluation of Corona and Line Models in Electromagnetic Transients Simulations". IEEE Trans. on PWD, Vol. 6, No. 1, p.p. 334-341, January 1991.

[4] J. R. Martí, "Accurate Modelling of Frequency-Dependent Transmission Lines in Electromagnetic Transient Simulations", IEEE Trans., Vol. PAS-101, 1982.

[5] H. W. Dommel, EMTP Theory Book. Second Edition. Microtran Power Systems Analysis Corporation. Vancouver, B.C. Canada, May 1992.

[6] EPRI, Transmission Line Reference Book - 345 kV and Above, 1975, Electric Power Research Institute. USA.

[7] J. Clade, C. Gary and C. Lefevre, "Calculation of Corona Losses Beyond the Critical Gradient in Alternating Voltage". IEEE Trans. on PAS, Vol. 88, No. 5, p.p. 695-703, May 1969.

[8] T. Giao and J. Jordan, "Modes of Corona Discharges in Air". IEEE Trans. on PAS, Vol. 87, No. 5, p.p. 1207-1215, May 1968.

[9] IEEE, EHV Transmission line Corona Effects. IEEE Tutorial Course. 72 CH0644-5 PWR. New York, 1972.

[10] F. W. Peek, Dielectric Phenomena in High Voltage Engineering. McGraw-Hill. 1915.

[11] C. F. Wagner, B. L. Lloyd, "Effects of Corona on Travelling Waves". AIEE Transactions, Vol. 74 - Pt. III, p.p. 858-872, Oct. 1955.

[12] C. F. Wagner, I. W. Gross, B. L.Lloyd, "High-Voltage Impulse Tests on Transmission Lines". AIEE Trans, Vol. 73-Pt. III. p. p. 196-210, April 1954.

[13] P. S. Maruvada, H. Menemenlis, R. Malewski, "Corona Characteristic of Conductor Bundles Under Impulse Voltages". IEEE Trans. PAS, Vol. 96, No. 1, p.p.102-115, Jan/Feb 1977.

[14] S. Maruvada, D. H. Nguyen, H. Hamadani-Zadeh, "Studies on Modeling Corona Attenuation of Dynamic Overvoltages". IEEE Trans. on PWD, Vol. 4, No. 2, p. p. 1441-1449, April 1989.

[15] C. Gary, G. Dragan, D. Critescu, "Attenuation of Travelling Waves Caused by Corona". CIGRE Report, 33-13, 1978.

[16] C. Gary, D. Critescu, G. Dragan, "Distortion and Attenuation of Travelling Waves Caused by Corona", CIGRE Report, Study Committee 33, 1989.

[17] A. Inoue. "High Voltage Travelling Waves with Corona Discharge on Bundled Conductors". IEEE PES Winter Meeting. A78 170-3. New York. Feb. 1978.

[18] R. Davis, R. W. Cook, "The Surge Corona Discharge", IEE Monograph No. 415, p.p. 230-239, November 1960.

[19] F. Castellanos, J. R. Martí, "Dynamic Corona Modelling in the EMTP with Simple Constant Parameter Circuit Components". Trans. Eng./Op. Division, Canadian Electrical Association Conference, Vol. 32, Montreal, Canada, March 1993.

[20] H. J. Koster, K. H. Weck, "Attenuation of Travelling Waves by Impulse Corona", CIGRE 33-18, 1981.

[21] N. H. C. Santiago, A. J. S. Junqueira, C. M. Portela, A. R. Pinto, "Attenuation of Surges in Transmission Lines due to Corona Effect Three Phase Modelling". 7th International Symposium on High Voltage Engineering. August 1991.

[22] N. Santiago, F. Castellanos, "Physical Aspects of Corona Effect During Transient Overvoltages and Their Simulation with Circuit Models". Proc. IASTED on Power Systems and Engineering, p. p. 9-14, August 1992.

[23] C. Christopoulos, "Propagation of Surges Above the Corona Threshold on a Line with a Lossy Earth Return", COMPEL, Vol. 4, No. 2, p.p. 91-102, 1985.

[24] H. M. Kudyan, C. H. Shih, "A Nonlinear Circuit Model for Transmission Lines in Corona", IEEE Trans. on PAS, Vol. 100, p.p. 1420-1430, March 1981.

[25] J. C. Portela, "Regimes Transitorios" (In portuguese). Vol. 2. COPPE/UFRJ. Brazil. 1983.

[26] M. T. Correia de Barros, "Efeito Coroa en Linhas de Transporte de Energia", (In portuguese), Doctoral Thesis, Instituto Superior Tecnico, Lisboa, Portugal,1985.

[27] M. M. Suliciu, I. Suliciu, "A Rate Type Constitutive Equation for the Description of the Corona Effect", IEEE Trans. on PAS, Vol. PAS-100, p.p. 3681-3685, Aug. 1981.

[28] J. R. Martí, F. Castellanos, N. Santiago, "A Wide Bandwidth Corona Model". Proceedings PSCC, 11th Power Systems Computation Conference, France, pp. 899-905, Aug. 1993.

[29] H. Hamadani-Zadeh, "Dynamic Corona Model and Frequency-Dependent Line Model for EMTP", Internal Report IREQ, Quebec, Canada, October 1986.

[30] C. Gary, A. Timotin, D. Critescu, "Prediction of Surge Propagation Influenced by Corona and Skin Effect", Proc. IEE, 130-A, p.p. 264-272, July 1983.

[31] K. C. Lee, "Non-Linear Corona Models in an ElectroMagnetic Transients Program (EMTP)", IEEE Trans. on PAS, PAS-102, p.p. 2936-2942, Sept. 1983.

[32] X. Li, O. P. Malik, Z. Zhao, "A Practical Mathematical Model of Corona for Calculation of Transients on Transmission Lines", IEEE PES Summer Meeting, 88 SM 579-5, 1988.

[33] M. Afghani, R. J. Harrington, "Charge-Model for Studying Corona During Surges on Overhead Transmission Lines", IEE Proc., Vol. 130, Pt. C, No.1, p.p. 16-21, January 1983.

[34] M. Abdel-Salam, E. Keith Stanek, "Mathematical-Physical Model of Corona from Surges on High-Voltage Lines", IEEE Trans. on Ind. Appl., Vol. 23, No. 3, p.p. 481-489, May/June 1987.

[35] M. Abdel-Salam, S. Abdel-Sattar, "Calculation of Corona V-I Characteristics of Monopolar Bundles Using the Charge Simulation Method", IEEE Trans. on Elec. Insul. Vol. 24, No. 4, p.p. 669-679, August 1989.

[36] F. Castellanos, J. R. Martí, "Incorporation of Corona on Transmission Lines in the EMTP", Trans. Eng./Op. Division, Canadian Electrical Association Conference, Vol. 33, Toronto, Canada, March 1994.

[37] S. Carneiro, "A Comparative Study of Some Corona Models and Their Implementation in the EMTP", Trans. CEA, Engineering and Operation Division, Vol. 27, 1988.

[38] N. Harid and R. T. Waters, "Statistical Study of Impulse Corona Inception Parameters on Line Conductors", IEE Proceedings-A, Vol. 138, No. 3, pp. 161-168, May 1991.

[39] C. de Jesus, M. T. Correia de Barros, "Modelling of Corona Dynamics for Surge Propagation Studies", IEEE Transactions on Power Delivery, Vol. PWRD-9, No. 3, pp. 1564-1569, July1994.

[40] J. R. Martí, F. Castellanos, N. Santiago, "Wide-Band Corona Circuit Model for Transient Simulations", IEEE Trans. on Power Systems, Vol. 10, No. 2, pp. 1003-1013, May 1995.

[41] R. T. Waters, D. M. German, A. E. Davies, N. Harid, H. SB. Eloyyan, "Twin Conductor Surge Corona", Fifth International Symposium on High Voltage Engineering, Federal Republic of Germany, 24-28 August 1987.

[42] A. Semlyen and W. G. Huang, "Corona Modelling for the Calculation of Transients on Transmission Lines", IEEE Transactions on Power Delivery, Vol. PWRD-1, No. 3, pp. 228-239, July 1986.

[43] W. G. Huang and A. Semlyen, "Computation of Electro-Magnetic Transients on Three-Phase Transmission Lines with Corona and Frequency Dependent Parameters", IEEE Transactions on Power Delivery, Vol. PWRD-2, No. 3, pp.887-898, July 1987.

[44] J. F. Guiller and M. Rioual, "Damping Model of Travelling Waves by Corona Effect Along Extra High Voltage Three Phase Lines", IEEE Transactions on Power Delivery, Vol. PWRD-10, No. 4, pp. 1851-1861, October 1995.

[45] L. Martí, "Simulation of Transients in Underground Cables with Frequency-Dependent Modal Transformation Matrices", IEEE Transactions on Power Delivery, Vol. PWRD-3, No. 3, pp. 1099-1110, July 1988.

[46] L. M. Wedepohl, "Application of Matrix Methods to The Solution of Travelling-Wave Phenomena in Polyphase Systems", Proc. IEE, Vol. 110, pp. 2200-2212, 1963.

[47] D. E. Hedman, "Propagation on Overhead Transmission Lines. I-Theory of Modal Analysis", IEEE Transactions PAS, pp. 200-205, March 1965.

[48] A. Semlyen, A. Dabuleanu, "Fast and Accurate Switching Transient Calculations on Transmission Lines with Ground Return using Recursive Convolutions", IEEE Trans. PAS, Vol. 94, pp. 561-571, March/April 1975.

[49] J. R. Martí, H. W. Dommel, L. Martí, V. Brandwajn, "Approximate Transformation Matrices for Unbalanced Transmission Systems", Proc. PSCC, 9th Power System Computation Conference, London, pp. 416-422, August 1987.

[50] J. F. Guillier, M. Rioual, M. Poloujadoff, "High Frequency Three Phases Line Model with Corona and Skin Effect", IERE France, p.p. 97-103, March 1992.

[51] H. Baher, Synthesis of Electrical Networks, New York, John Wiley and Sons Ltd, 1984.

[52] J. R. Martí, B. W. Garrett, H. W. Dommel and L. M. Wedepohl, "Transients Simulation in Power Systems: Frequency Domain and Time Domain Analysis", Canadian Electrical Association, CEA Transactions, Montreal, Quebec, March 1985.

[53] F. Castellanos and J. R. Martí, "Phase-Domain Multiphase Transmission Line Models", Proc. IPST'95, International Conference on Power Systems Transients, Lisbon, pp. 17-22, Sept. 1995.

[54] J. L. Naredo, "The Effect of Corona on Wave Propagation on Transmission Lines", Ph. D. Thesis, The University of British Columbia, Vancouver, Canada, August 1992.

[55] F. Castellanos and J. R. Martí, "Exact Modelling of Asymmetrical Multiple-Circuit Transmission Lines in EMTP Simulations", Trans. Eng./Op. Division, Canadian Electrical Association Conference, Montreal, Canada, April 1996.

[56] H. V. Nguyen, H. W. Dommel, J. R. Martí, "Direct Phase-Domain Modelling of Frequency-Dependent Overhead Transmission Lines", PES Summer Meeting, 96SM458-0-PWRD, Denver, USA, Aug. 1996.

[57] T. Noda, N. Nagaoka, A. Ametani, "Further Improvements to a Phase-Domain ARMA Line Model in Terms of Convolution, Steady-State Initialization and Stability", PES Summer Meeting, 96 SM 457-2-PWRD, Denver, USA, Aug. 1996.

[58] G. Angelidis, A. Semlyen, "Direct Phase-Domain Calculation of Transmission Line Transients Using Two-Sided Recursions", IEEE Trans. on PWRD, Vol. 10, No. 2, pp. 941-949, April 1995.

[59] F. Castellanos, J. R. Martí and F. Marcano, "Phase-Domain Multiphase Transmission Line Models", Invited paper Special Issue on Electromagnetic Transients, International Journal of Electrical Power & Energy Systems, London, England, To be published March 1997.

[60] F. J. Marcano, "Modelling of Transmission Lines Using Idempotent Decomposition", Master Thesis, The University of British Columbia, Vancouver, Canada, August 1996.

[61] H. M. Barros, S. Carneiro, R. M. Azevedo, "An Efficient Recursive Scheme for the Simulation of Overvoltages on Multiphase Systems Under Corona", IEEE Trans. on Power Delivery, Vol. 10, No. 3, p.p. 1443-1452, July 1995.

[62] H. M. Barros, R. M. Azevedo, S. Carneiro, "A Comparison of Frequency-Dependent Models in Connection with Implicit Segmentation Schemes", Proc. International Conference on Power Systems Transients, p.p. 29-34, Lisbon, Portugal, Sept. 1995.

[63] S. Carneiro, J. R. Martí, H. W. Dommel, H. M. Barros, "An Efficient Procedure for the Implementation of Corona Models in ElectroMagnetic Transients Programs", IEEE Transactions on Power Delivery, Vol. 9, No. 2, p.p. 849-855, April 1994.

[64] M. T. Correia de Barros, "Identification of the Capacitance Coefficients of Multiphase Transmission Lines Exhibiting Corona Under Transient Conditions", IEEE Transactions on Power Delivery, Vol.10, No. 3, p.p. 1642-1648, July 1995.

[65] A. Semlyen and A. Dabuleanu, "Fast and Accurate Switching Transient Calculations on Transmission Lines with Ground Return Using Recursive Convolutions",

IEEE Transactions on Power, Apparatus and Systems, Vol. PAS-94, p.p. 561-571, March/April 1975.

[66] F. Castellanos, J. R. Martí, "Full Frequency-Dependent Phase-Domain Transmission Line Model", Paper 96SM-569PWRS. To be published in IEEE Trans. on Power Systems. Accepted, June 1996. Presented at PES-IEEE Summer Power Meeting, , Denver, USA, 6 journal pages, Aug. 1996.

A. APPENDIX A

MODELLING OF MULTIPHASE FREQUENCY CONSTANT LUMPED ELEMENTS

A special case of the modelling of a multiphase line using the z-line model exists when the matrix $[\mathbf{Z}^{loss}(\omega)]$ is evaluated at only one particular frequency (ω_o) and synthesized with only one *R-L* block. In this case there is only one frequency at which the original matrix matches the approximation and it is equivalent, in terms of computational effort, to using a "constant-parameter" line model. The general method explained in section 3.4 can be used to obtain a normal z-line representation by setting the number of synthesizing blocks to one ($m = 1$). However, an alternative formulation can be written in terms of the corresponding parallel *R-L* blocks. This method is presented here because it could also be used to represent other power system elements such as transformers, machines and others.

The matrix $[\mathbf{Z}^{loss}(\omega_o)]$ represents, mathematically, a resistance and an inductance in series. Actually, the minimal solution as represented by equations (3-12) and (3-13) is a one block parallel *R-L* combination around the given ω_o frequency. Each element of the matrix $[\mathbf{Z}^{loss}(\omega_o)]$ can be replaced by its equivalent parallel *R-L* block elements through the equations:

$$R_{ij}^{par} = \frac{(\omega_o L_{ij})^2}{R_{ij}} + R_{ij} \quad \text{and} \quad L_{ij}^{par} = \frac{R_{ij}^2}{\omega_o L_{ij}} + L_{ij} \quad \text{for } i \neq j$$

$$R_{ii}^{par} = \frac{(\omega_o L_{ii})^2}{R_{ii} - R_{iio}} + (R_{ii} - R_{iio}) \quad \text{and} \quad L_{ii}^{par} = \frac{(R_{ii} - R_{iio})^2}{\omega_o L} + L \tag{A-1}$$

where R and L are the real and imaginary parts of the corresponding element of $[\mathbf{Z}^{loss}(\omega_o)]$, and R^{par} and L^{par} the resulting equivalent elements of the parallel block.

This alternative multiphase $[\mathbf{Z}^{loss}(\omega_o)]$ equivalent can be implemented in an EMTP's type solution using the procedure explained in [5] for coupled R-L elements and using the following discrete-time equations to calculate the equivalent resistance matrix $[\mathbf{R}^{eq}]$ and the history current-source vector $\mathbf{h}_{km}$.

$$[\mathbf{R}^{eq}] = [\mathbf{R}_o] + [\mathbf{R}^{eqpar}] \tag{A-2}$$

with $[\mathbf{R}^{eqpar}]$ being the equivalent multiphase resistance for the discretize parallel R^{par}-L^{par} block and $[\mathbf{R}_o]$ a diagonal matrix with the dc resistances of each conductor. For the history source,

$$\mathbf{h}_{km}(t) = [\mathbf{A}]v_{km}(t - \Delta t) + [\mathbf{B}]\mathbf{h}(t - \Delta t)$$

with

$$[\mathbf{A}] = 2[\mathbf{R}^{eq}]^{-1}[\mathbf{R}^{eqpar}]\left[\frac{2\mathbf{L}^{par}}{\Delta t}\right][\mathbf{R}^{eqpar}][\mathbf{R}^{eq}]^{-1} \tag{A-3}$$

and

$$[\mathbf{B}] = [\mathbf{R}^{eq}]^{-1}\left\{[\mathbf{R}^{eq}] - 2[\mathbf{R}_o][\mathbf{R}^{eqpar}]\left[\frac{2\mathbf{L}^{par}}{\Delta t}\right]^{-1}\right\}$$

This minimum one-block realization acts basically as a filter and a suitable (ω_o) frequency must be chosen to calculate the parameters. For the case of transmission lines a good wide-band fitting is accomplished for the elements of $[\mathbf{Z}^{loss}(\omega)]$ if the frequency (ω_o) is high enough to account for the highest frequency of interest.

A complete line model was developed using this approach [53] and simulations showed that this model gives better results than the cp-line constant-parameter line model (with the same computational effort) and its accuracy is even comparable to that of the fd-line frequency-dependent line model (with much less computational effort).